UNIVERSITY OF CALIFORNIA,
IRVINE

Merger Histories of Dark Matter Halos in ΛCDM and Implications for the Evolution of Milky Way-size Galaxies

DISSERTATION

submitted in partial satisfaction of the requirements
for the degree of

DOCTOR OF PHILOSOPHY

in Physics

by

Kyle Robert Stewart

Dissertation Committee:
Professor James Bullock, Chair
Professor Elizabeth Barton
Professor Manoj Kaplinghat

2009

DEDICATION

To God.

I can do all things through Him who gives me strength.

To my parents,

who always encouraged me to "reach for the stars."

(Though I doubt they realized I would "reach for the stars" quite so... literally.)

To my wife, Tania,

whose love makes me strong when I am weak.

The heavens declare the glory of God;

the skies proclaim the work of his hands.

Day after day they pour forth speech;

night after night they display knowledge.

There is no speech or language

where their voice is not heard.

Their voice goes out into all the earth,

their words to the ends of the world.

– Psalms 19:1-4 (NIV)

TABLE OF CONTENTS

LIST OF FIGURES

LIST OF TABLES

ACKNOWLEDGMENTS

I have had the privilege to work with many wonderful and talented people during my graduate career at University of California, Irvine. First and foremost, I would like to thank my advisor, James Bullock, whose incredible enthusiasm for science is matched by his genuine and heartfelt concern for his students' welfare and growth. James has the incredible ability to encourage students to develop projects that match their personal interests, while simultaneously molding such projects so that they are as scientifically relevant as possible. I would also like to thank Betsy Barton, who has continually challenged me to expand my scientific horizons and explore new topics of study. Much of this thesis attempts to bridge theoretical expectations with observations: a task that would have been impossible without Betsy's input and advice. I would like to thank Risa Wechsler at Stanford University, who provided the cosmological simulations' merger trees utilized in most of the work presented here. Her willingness to share her merger tree data, as well as her overall expertise and input over the years has been vital to much of this work.

I would also like to thank postdoc Jeff Cooke for many useful conversations, and postdoc Tobias Kaufmann for his invaluable expertise in recent months, helping me make a transition into a related subfield of galaxy formation simulations. The work presented here also benefitted from contributions of many others, and I would like to thank collaborators Ari Maller, Andrew Zentner, Manoj Kaplinghat, Joel Berrier, Chris Purcell, and Erik Tollerud for their numerous insights and advice.

I would like to thank all of my fellow graduate students, and all the postdocs in the astronomy group at UCI for countless conversations over lunches and astro-coffees, or while passing by each other in the hallway, etc. I would especially like to thank my office mate Chris Purcell for his constant willingness to pause whatever he's doing to discuss computer bugs, programming tips, or scientific topics with me over the years. I'd also like to thank Erik Tollerud, Devdeep Sarkar and Jonelle Walsh for acting as my "lifeline" to the various departmental activities and social functions. Without their outgoing and friendly efforts to keep me involved in the astronomy group's social activities, I would have no doubt spent my graduate years secluded in the corner of my office, doing research whilst interacting with no one.

I would like to thank the National Science Foundation for its support, as the bulk of work presented here was funded by NSF grant AST $05-07916$. I also like to thank the Center for Cosmology for its support, and the American Astronomical Society for permitting me to present published material as part of this thesis. Chapter 2, Chapter 3 and Chapter 4 have been published in The Astrophysics Journal as Stewart et al. (2008, 2009a,b) respectively.

I thank my parents for supporting me, both financially and otherwise, throughout my life. They have done more for me than I can ever list here, and they have always encouraged me to follow my dreams. Without their guidance and encouragement, I

would never have developed into the person I am today, nor could I have come this far. Finally, I thank my wife, Tania. Without her love and support, I could never have survived the rigors of graduate school. She has taught me so much about life, and about myself, and I am a better person today, thanks to her. I cannot imagine life without her.

CURRICULUM VITAE

Kyle Robert Stewart

CONTACT INFORMATION

2140 Frederick Reines Hall
Department of Physics and Astronomy
University of California, Irvine
Irvine, CA 92697 USA

Office: (949) 824-2892
Email: stewartkuci.edu
Web: www.physics.uci.edu/∼stewartk
Citizenship: United States

RESEARCH INTERESTS

Theoretical Cosmology; Galaxy Formation & Evolution; Dark Matter; Cosmological Simulations; Galaxy Simulations; Galaxy Mergers

EDUCATION

Doctor of Philosophy in Physics **2009**
University of California, Irvine *Irvine, California*

Master of Science in Physics **2006**
University of California, Irvine *Irvine, California*

Bachelor of Science in Astrophysics **2004**
University of California, Los Angeles *Los Angeles, California*

RESEARCH EXPERIENCE

Graduate Student Researcher **2005–2009**
University of California, Irvine *Irvine, California*
PI: James Bullock, Ph.D.

Undergraduate Research Assistant **2003–2004**
University of California, Los Angeles *Los Angeles, California*
PI: Matt Malkan, Ph.D.

TECHNICAL SKILLS

Operating Systems:
Proficient in: Windows, Linux

Programming & Software:
Proficient in: IDL, TIPSY
Familiar with: C++, Java, Mathematica, PKDGRAV, GASOLINE

TEACHING EXPERIENCE

Teaching Assistant: Introduction to Astronomy **Spring 2006**
University of California, Irvine: Course 20A *Irvine, California*
3 discussion sections, grading, office hours

Teaching Assistant: Cosmology **Winter 2006**
University of California, Irvine: Course 20B *Irvine, California*
4 discussion sections, grading, office hours

Teaching Assistant: Classical Physics **Spring 2005**
University of California, Irvine: Courses 7B, 7LB *Irvine, California*
2 discussion sections, grading, office hours
3 tutorial labs, office hours, tutorial center

Teaching Assistant: Basic Physics Lab II **Winter 2005**
University of California, Irvine: Course 3LB *Irvine, California*
3 experimental laboratory sections, grading, office hours

Teaching Assistant: Fundamentals of Experimental Physics **Fall 2004**
University of California, Irvine: Course 52A *Irvine, California*
3 experimental laboratory sections, grading, office hours

OUTREACH

University of California, Irvine **2008**
Participated in presentations to local elementary schools

SELECTED HONORS AND AWARDS

NASA Postdoctoral Program (NPP) Fellowship **2009**

PUBLICATIONS AND PRE-PRINTS

Mg II Absorption Systems in a Cosmological Context **K.R. Stewart**, T. Kaufmann, J. Bullock, E. Barton, J. Diemand, L. Mayer, P. Madau, J. Wadsley, A. Maller (tentative title and author list), **in prep.**

Stealth Galaxies in the Halo of the Milky Way J.S. Bullock, **K.R. Stewart**, M. Kaplinghat, E.J. Tollerud, **in prep.**

Mergers and Bulge Formation in Lambda-CDM: Which Mergers Matter? P. Hopkins, K. Bundy, D. Croton, L. Hernquist, D. Keres, S. Kochfar, **K.R. Stewart**, A. Wetzel, and J. Younger, MNRAS submitted, **2009**

Invisible Major Mergers: Why the Definition of a Galaxy "Merger Ratio" Matters

K.R. Stewart, ArXiv:0902.2214 [astro-ph], to appear in proceedings of "Galaxy Evolution: Emerging Insights and Future Challenges," **2009**

Gas-rich Mergers in LCDM: Disk Survivability and the Baryonic Assembly of Galaxies **K.R. Stewart**, J.S. Bullock, R.H. Wechsler, and A.H. Maller, ApJ, 702, 307, **2009**

The Effects of Gas on Morphological Transformation in Mergers: Implications for Bulge and Disk Demographics P.F. Hopkins, R.S. Somerville, T.J. Cox, L. Hernquist, S. Jogee, D. Keres, C.P. Ma, B. Robertson, and **K.R. Stewart**, MNRAS, 397, 802, **2009**

Galaxy Mergers and Dark Matter Halo Mergers in LCDM: Mass, Redshift, and Mass-Ratio Dependence **K.R. Stewart**, J.S. Bullock, E.J. Barton, R.H. Wechsler, ApJ, 702, 1005, **2009**

Mergers and Disk Survival in LCDM J.S. Bullock, **K.R. Stewart**, and C.W. Purcell, Invited Contribution, IAU Symposium 254, **2008**

The Assembly of Galaxy Clusters J.C. Berrier, **K.R. Stewart**, C.W. Purcell, E.J. Barton, and R.H. Wechsler, ApJ, 690, 1292, **2008**

A Candidate Brightest Proto-Cluster Galaxy at z = 3.03 J. Cooke, E.J. Barton, J.S. Bullock, **K.R. Stewart**, and A.M. Wolfe, ApJ, 681, 57, **2008**

Merger Histories of Galaxy Halos and Implications for Disk Survival **K.R. Stewart**, J.S. Bullock, R.H. Wechsler, A.H. Maller, and A.R. Zentner, ApJ, 653, 597, **2008**

SEMINARS AND COLLOQUIA

Merger Histories of LCDM Galaxies: Disk Survivability and the Deposition of Cold Gas via Mergers, Kavli Institute for Cosmological Physics, Open Group Seminar, The University of Chicago. Nov. 2008.

Merger Histories of LCDM Galaxies: Disk Survivability and the Deposition of Cold Gas via Mergers, Center for Cosmology and AstroParticle Physics Seminar, the Ohio State University, Oct. 2008.

Merger Histories of LCDM Galaxies: Disk Survivability and the Deposition of Cold Gas via Mergers, Berkeley Cosmology Group Seminar, University of California, Berkeley, Sept. 2008.

Merger Histories of LCDM Galaxies: Disk Survivability and the Deposition of Cold Gas via Mergers, KIPAC tea talk, Kavli Institute for Particle Astrophysics and Cosmology, Stanford University, Aug. 2008.

CONTRIBUTED CONFERENCE TALKS (OR POSTERS)

Cloud Formation in a Cosmological Context and Implications for Absorption-Selected Galaxies, Hunting for the Dark: the Hidden Side of Galaxy Formation, Malta, Oct. 2009 (Poster)

Cool Halo Gas in a Cosmological Context, Galaxy Formation Workshop, University of California, Santa Cruz, Aug. 2009.

Merger Histories of LCDM Galaxies: Disk Survivability and the Deposition of Cold Gas via Mergers, 213th AAS Meeting, Long Beach, CA, Jan. 2009.

Merger Histories of LCDM Galaxies: Gas Fractions and Disk Survivability, 8th Annual Theoretical Astrophysics in Southern California Meeting, University of California, Irvine, Oct. 2008.

Galaxy Merger Fractions and Disk Survivability, Back to the Galaxy II (Scientific Hightlights Section), University of California, Santa Barbara, Oct. 2008.

Merger Histories of DM Halos and the Baryonic Assembly of Galaxies, Galaxy Formation Workshop, University of California, Santa Cruz, Aug. 2008.

Merger Histories of Galaxy Halos, and Implications for Disk Survival, Galactic Structure and Structure of Galaxies Workshop, Ensenada, Baja California, Mexico, Mar. 2008 (Poster)

Merger Histories of Galaxy-sized Dark Matter Halos, and Implications for Disk Survival, 7th Annual Theoretical Astrophysics in Southern California Meeting, University of California, Los Angeles, Nov. 2007

Merger Histories of Galaxy-sized Dark Matter Halos, Galaxy Formation Workshop, University of California, Santa Cruz, Aug. 2007

ABSTRACT OF THE DISSERTATION

Merger Histories of Dark Matter Halos in ΛCDM
and Implications for the Evolution of Milky Way-size Galaxies

By

Kyle Robert Stewart

Doctor of Philosophy in Physics

University of California, Irvine, 2009

Professor James Bullock, Chair

There is a concern in galaxy formation that mergers are too common in ΛCDM to explain the prominence of thin disk-dominated galaxies in the local universe. In my dissertation, I analyze merger histories of dark matter halos from high resolution N-body simulations and compare dark halo merger statistics to the observable properties of galaxies, in order to study the implications of cosmologically motivated merger histories. I use empirical relations between a galaxy's dark matter halo mass, stellar mass, and cold gas mass to investigate these merger histories in the context of galaxy evolution, focusing on a dark matter mass regime within an order of magnitude of the Milky Way.

The principle results of this dissertation may be summarized as follows. Firstly, 70% of Milky Way-size halos have accreted an object with more than twice the mass of the Milky-Way's disk in the past 10 Gyr. To meet the observed fraction of disk dominated galaxies, mergers of this size must not always destroy galactic disks. Secondly, The merger rate of dark halos increases strongly with redshift. A simple 'universal' fitting formula describes these merger rates as a function of halo mass, merger mass ratio, and redshift. Thirdly, the fraction of halos have ever experienced a gas poor major

merger roughly matches the observed early-type morphological fractions within the regime $M = 10^{11-13} M_{\odot}$, providing a possible solution to disk survivability, if gas rich mergers do not destroy disk-dominated morphologies. Fourthly, because the mapping between dark matter halo mass and galaxy stellar mass (or baryonic mass) is a non-trivial function, it is important to distinguish between definitions of a merger "mass ratio" that use dark matter, stellar, or galaxy baryonic masses as a means of comparison. For example, major dark matter mergers in smaller galaxies ($M_{\rm DM} < 10^{11} M_{\odot}$) typically corresponds to very minor *stellar* mergers. Finally, we use a higher resolution simulation to focus on the substructure of Milky Way-sized galaxies. We predict a population of "stealth" galaxies: low-luminosity dwarf galaxies in the halo of the Milky Way with surface brightnesses so low they are unobservable with current methods.

Chapter 1

Introduction

In the current Λ Cold Dark Matter (CDM) paradigm, dark matter (DM) constitutes $\sim 83\%$ of the matter density of the universe (Spergel et al., 2007), so that the large scale structures in the universe are not dominated by normal "baryonic" matter, but by the behavior of dark matter (and dark energy, in the form of a cosmological constant, Λ, which causes the observed acceleration in the universe at later times.) The term "cold" in describing dark matter refers to non-relativistic particle velocities, which allows dark matter to clump gravitationally on small scales first. Thus, in CDM cosmologies, the universe forms hierarchically, with less massive dark matter halos forming first, and halos merging together to form more massive halos over time. In this paradigm, since dark matter dominates the matter density of the universe, all baryonic matter (galaxies) are expected to reside within the centers of massive dark matter halos.

In this picture of galaxy formation, it is important to understand the implications of dark matter halo mergers (galaxy mergers). The gravitational impact of so called "major mergers" (in which the ratio of dark matter halo masses $\gtrsim 1/3$) are believed to

play an important role in shaping galaxy morphologies (e.g., Toomre & Toomre, 1972; Bournaud et al., 2007). They also drive large supplies of gas (when gas is present in the progenitor galaxies) into the central regions, triggering star formation, fueling supermassive black holes and Active Galactic Nuclei (AGN) activity (e.g., Mihos & Hernquist, 1996; Barton et al., 2007). They also contribute to the direct deposition of gas and stars into the "main" galaxy (usually defined as the most massive progenitor). So called "minor mergers" (typically with merger mass ratios between $\sim 1/10 - 1/3$) may aid in the creation of thick disk components in disk-dominated galaxies (e.g. Quinn et al., 1993; Purcell et al., 2009), cause anti-truncation (Younger et al., 2007), add angular momentum to the main galaxy, and contribute to extended diffuse light components around galaxies (e.g., Purcell et al., 2007).

However, there is concern that mergers may in fact be *too* common in ΛCDM to explain the observed fractions of disk-type systems (with stellar dynamics dominated by ordered rotation) and bulge-type galaxies (with dynamics dominated by random motions). Since mergers are relatively common, and mergers are expected to disrupt or even destroy disk-dominated morphologies, it is difficult to explain how $\sim 70\%$ of Milky Way-size galaxies are morphologically classified as "disk-dominated." There is also a concern that the ΛCDM model predicts thousands of subhalos within the halo of the Milky Way that should host galaxies, which have not been observed.

The goal of this thesis is to use cosmological simulations of dark matter structure in order to derive theoretical expectations for galaxy evolution, specifically in roughly Milky Way-sized galaxies ($M_{\rm DM} \sim 10^{12} M_{\odot}$). The structure of the thesis is as follows. In Chapter 2 we analyze thousands of cosmological merger histories for existing Milky Way-sized halos at $z = 0$ in the simulation, then apply these statistics to the issue of disk-galaxy survivability, comparing to observed morphological fractions of galaxies in the local universe. In Chapter 3 we focus on more instantaneous merger rates of dark

matter halos as a function of redshift, merger mass ratio, and halo mass. We compare our theoretical findings to observational indications of the merger rate, such as the morphologically disturbed fraction or close-pair count statistics of massive galaxies as a function of redshift. In Chapter 4 we revisit dark matter halo merger statistics in light of disk survival, but we used empirically motivated techniques for approximating the stellar mass and cold gas mass within a dark matter halo, as a function of halo mass. We then investigate the cosmologically expected fractions of major *gas-poor* mergers (galactic cold gas fractions $< 50\%$), based on recent simulation results indicating that gas-rich mergers may preserve disk-dominated morphologies (Brook et al., 2004; Robertson et al., 2006a; Governato et al., 2009). In Chapter 5 we take a brief look at how varying definitions of a merger "mass ratio" (defined either by dark matter halo masses, galaxy stellar masses, or total galaxy baryonic masses) may impact comparisons between observations and theory. Finally, in Chapter 6 we analyze a much higher resolution simulation, "Via Lactea II" (Diemand et al., 2008), that allows us to accurately describe the substructure of a single Milky Way-size halo. Using a similar model as in previous chapters to assign a central galaxy's stellar mass as a function of halo mass, we develop a model from this simulation that is consistent with the observed dwarf galaxies around the Milky Way, and predicts a population of heretofore undiscovered "stealth" galaxies in the Milky Way, which have surface brightnesses too low to be observed with current methods. We touch upon avenues of future work in Chapter 7 and summarize our findings with some concluding remarks in Chapter 8.

Chapter 2

Merger Histories of DM Halos and Implications for Disk Survival

2.1 Chapter Abstract

We study the merger histories of galaxy dark matter halos using a high resolution ΛCDM N-body simulation. Our merger trees follow $\sim 17,000$ halos with masses $M_0 = (10^{11} - 10^{13})M_\odot$ at $z = 0$ and track accretion events involving objects as small as $m \simeq 10^{10}M_\odot$. We find that mass assembly is remarkably self-similar in m/M_0, and dominated by mergers that are $\sim 10\%$ of the final halo mass. While very large mergers, $m \gtrsim 0.4\,M_0$, are quite rare, sizeable accretion events, $m \sim 0.1\,M_0$, are common. Over the last ~ 10 Gyr, an overwhelming majority ($\sim 95\%$) of Milky Way-sized halos with $M_0 = 10^{12}M_\odot$ have accreted at least one object with greater total mass than the Milky Way disk ($m > 5 \times 10^{10}M_\odot$), and approximately 70% have accreted an object with more than twice that mass ($m > 10^{11}M_\odot$). Our results raise serious concerns about the survival of thin-disk dominated galaxies within the

current paradigm for galaxy formation in a ΛCDM universe. In order to achieve a $\sim 70\%$ disk-dominated fraction in Milky Way-sized ΛCDM halos, mergers involving $m \simeq 2 \times 10^{11} M_{\odot}$ objects must not destroy disks. Considering that most thick disks and bulges contain old stellar populations, the situation is even more restrictive: these mergers must not heat disks or drive gas into their centers to create young bulges.

2.2 Introduction

In the cold dark matter (CDM) model of structure formation, dark matter halos form via the continuous accretion of smaller systems (Peebles, 1982; Blumenthal et al., 1984; Davis et al., 1985; Fakhouri & Ma, 2008; Neistein & Dekel, 2008; Cole et al., 2008a). Mergers of the type predicted can help explain many properties of the observed universe. Major mergers are believed to play an important role in shaping the Hubble sequence (Toomre & Toomre, 1972; Barnes, 1988; Hernquist, 1993; Naab & Burkert, 2003; Khochfar & Burkert, 2005; Cox et al., 2006a; Robertson et al., 2006b,a,c; Maller et al., 2006; Jesseit et al., 2007; Bournaud et al., 2007) and triggering star formation and AGN activity (Mihos & Hernquist, 1996; Kolatt et al., 1999; Cox et al., 2006a; Woods et al., 2006; Barton et al., 2007). Minor mergers may help explain the origin of thick disks (Quinn et al., 1993; Walker et al., 1996; Abadi et al., 2003; Brook et al., 2004; Dalcanton et al., 2005; Kazantzidis et al., 2008; Hayashi & Chiba, 2006), cause anti-truncation (Younger et al., 2007), and produce extended diffuse light components around galaxies (Johnston et al., 1996; Helmi & White, 1999; Bullock et al., 2001b; Bullock & Johnston, 2005; Purcell et al., 2007; Bell et al., 2008). However, there is lingering concern that mergers are too common in CDM cosmologies for thin disk-dominated systems to survive (Toth & Ostriker, 1992; Wyse, 2001; Kormendy & Fisher, 2005; Kautsch et al., 2006). In this chapter

we present the merger statistics necessary for addressing this issue.

The formation of disk galaxies within hydrodynamic simulations in hierarchical CDM cosmologies has proven problematic (e.g. Navarro & Steinmetz, 2000). While there have been some successes in forming galaxies with disks in cosmological simulations (Abadi et al., 2003; Sommer-Larsen et al., 2003; Brook et al., 2004; Robertson et al., 2004; Kaufmann et al., 2007a; Governato et al., 2007), the general problem is far from resolved. The resultant disks are often fairly thick and accompanied by large bulges, and the systems that form disks tend to have special merger histories. The resultant thick disk and bulge stars also tend towards a broad range of stellar ages, instead of being dominated by predominantly old stars. Moreover, the successes depend strongly on effective models that describe physics on scales far below the simulation resolution, which are poorly understood. Given the current difficulties in understanding *ab initio* disk formation, one can consider a less ambitious, but more well-posed question. Even if disk galaxies can form within CDM halos, can they survive the predicted merger histories?

Unfortunately, the prevalence of thin-disk or even disk-dominated galaxies in the universe is difficult to quantify with large observational samples. Some promising approaches use asymmetry vs. concentration to define morphological type (e.g., Ilbert et al., 2006), and some use a combination color and concentration indicators (e.g. Choi et al., 2007; Park et al., 2007). Despite the wide range of definitions, the general consensus in the literature is that $\sim 70\%$ of $\sim 10^{12} h^{-1} M_{\odot}$ halos host disk-dominated, late-type galaxies (e.g. Weinmann et al., 2006; van den Bosch et al., 2007; Ilbert et al., 2006; Choi et al., 2007; Park et al., 2007). We adopt this number for the sake of discussion in what follows, but none of our primary results on merger statistics depend on this number.

Also relevant to the discussion of galaxy merger histories is the prevalence of pure

disk galaxies in the universe. Kautsch et al. (2006) have compiled a statistically meaningful sample of edge-on disk galaxies and found that $\sim 16\%$ of these objects are "simple disks" with no observable bulge component. In principle, this statistic places strong constraints on the merger histories of galaxies. Moreover, a large fraction of disk galaxies with bulges contain pseudo-bulges, which may be the products of secular processes and not the remnants of an early merger event (e.g. Kormendy & Kennicutt, 2004; Carollo et al., 2007). These cases provide further motivation to quantify the predicted merger histories of galaxy halos in the favored CDM cosmology.

Here we use a large dissipationless cosmological ΛCDM N-body simulation to track the merger histories of an ensemble of $\sim 17,000$ halos with $z = 0$ masses $M_0 = 10^{11} - 10^{13} h^{-1} M_\odot$. We focus on halos of fixed mass at $z = 0$, and concentrate specifically on Milky Way-sized systems, $M_0 \simeq 10^{12} h^{-1} M_\odot$. We categorize the accretion of objects as small as $m \simeq 10^{10} h^{-1} M_\odot$ and focus on the infall statistics into *main progenitors* of $z = 0$ halos as a function of lookback time. As discussed below, the *main progenitor* is defined to be the most massive progenitor of a $z = 0$ halo tracked continuously back in time.

A *merger* is defined here to occur when an infalling halo first crosses within the virial radius of the main progenitor. In most cases we do not track subhalo evolution after accretion. We have chosen to track mergers in this way in order to provide a robust prediction. An understanding of an accreted halo's subsequent orbital evolution and impact with the central disk region is essential for any complete understanding of *galaxy* merger statistics. However, this evolution will be sensitive to the baryonic distribution within both the main progenitor halo and the satellites themselves. The *halo* merger rate we present is a relatively clean measure that can be used as a starting point for more detailed investigations of galaxy–galaxy encounters. Still, it is worth pointing out that for most of the mergers we consider, impacts with the central disk

region should occur relatively shortly after accretion. As we show in the Appendix, events with $m \gtrsim 0.1M_0$ typically happen at a redshift z when the main progenitor mass, M_z, is significantly smaller than M_0, such that the merger ratio is fairly large $m/M_z \gtrsim 0.2$. Therefore, even ignoring the enhanced orbital decay that will be caused by a central disk potential, the dynamical friction decay times are expected to be short for these events, with central impacts occurring within $\tau \lesssim 3$ Gyr for typical orbital parameters (Boylan-Kolchin et al., 2008; Zentner et al., 2005; Zentner & Bullock, 2003). As discussed in conjunction with Figure 2.5 in §2.4, destruction times of ~ 3 Gyr are consistent with our measurements of subhalo evolution.

The outline of this chapter is as follows. In §2.3 we discuss the numerical simulations used and the method of merger tree construction. In §2.4 we present our principle results, which characterize the accretion mass functions of halos and the fraction of halos with mergers as a function of lookback time. In §2.5 we discuss these results in reference to the problem of disk survival in a hierarchical universe, and we summarize our main conclusions in §2.6.

2.3 The Simulation

Our simulation consists of 512^3 particles, each with mass $m_p = 3.16 \times 10^8 h^{-1} M_\odot$, evolved within a comoving cubic volume of $80h^{-1}$ Mpc on a side using the Adaptive Refinement Tree (ART) N-body code (Kravtsov et al., 1997, 2004). The cosmology is a flat ΛCDM model, with parameters $\Omega_M = 1 - \Omega_\Lambda = 0.3$, $h = 0.7$, and $\sigma_8 = 0.9$. The simulation root computational grid consists of 512^3 cells, which are adaptively refined to a maximum of eight levels, resulting in a peak spatial resolution of $1.2h^{-1}$ kpc, in comoving units. This simulation and the methods we use to construct merger trees have been discussed elsewhere (Allgood et al., 2006; Wechsler et al., 2006). Here

we give a brief overview and refer the reader to those papers for a more complete discussion.

Field dark matter halos and subhalos are identified using a variant of the bound density maxima algorithm (Klypin et al., 1999a). A *subhalo* is defined as a dark matter halo whose center is positioned within the virial radius of another, more massive halo. Conversely, we define a *field halo* to be a dark matter halo that does not lie within the virial radius of a larger halo. The virial radius is defined as the radius of a collapsed self gravitating dark matter halo within which the average density is Δ_{vir} times the mean density of the universe. For the family of flat cosmologies ($\Omega_m + \Omega_\Lambda = 1$) the value of Δ_{vir} can be approximated by (Bryan & Norman, 1998):

$$\Delta_{vir} = \frac{18\pi^2 + 82(\Omega_m(z) - 1) - 39(\Omega_m(z) - 1)^2}{\Omega_m(z)}. \tag{2.1}$$

Masses, M, are defined for field halos as the mass enclosed within the virial radius, so that $M = (4\pi/3)R^3\Omega_m\rho_c\Delta_{vir}$. With these definitions, the virial radius for halos of mass M at $z = 0$ is given by:

$$R \simeq 205h^{-1}\mathrm{kpc}\ \left(\frac{M}{10^{12}h^{-1}M_\odot}\right)^{1/3}. \tag{2.2}$$

Note that this mass definition based on a fixed overdensity is largely conventional, and is traditionally used as a rough approximation for the radius within which the halos are virialized. We refer the reader to the recent work of Cuesta et al. (2008) for further discussion of this issue.

Halo masses become more difficult to define in crowded environments. For example, if two halos are located within two virial radii of each other, mass double-counting can become a problem. Also, subhalos can become tidally stripped if they are accreted into a larger halo. While the stripped material typically remains bound to the larger

host halo, it is no longer bound to the smaller subhalo and should not be included in the subhalo's mass. In these cases, the standard virial over-density definitions are not appropriate. In order to overcome this ambiguity, we always define a halo's radius and mass as the minimum of the virial mass and a "truncation mass" – defined as the mass within the radius where the log-slope of the halo density profile becomes flatter than -0.5. This definition of truncation mass is a relatively standard practice when dealing with simulations of this kind (e.g. Klypin & Holtzman, 1997; Kravtsov et al., 2004; Zentner et al., 2005), and we follow this convention to remain consistent with other work in this field. In practice, our field halos have masses and radii defined by the standard virial relations ($\sim 98\%$ of all non- subhalos). It is fair then to interpret our merger rates as infall rates into halo virial radii. The masses of objects just prior to infall are more likely affected by this definition, but the overall effect on our results is not large. As a test, we have redone our main analysis using an (extrapolated) virial mass for infalling halos. The results on fractional merger rates change only at the $\sim 5\%$ level.

In the event that a halo experiences a close pass with another halo—entering within the virial radius for a short time, then exiting the virial radius never to return—the two halos are considered isolated, even though one may lie within the virial radius of the other. Conversely, if the smaller halo falls back within the virial radius and the two halos subsequently merge together, then we continue to consider the smaller halo a subhalo even during the time when it lies outside the virial radius of its host. This has been referred to as the "stitching" method—as opposed to "snipping," which would count the above example as two separate mergers (Fakhouri & Ma, 2008).

By constructing mass functions, we find that these halo catalogs are complete to a minimum mass $10^{10}h^{-1}M_{\odot}$. This allows us to measure the accretion of objects 10 times smaller than $10^{11}h^{-1}M_{\odot}$ halos, or objects up to 1000 times smaller than

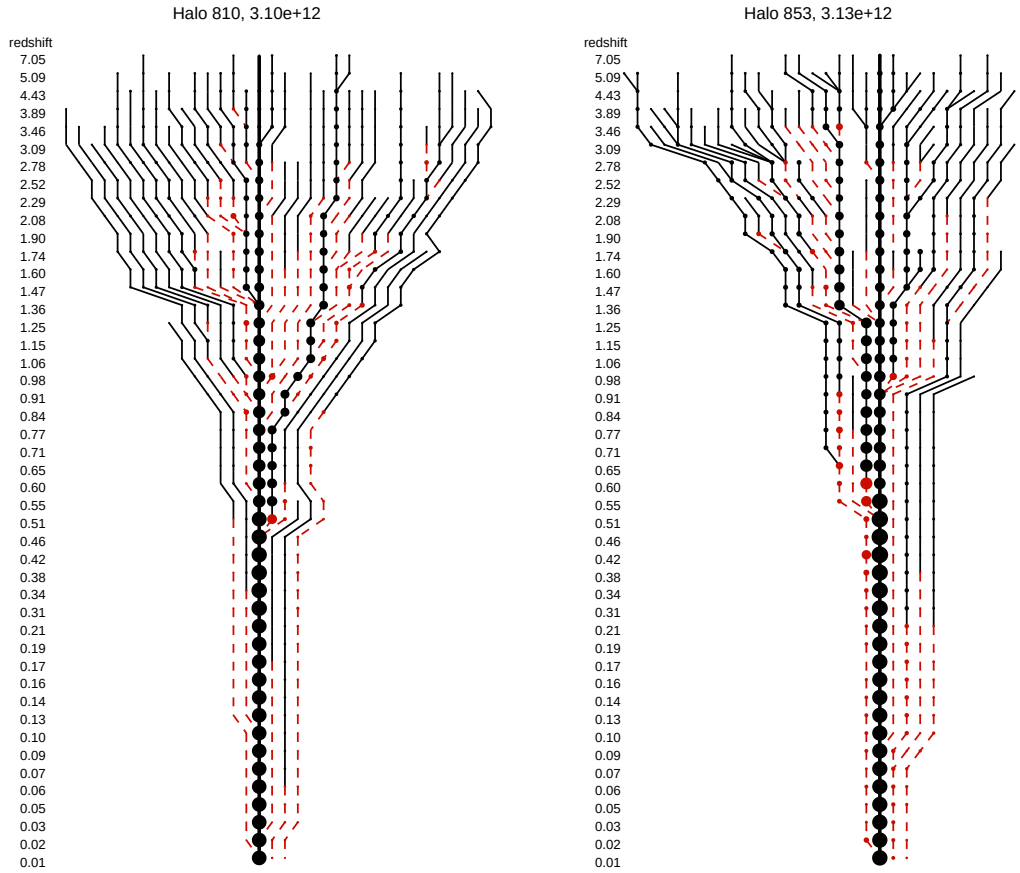

Figure 2.1: Sample merger trees, for halos with $M_0 \simeq 10^{12.5} h^{-1} M_\odot$. Time progresses downward, with the redshift z printed on the left hand side. The bold, vertical line at the center corresponds to the main progenitor, with filled circles proportional to the radius of each halo. The minimum mass halo shown in this diagram has $m = 10^{9.9} h^{-1} M_\odot$. Solid (black) and dashed (red) lines and circles correspond to isolated field halos, or subhalos, respectively. The dashed (red) lines that do not merge with main progenitor represent surviving subhalos at $z = 0$. *Left:* A "typical" merger history, with a merger of mass $m \simeq 0.1 M_0 \simeq 0.5 M_z$ at $z = 0.51$. *Right:* A halo that experiences an unusually large merger $m \simeq 0.4 M_0 \simeq 1.0 M_z$ at $z = 0.65$.

$10^{13} h^{-1} M_\odot$ halos. In all cases, we denote the mass of an accreted object as m. Overall we have a total of 17,241 halos in our sample with $M_0 > 10^{11} h^{-1} M_\odot$, and (6642, 2479, 911, and 298) halos in logarithmically-spaced mass bins centered on $\log M_0 =$ (11.5, 12.0, 12.5, and 13.0) respectively, in units of $h^{-1} M_\odot$.

Our merger tree construction mirrors that described in Kravtsov et al. (2004) and uses 48 stored timesteps that are approximately equally spaced in expansion factor

between the current epoch $a = (1+z)^{-1} = 1.0$ and $a = 0.0443$. We use standard terminologies for *progenitors* and *descendant*. Any halo at any timestep may have any number of *progenitors*, but a halo may have only one *descendant* — defined to be the single halo in the next timestep that contains the majority of this halo's mass. We use the terms "merger" and "accretion" interchangeably to designate the infall of a smaller halo into the virial radius of a larger one. The term *main progenitor* is used to reference the most massive progenitor of a $z = 0$ halo tracked continuously back in time.

Throughout most of this work we present results in terms of absolute mass thresholds on the infalling mass m. Our principle statistics are quantified using the infalling mass thresholds in terms of the final $z = 0$ mass of the main progenitor halo (e.g. $m > 0.1M_0$). Indeed, many of our results are approximately self-similar with respect to halo mass when the infalling mass cut is defined in this scaled manner. By definition, the maximum mass that a merging halo can have is $m = 0.5M_0$. Note that it is common in the literature to study the *merger ratio* of an infalling object, m/M_z, where M_z is the main progenitor mass at the redshift z, just prior to the merger. Here, M_z *does not* incorporate the mass m itself and therefore m/M_z has a maximum value of 1.0. A parallel discussion that uses m/M_z is presented in the Appendix, but the absolute mass thresholds are used as our primary means to quantify merger statistics in the main part of this chapter. We make this choice for two reasons. First, it is relatively easy to understand completeness effects using a fixed threshold in m, while completeness in m/M_z will vary as a function of time and will change from halo to halo depending on its particular mass accretion history. Second, an event with $m/M_z \sim 1$ does not necessarily imply that the infalling object m is large compared to the final halo mass M_0. In order to be conservative, we would like to restrict ourselves to mergers that are large in an absolute sense compared to typical galaxy masses today.

Figure 2.1 shows two pictorial examples of merger trees for halos with approximately equal $z = 0$ masses $M_0 \simeq 10^{12.5} h^{-1} M_\odot$. Time runs from top to bottom and the corresponding redshift for each timestep is shown to the left of each tree. The radii of the circles are proportional to the halo radius $R \sim M^{1/3}$, while the lines show the descendent–progenitor relationship. The color and type of the connecting lines indicate whether the progenitor halo is a field halo (solid black) or a subhalo (dashed red). The most massive progenitor at each timestep — the main progenitor — is plotted in bold down the middle. The ordering of progenitor halos in the horizontal direction is arbitrary. Once a halo falls within the radius of another halo, it becomes a subhalo and its line-type changes from black solid to red dashed. When subhalo lines connect to a black line this corresponds to a central subhalo merger or to a case when the subhalo has been stripped to the point where it is no longer identified. When field halos connect directly to a progenitor without becoming subhalos in the tree diagram it means that the subhalo is stripped or merged within the timestep resolution of the simulation. Halos that are identified as subhalos of the main halo at $z = 0$ are represented by the dashed-red lines that reach the bottom of the diagram without connecting to the main progenitor line.

Note that the extent to which we can track a halo after it has become a subhalo, and the point at which a subhalo is considered "destroyed" is dependent both on spacing of our output epochs and mass resolution of the simulation. This is another reason why we count mergers when a halo falls within the virial radius (when the lines in Figure 2.1 change from solid-black to dashed-red) and not when a subhalo experiences a central merger with its host.

The left diagram ("halo 810") in Figure 2.1 shows a fairly typical merger history, with a merger of mass $m \simeq 0.1 M_0$ at $z \simeq 0.51$. The merger ratio at the time of the merger was $m/M_z \simeq 0.5$. The right diagram ("halo 853") shows a very rare type

of merger history with a massive event $m \simeq 0.4M_0$ at $z \simeq 0.65$. This was a nearly equal-mass accretion event at the time of the merger, $m/M_z \simeq 1.0$. Note that neither of these large mergers survive for long as resolved subhalos — they quickly lose mass and merge with the central halo. Each of these halos has two $\sim 10^{10}h^{-1}M_\odot$ subhalos that survive at $z = 0$.

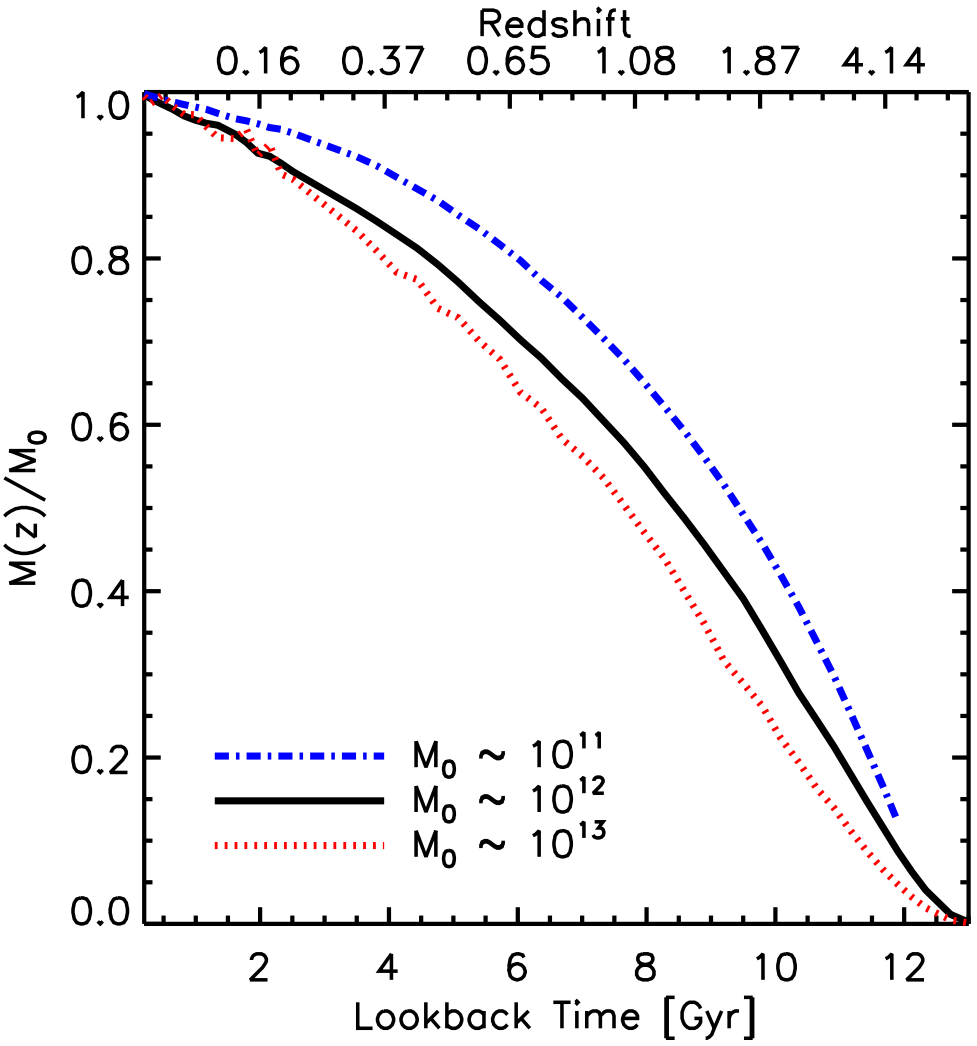

Figure 2.2: Average mass accretion histories for three bins in halo mass, as a function of lookback time. Each bin gives the average for bins of size $\log M_0 = 0.5$, centered on the stated value. More massive halos accreted a larger fraction of their mass at late times.

2.4 Results

2.4.1 Accretion Histories and Mass Functions

The literature is rich with work on the cumulative mass accretion histories of halos as a function of redshift (e.g Wechsler et al., 2002; Zhao et al., 2003; Tasitsiomi et al., 2004; Li et al., 2007, and references therein). We begin by re-examining this topic for the sake of completeness. Figure 2.2 shows average main progenitor mass accretion histories, $M_z = M(z)$, for halos of three characteristic final masses, $M_0 = M(z = 0)$. We confirm previous results that halo mass accretion histories are characterized by an initial rapid accretion phase followed by a slower accretion phase, and that more massive halos experience the rapid accretion phase later than less massive halos (Wechsler et al., 2002). Milky Way-sized halos with $M_0 = 10^{12}h^{-1}M_\odot$ will, on average, accrete half of their mass by $z \simeq 1.3$, corresponding to a lookback time of ~ 8.6 Gyr.

While Figure 2.2 provides some insight into *when* mass is accreted into halos, we are also interested in characterizing *how* this mass is accreted. (Ultimately, we will present merger statistics for a joint distribution of both time *and* mass ratio.) Now we investigate the mass function $n(m)$ of objects larger than m that have merged into the main progenitor over its history. The solid line in Figure 2.3 shows $n(m)$ averaged over halos in the $M_0 = 10^{12}h^{-1}M_\odot$ bin, plotted as a function of m/M_0. On average, Milky Way-sized halos with $M_0 \simeq 10^{12}h^{-1}M_\odot$ experience ~ 1 merger with objects larger than $m \sim 10^{11}h^{-1}M_\odot$, and ~ 7 mergers with objects larger than $m \sim 10^{10}h^{-1}M_\odot$ over the course of their lives.

For some purposes, an analytic characterization of the accreted mass function will be useful. We have investigated the average $n(m)$ function for halos in the mass range $M_0 = 10^{11.5} - 10^{13}h^{-1}M_\odot$ and find that the shape of this function is remarkably

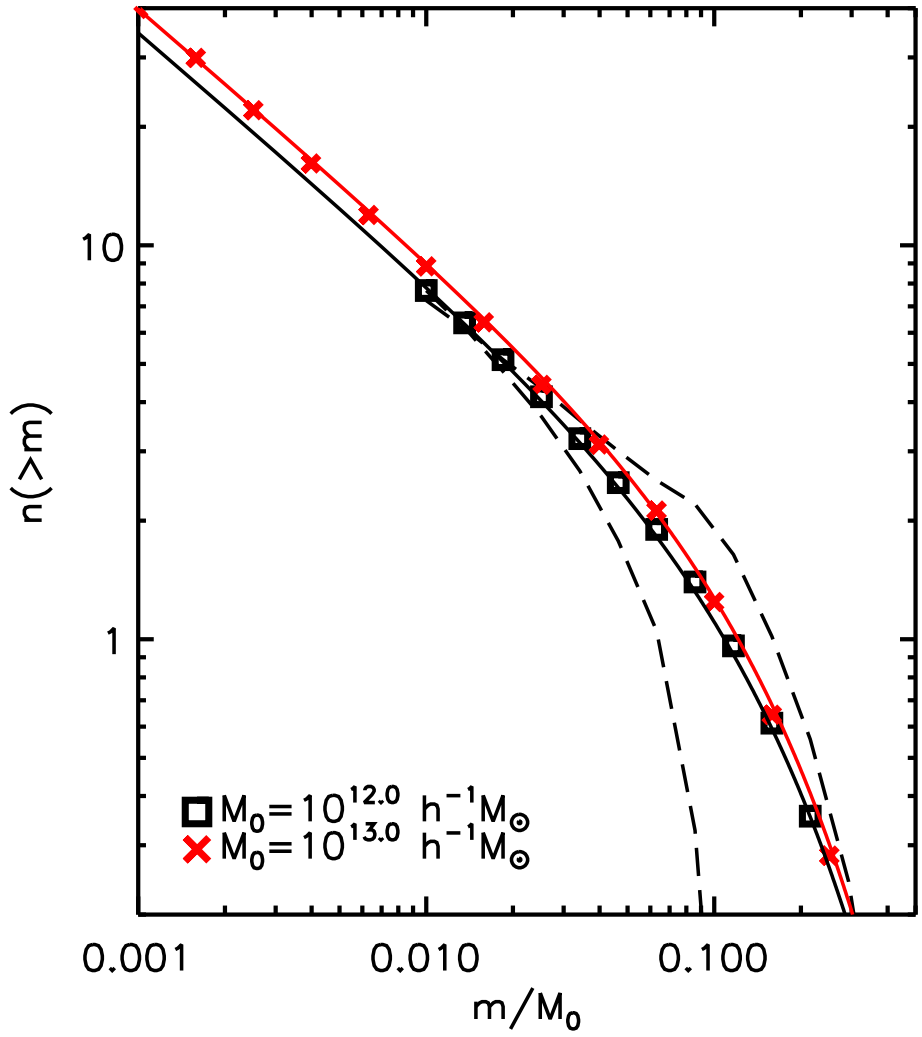

Figure 2.3: Mass functions of accreted material, with respect to the final halo mass. Lines show the cumulative number of mergers that a halo experiences with objects larger than m/M_0, integrated over the main progenitor's formation history. The (black) squares show the average for $10^{12}h^{-1}M_\odot$ halos; (red) crosses show the average for $10^{13}h^{-1}M_\odot$ halos. Lines through the data points show the fits given by Equation 2.1. The upper/lower dashed lines indicate the $\sim 25\%/20\%$ of halos in the $10^{12}h^{-1}M_\odot$ sample that have experienced exactly two/zero $m \geq 0.1M_0$ merger events. Approximately 45% of halos have exactly one $m \geq 0.1M_0$ merger event; these systems have mass accretion functions that resemble very closely the average.

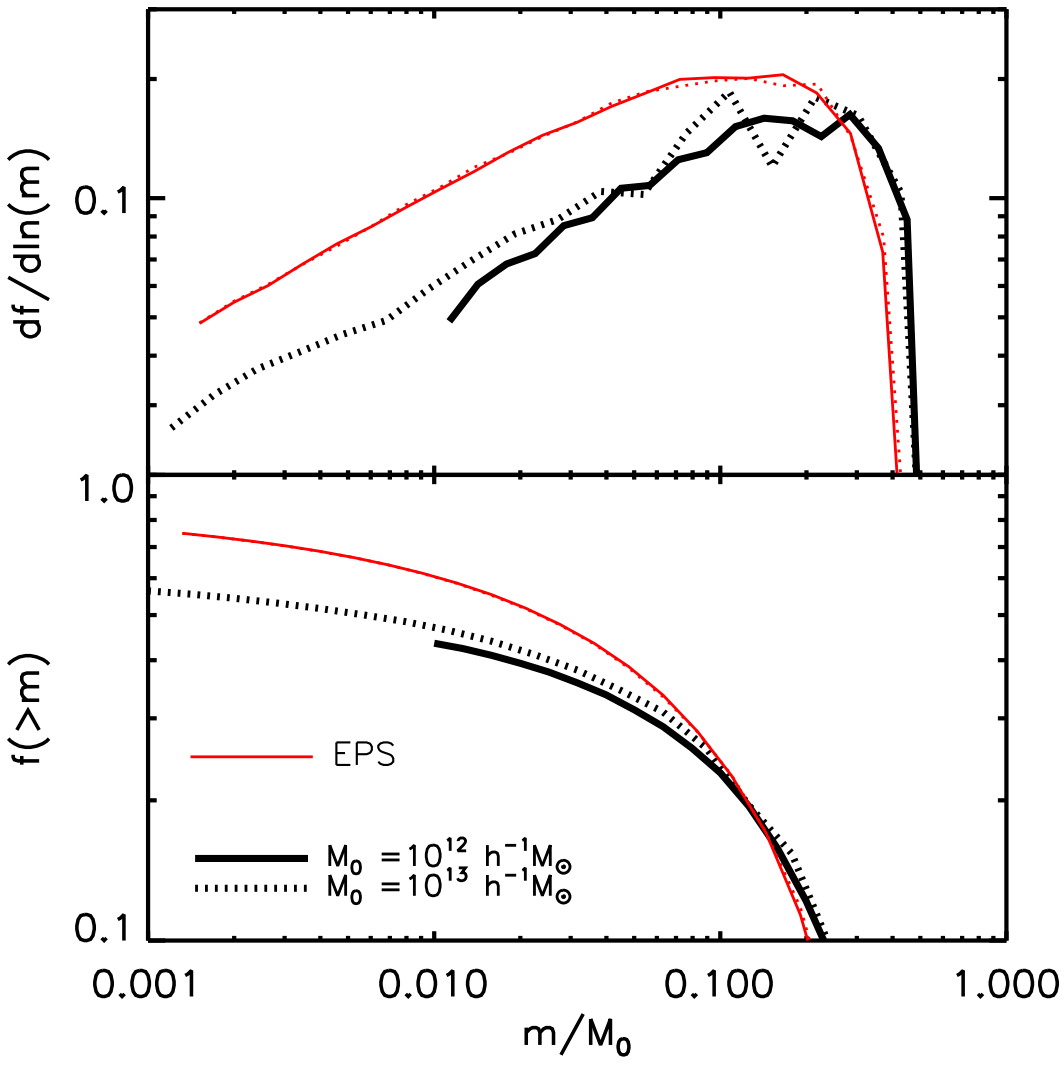

Figure 2.4: The fraction of halo's final mass M_0 accreted from objects of mass m/M_0, integrated over time. The differential (upper) and cumulative (lower) mass fractions are shown. The thick (black) lines show simulation results and the thin (red) lines show the prediction from standard Extended Press Schechter (EPS). Accretions with $m \simeq (0.03 - 0.3)M_0$ dominate the mass buildup in halos of all M_0. The distributions are approximately self-similar with host halo mass. This is in reasonably good agreement with the EPS expectation, although the EPS fractions systematically sit above the simulation results.

similar over this range (smaller M_0 were neglected in order to achieve a reasonable range in m/M_0). Specifically, we find that $n(m)$ is well-characterized by a simple function of $x \equiv m/M_0$:

$$n(> x) = A\, x^{-\alpha}\, (0.5 - x)^{\beta}, \tag{2.3}$$

with $\beta = 2.3$, $\alpha = 0.61$, and $x \leq 0.5$ by construction. Interestingly, we find that the overall normalization increases monotonically with halo mass, and that the trend can be approximated as $A(M_0) \simeq 0.47 \log_{10}(M_0) - 3.2$, where M_0 is in units of $h^{-1}M_\odot$. This mass-dependent normalization, together with Equation 2.3, reproduces our measured $n(m)$ functions quite well — to better than 5% at all m in smaller halos ($M_0 = 10^{11.5} - 10^{12} h^{-1} M_\odot$), and (somewhat worse) to 15% at higher masses ($M_0 = 10^{12.5} - 10^{13} h^{-1} M_\odot$). [1]

We would also like to understand the scatter in the accreted mass function from halo to halo at fixed M_0. It is not appropriate to simply describe the variation in $n(m)$ at a fixed mass, because the total mass accreted is constrained to integrate to less than M_0. This means that the number of small objects accreted may be anti-correlated with the number of large objects accreted. With this in mind, we provide an illustration of the scatter with the two dashed lines in Figure 2.3. The upper dashed line shows the average $n(m)$ for the $\sim 25\%$ of halos that have experienced exactly two accretion events larger than $m = 0.1M_0$. The lower dashed line shows the average $n(m)$ for the $\sim 20\%$ of halos that have experienced exactly zero $m > 0.1M_0$ accretion events. Approximately $\sim 45\%$ of halos have exactly one $m > 0.1M_0$ event, and these have an average accreted mass function that is very similar to the overall average shown by solid (black) line in Figure 2.3. Halos with fewer large mergers show a slight tendency to have more small mergers, but the effect is not large.

[1] The quoted errors are restricted to $n > 0.05$.

Figure 2.4 presents some of the same information shown in Figure 2.3, but now in terms of the mass fraction, $f(m)$, accreted in objects larger than m for $M_0 = 10^{12}$ and $10^{13}h^{-1}M_\odot$ halos (thick lines, see legend). The upper panel in Figure 2.3 shows the differential fraction, $\mathrm{d}f/\mathrm{d}\ln m = (-m^2/M_0)\mathrm{d}n/\mathrm{d}m$, while the lower panel plots the integrated fraction $f(m)$. As before, we have normalized the accreted masses, m, by the final $z = 0$ main progenitor mass M_0. We find that $f(> m)$ is also well fit by Equation 2.3 (to better than 10% across all masses $M_0 = 10^{12} - 10^{14}h^{-1}M_\odot$)[2]. As before, $x \equiv m/M_0$, but now $A(M_0) \simeq 0.17\log_{10}(M_0) - 0.36$, with M_0 still in units of $h^{-1}M_\odot$. The best fit parameters are $\alpha = 0.05$, and $\beta = 2.3$. The lines are truncated at $m/M_0 = 0.01$ and 0.001, corresponding to our fixed resolution limit at $m = 10^{10}h^{-1}M_\odot$. The thin (red) lines of the same line types show the same quantities predicted from Extended Press Schechter (EPS Lacey & Cole, 1993) Monte-Carlo merger trees. Each of these lines is based on 5000 trees generated using the Somerville & Kolatt (1999) algorithm.

In broad terms, the mass spectrum of accreted objects agrees fairly well with the EPS expectations, especially considering the relative ambiguity associated with defining halo masses in simulations (e.g. Cohn & White, 2008; Diemand et al., 2007; Cuesta et al., 2008). However, it is worth discussing the similarities and differences in some detail. It is a well-known expectation from EPS that the total mass accreted into a halo of mass M_0 is dominated by objects of mass $m \sim 0.1M_0$ (Lacey & Cole, 1993; Zentner & Bullock, 2003; Purcell et al., 2007; Zentner, 2007). Our simulations reveal that indeed $m \simeq (0.03 - 0.3)M_0$ objects are the most important contributors to the final halo mass.

EPS trees predict self-similar mass fractions across all halo masses. Our more massive halos, however, show a slight tendency to have more of their mass accreted in collapsed

[2]The quoted errors are restricted to $f > 0.1$.

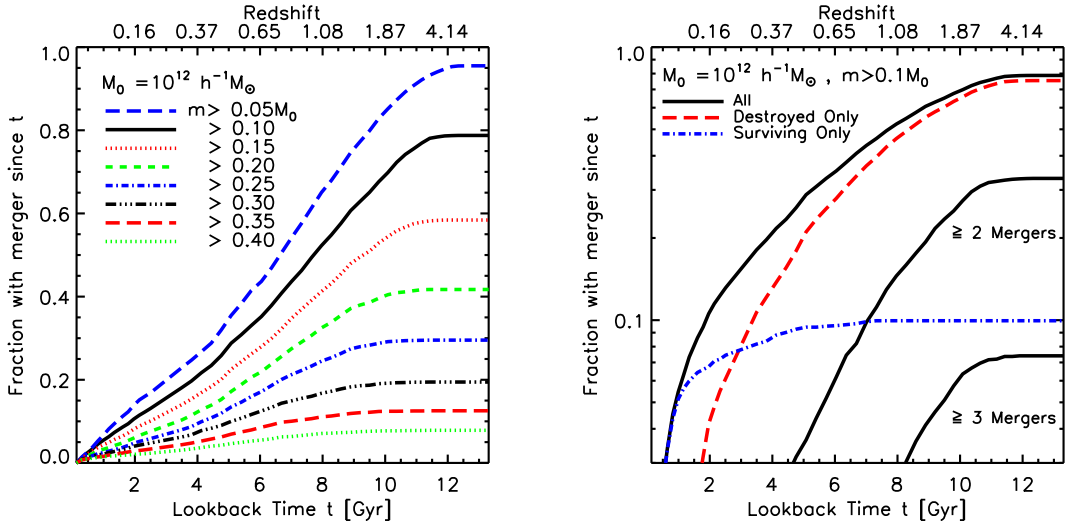

Figure 2.5: *Left:* The fraction of Milky Way-sized halos, $M_0 \simeq 10^{12}h^{-1}M_\odot$, that have experienced at least one merger larger than a given mass threshold, m, since lookback time t. *Right:* The three solid (black) lines show the fraction of $M_0 \simeq 10^{12}h^{-1}M_\odot$ halos that have experienced at least one, two, or three mergers larger than $m = 0.1M_0$ in a lookback time t. The upper solid line is the same as the solid line in the left panel. The dashed (red) line include only mergers that are "destroyed" before $z = 0$ (*i.e.* lose $> 80\%$ of their mass by $z = 0$). Conversely, the dot-dashed (blue) line shows the fraction of halos with at least one merger that "survives" as a subhalo as a function of lookback time to the surviving halo's merger. Large accretions of $m > 0.1M_0$ typically do not survive for more than ~ 3 Gyr after accretion.

objects, across all scaled masses m/M_0. As discussed in association with Equation 2.3 above, the overall normalization of the mass spectrum is slightly higher for our more massive halos. For example, the mass accreted in objects larger than $m = 0.01M_0$ is $\sim 45\%$ for $M_0 = 10^{12}$ halos and $\sim 50\%$ for $M_0 = 10^{13}$ halos. Both of these fractions are low compared to the $\sim 65\%$ expected from the semi-analytic EPS merger trees.

It is interesting to estimate the *total* mass fraction accreted in collapsed objects ($m >$

0) by extrapolating the $n(m)$ fit given in Equation 2.3 to $m \to 0$. We find

$$\begin{aligned} f(>0) &= \int_0^{0.5M_0} \frac{\mathrm{d}f}{\mathrm{d}m}\,\mathrm{d}m \\ &= \int_0^{0.5} A\,x^{1-\alpha}\,(0.5-x)^{\beta}\,\mathrm{d}x \\ &\simeq 0.24\,A. \end{aligned} \tag{2.4}$$

In the second step, β and α are the shape parameters in Equation 2.3. In the last step we have used our best fit parameters $\alpha = 0.61$ and $\beta = 2.3$. Using Equation 2.2 for $A(M_0)$, we find that the total accreted mass fraction (in virialized halos) increases from $f \simeq 0.50$ to 0.70 as M_0 varies from $10^{11.5}$ to $10^{13}h^{-1}M_\odot$. This suggests that a significant fraction ($\sim 30-50\%$) of dark halo mass is accreted in the form of "diffuse", unvirialized material, and that smaller halos have a higher fraction of their mass accreted in this diffuse form. Of course, our conclusion on "diffuse" accretion may be due, at least in part, to difficulties in precisely defining halo masses—and, in particular, in defining halo masses in dense environments where mergers are occurring rapidly. It is also possible that the accreted mass function steepens below our resolution limit, resulting in a lower diffuse fraction than we expect from our extrapolation, but there is no clear physical reason to expect such a steepening.

2.4.2 Merger Statistics

Understanding how galaxy mergers can affect galaxy transformations and morphological fractions necessarily requires an understanding of halo merger statistics. Of specific interest is the overall fraction of halos that have had mergers within a given look back time.

The left panel of Figure 2.5 shows the fraction of Milky Way-sized halos ($M_0 \sim 10^{12}h^{-1}M_\odot$) that have experienced *at least one* "large" merger within the last t Gyr. The different line types correspond to different absolute mass cuts on the accreted halo, from $m > 0.05\,M_0$ to $m > 0.4\,M_0$. The tendency for lines to flatten at large lookback times is a physical effect and *is not an artifact of limited resolution*. Specifically, the lines flatten at high z because the halo main progenitor masses, M_z, become smaller than the mass threshold on m (see Figure 2.2). We find that while less than $\sim 10\%$ of Milky Way-sized halos have *ever* experienced a merger with an object large enough to host a sizeable disk galaxy, ($m > 0.4\,M_0 \simeq 4\times10^{11}h^{-1}M_\odot$), an overwhelming majority ($\sim 95\%$) have accreted an object more massive than the Milky Way's disk ($m > 0.05M_0 \simeq 5\times10^{10}h^{-1}M_\odot$). Approximately 70% of halos have accreted an object larger than $m \simeq 10^{11}h^{-1}M_\odot$ in the last 10 Gyr.

While the left panel of Figure 2.5 illustrates the fraction of halos with at least one merger in a given time, the right panel of Figure 2.5 provides statistics for multiple mergers. We again focus on $M_0 \sim 10^{12}h^{-1}M_\odot$ halos, but restrict our statistics to accretions with $m > 0.1\,M_0 \simeq 10^{11}h^{-1}M_\odot$. The upper solid (black) line shows the fraction of halos with at least one accretion event within the last t Gyr. This reproduces the solid (black) line in the left-hand panel, but now the vertical scale is logarithmic. The middle and lower solid (black) lines in the right panel show the fraction of halos with at least two and at least three mergers larger than $0.1\,M_0$ in the past t Gyr, respectively. Roughly $\sim 30\%$ of Milky Way-sized halos have experienced at least two accretion events larger than $\sim 10^{11}h^{-1}M_\odot$. Multiple events of this kind could be important in forming elliptical galaxies (Hernquist, 1993; Boylan-Kolchin et al., 2005; Robertson et al., 2006b; Naab et al., 2006).

As discussed above, our merger events are defined at the time when the accreted halos first cross within the virial radius of the main progenitor. This definition allows us to

focus on a robust statistic that is less likely to be affected by baryonic components. In §2.5, we speculate on the implications of these results for disk stability. In this context, one may be concerned that some fraction of our identified "mergers" will never interact with the central disk region, but instead remain bound as surviving halo substructure. We expect this effect to be most important for smaller accretions, as larger merger events will decay very quickly.

The dashed (red) line in Figure 2.5 shows a statistic that is analogous to the upper black line — the fraction of halos that have had at least one merger in the last t Gyr — except we have now restricted the analysis to include only objects that are "destroyed" before $z = 0$. We define an object to be "destroyed" if it loses more than 80% of the mass it had at accretion because of interactions with the central halo potential. (Our results are unchanged if we use $70 - 90\%$ thresholds for mass loss). Likewise, the dot-dashed (blue) line shows the same statistic restricted to "surviving" objects. Only $\sim 10\%$ of Milky Way-sized halos have surviving massive substructures at $z = 0$ that are remnants of $m \simeq 10^{11} h^{-1} M_{\odot}$ accretion events. These survivors were typically accreted within the last ~ 3 Gyr.

We conclude that large accretions that happened more than ~ 3 Gyr ago would have had significant interactions with the central disk regions of the main progenitor. Indeed, this must be the case if the Milky Way is "typical". The most massive Milky Way satellite, the LMC, was likely accreted with a mass no larger than $m \sim 4 \times 10^{10} h^{-1} M_{\odot}$ (van der Marel et al., 2002; Robertson et al., 2005). According to Figure 2.3, we expect that the Milky Way has accreted at least ~ 3 objects that are larger than the LMC over its history. The expectation is that most of the larger objects that were accreted have been shredded by the central galaxy potential, and have deposited their stars in the extended stellar halo (Bullock & Johnston, 2005). Interestingly, a recent re-analysis of the LMC's motion suggests that it is indeed on

its first passage about the Milky Way (Besla et al., 2007), as we would expect for surviving, massive satellites.

Given that galaxy morphology fractions are observed to change systematically as a function of luminosity or mass scale (e.g. Park et al., 2007), we are also interested in exploring merger fractions as a function of M_0. The left panel of Figure 2.6 shows the fraction of halos that have had a merger larger than $m = 0.1\,M_0$ within the last $t = 2,\ 4,\ ...\ 12$ Gyr, as indicated by the t labels. The right panel shows the same statistic computed for larger $m > 0.3\,M_0$ accretion events. The most striking result is that the merger fraction is fairly independent of M_0. This suggests that halo merger statistics alone cannot explain the tendency for early-type spheroidal galaxies to reside in more massive halos. Baryon physics must instead play the primary role in setting this trend. (The right-panel in Figure 2.6 does show evidence that halos larger than $M_0 \sim 3 \times 10^{12} h^{-1} M_\odot$ have a higher fraction of recent ($t \lesssim 2$ Gyr) large ($m > 0.3 M_0$) events, but the overall merger fraction is small ($\lesssim 10\%$), even for group-sized halos with $M_0 \simeq 10^{13} h^{-1} M_\odot$.) When counting *instantaneous* merger rates there appears to be a relatively universal merger rate across a wide range of host masses $M_0 \sim 10^{12}$–10^{14} (Fakhouri & Ma, 2008). Given this uniformity, we speculate that the weak trend we see in Figure 2.6 may ultimately be a direct result of the trend for more massive halos to form later, as shown in Figure 2.2.

If a merger occurs early enough, we might expect the main progenitor halo to grow significantly after the merger. The fraction of mass accreted since the last merger is potentially important, as, for example, it could enable the regrowth of a destroyed disk. One could reason that the fraction of halos that experience a large merger and then subsequently fail to accrete a significant amount of mass is the most relevant statistic for evaluating the probability of disk formation. However, we find that in most cases, very little mass is accreted after an event that is large relative to M_0.

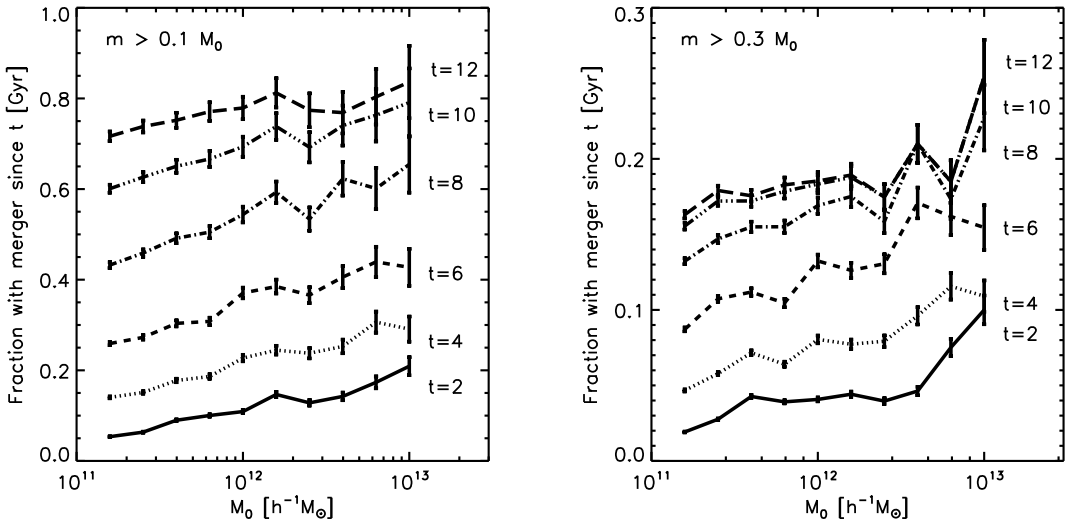

Figure 2.6: The fraction of halos of mass M_0 at $z = 0$ that have experienced a merger with an object more massive than $0.1M_0$ (left) and $0.3M_0$ (right) in the last t Gyr. Error bars are Poissonian based on the number of halos used in each mass bin. Note the fairly weak mass dependence.

Figure 2.7 shows the average *fraction* ($\Delta M/M_0$) of a halo's final mass M_0 that is accreted since the last large merger. Each curve corresponds to a different threshold in m. As in Figure 2.6, the overall trend with final mass M_0 is very weak. We define the accreted mass by $\Delta M = M_0 - M_{\rm m}$, where $M_{\rm m}$ is the mass of the host halo's main progenitor *after* the most recent large merger. The upper (solid, black) line includes all halos that have had at least one event larger than $m = 0.1\,M_0$ and the lowest line (long-dashed, red) includes all halos that have had at least one merger larger than $m = 0.35\,M_0$. This shows that the fractional mass accreted since a merger is a decreasing function of m/M_0. It also shows that the fraction is typically small, with $\Delta M/M_0 \lesssim 30\%$ (10%) for $m \gtrsim 0.1\,M_0$ ($0.3\,M_0$) mergers. These trends are a consequence of the fact that we are doing this calculation at a fixed M_0 — if a merger m is large compared to M_0, then there is little room in the mass budget for new material to be accreted after the merger. This implies, for example, that if a disk is destroyed as a result of a large-m/M_0 accretion event, it is unlikely that a new

"disk-dominated" system can be regrown from material that is accreted into the host halo after the merger. However, gaseous material involved in the merger may re-form a disk (see e.g. Zurek et al., 1988; Robertson et al., 2006b).

2.5 Discussion

2.5.1 Milky Way Comparison

The Milky Way has a dark matter halo of mass $M_0 \simeq 10^{12} h^{-1} M_\odot$ (Klypin et al., 2002), and its stellar mass is dominated by a thin disk of mass $\simeq 3.5 \times 10^{10} M_\odot$ (Klypin et al., 2002; Widrow & Dubinski, 2005). The thin disk has vertical scale height that is just $\sim 10\%$ of its radial scale length (Siegel et al., 2002; Jurić et. al, 2008; Newberg et al., 2006), and contains stars as old as ~ 10 Gyr (Nordström et al., 2004). Moreover, stars in the local thick disk are predominantly older than ~ 10 Gyr, and the bulge is old as well. This suggests that there was not significant merger activity in the Milky Way to drive gas towards the bulge or to thicken the disk in the past ~ 10 Gyr (Wyse, 2001).

Based on our results, a galaxy like the Milky Way would seem rare in a ΛCDM universe. Roughly 70% of dark matter halos of mass $M_0 \simeq 10^{12} h^{-1} M_\odot$ have experienced a merger with a halo of mass $10^{11} h^{-1} M_\odot$ in the past ~ 10 Gyr. A merger of this size should thicken the existing disk and drive gas into the center of the galaxy to create a bulge (Kazantzidis et al., 2008). If the Milky Way has *not* experienced a merger of this magnitude, that would make our galaxy a rare occurrence ($\lesssim 30\%$ of halos). On the other hand, if the Milky Way *has* experienced such a merger, it is difficult to understand its observed late-type morphology and thin-disk properties.

2.5.2 Morphological Fractions and Thick Disks

The degree to which the Milky Way halo is typical for its mass is becoming better understood thanks to the advent of large, homogeneous astronomical sky surveys. As mentioned in the introduction, broad-brush categorizations of "late type" vs. "early type" suggest that $\sim$ 70% of Milky Way-sized halos host late-type galaxies (e.g. Weinmann et al., 2006; van den Bosch et al., 2007; Ilbert et al., 2006; Choi et al., 2007; Park et al., 2007). The degree to which "late-type" is synonymous with "thin disk-dominated" is difficult to quantify with current data sets, but for the sake of this discussion, we will assume that this is the case. Also discussed earlier were the results of Kautsch et al. (2006), who found that $\sim 16\%$ of disk galaxies are bulgeless systems. This suggests that $\sim (0.7)(0.16) \sim 11\%$ of Milky Way-sized halos host pure disk galaxies.

The observed morphological fractions may be compared to the halo merger fractions presented in Figure 2.5. These results show that an overwhelming majority of Milky Way-sized halos ($\sim$ 95%) experience at least one merger larger than the *current* mass of the Milky Way disk ($\gtrsim 5 \times 10^{10} h^{-1} M_{\odot}$). Figure 2.3 shows that a typical $M_0 \simeq 10^{12} h^{-1} M_{\odot}$ halo has merged with $\sim 2-3$ objects of this size over its history. It is possible that mergers of this characteristic mass are responsible for creating thick disk components in most galaxies (Walker et al., 1996; Dalcanton & Bernstein, 2002). More detailed simulations will be required to test whether disks are destroyed or overly thickened by the predicted infall of $m \sim 5 \times 10^{10} h^{-1} M_{\odot}$ objects, and whether these thickening events happen too late to explain thick disks as old as those observed (Dalcanton & Bernstein, 2002). Understanding how bulgeless galaxies could exist in halos with mergers of this kind is a more difficult puzzle.

Perhaps more disturbing for the survival of thin disks are the statistics of more sub-

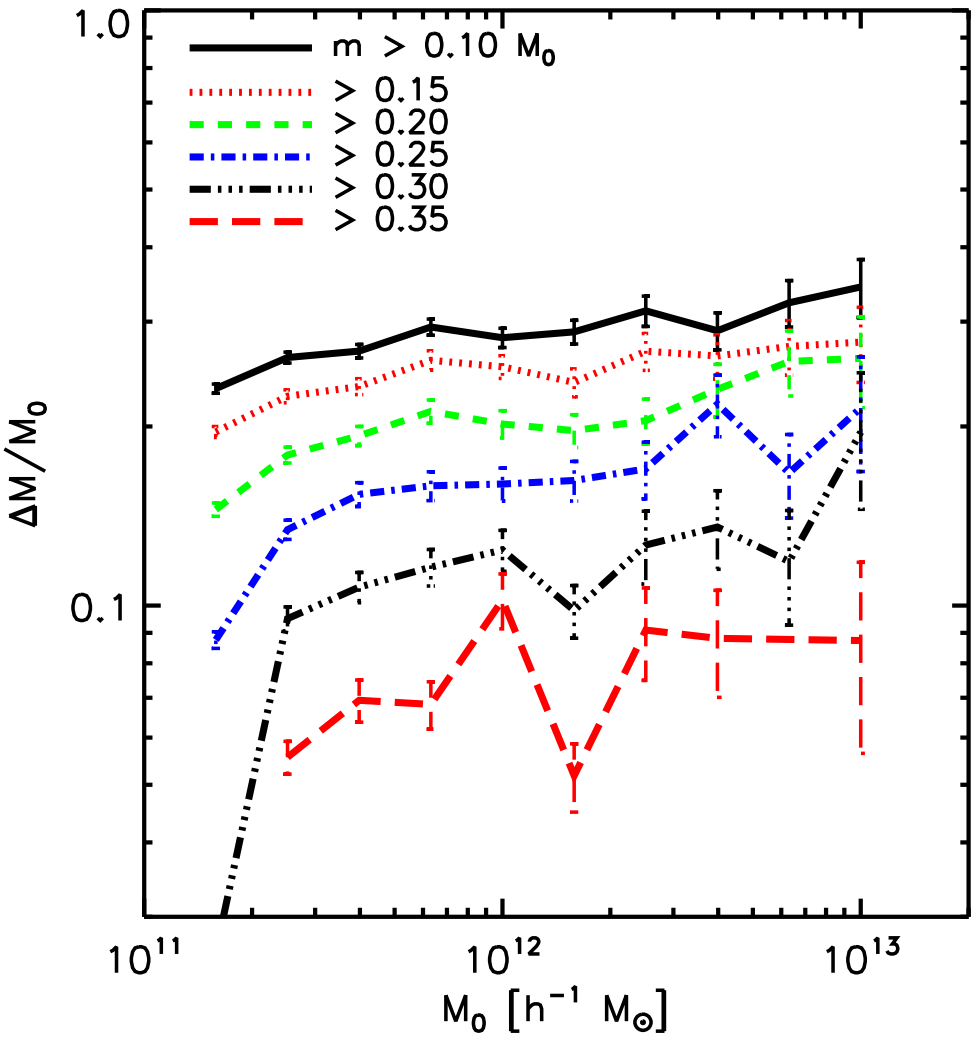

Figure 2.7: The average fractional change in a halo's main progenitor mass $\Delta M/M_0$ since its last large merger, shown as a function of the halo's $z = 0$ mass M_0. Each line includes only halos that have had a merger larger than the m value indicated (*i.e.* only halos that have had a $m > 0.35M_0$ accretion event are included in the lowest line). Error bars shown are Poisson on the number of halos used in the average.

stantial merger events. Figure 2.5 shows that $m \gtrsim 10^{11}h^{-1}M_\odot$ accretions are quite common in Milky Way-sized halos, with $\sim 70\%$ of $M_0 \simeq 10^{12}h^{-1}M_\odot$ objects experiencing such a merger in the past ~ 10 Gyr. Of course, the impact that these events will have on a central disk will depend on orbital properties, gas fractions, and star formation in the merging systems. Generally, however, a merger with an object ~ 4

times as massive as the Milky Way thin disk would seem problematic for its survival.

We find that a small fraction of a halo's final mass is typically accreted into the main progenitor subsequent to $m \sim 0.1M_0$ mergers — this suggests that the regrowth of a dominant disk from material accreted *after* such a merger will be difficult (see Figure 2.7). We conclude that if $\sim$ 70% of Milky Way-sized halos contain disk-dominated galaxies, and if the adopted ΛCDM cosmology is the correct one, then mergers involving $m \simeq 10^{11}h^{-1}M_{\odot}$ objects must not result in the destruction of galaxy disks. This is a fairly conservative conclusion because if we naively match the percentages of mergers with an early-type fraction of $\sim 30\%$, then Figure 2.5 suggest that the critical mass scale for disk survival is significantly larger, $m \gtrsim 2\times10^{11}h^{-1}M_{\odot}$. Specifically, mergers involving objects that are ~ 5 times the current Milky Way disk mass must not (always) destroy disks.

We remind the reader that the lookback times depicted in Figures 2.5 and 2.6 correspond specifically to the times when infalling halos first fall within the main progenitor's virial radius. Our estimates suggest that the corresponding central impacts should occur $\sim$3 Gyr later for the mass ratios we consider. Therefore, when we quote merger fractions to a lookback time of $\sim$10 Gyr, this will correspond to an actual impact $\sim$7 Gyr ago. Of course, the infalling systems will also lose mass as they fall towards the central galaxy. As we have emphasized, the detailed evolution of merging objects can only be determined with focused simulations, and the outcome of the subsequent mergers will depend on the baryonic components and orbital properties of the systems involved.

Kazantzidis et al. (2008) have performed a focused N-body simulation in order to investigate the morphological response of a thin, Milky Way type stellar disk galaxy to a series of impacts with 6 satellite halos [3] of mass $m \simeq (1-2)\times10^{10}M_{\odot}$ ($\sim 30-60\%$

[3]We note that their 6 accretions were chosen from a high-resolution N-body simulation, and that

of the disk mass). They find that a dominant "thin" stellar disk component survives the bombardment, although its scale-height was seen to increase from 250 pc to ~ 400 pc, and a second ~ 1.5 kpc "thick" component was also created. In addition, a new central bar / bulge component was also generated in these fairly small encounters. While it is encouraging to see that a thin disk can survive some bombardment, mergers with objects ~ 6 times as massive as those considered by Kazantzidis et al. should be very common in Milky Way-sized halos. It remains to be seen how the infall of $m \simeq 10^{11} h^{-1} M_{\odot}$ objects will affect the morphologies of thin, $\sim 4 \times 10^{10} M_{\odot}$ stellar disks. Moreover, the merger history considered by Kazantzidis et al. extended to fairly recent events. While there was no explicit star formation prescription in these simulations, one would expect a broad range of stellar ages in the thickened disk stars in this case, instead of a predominantly old population—as seems to be observed in actual galaxies.

2.5.3 Morphology–Luminosity Trends

Another well-established observational trend is the morphology–luminosity relation (recently, Choi et al., 2007; Park et al., 2007), which, when interpreted in terms of a morphology–halo mass relation, demonstrates that the fraction of late-type galaxies contained within dark matter halos is anti-correlated with the mass of the halo (Weinmann et al., 2006). For large galaxy halos, $M_0 \simeq 10^{13} h^{-1} M_{\odot}$, the late-type fraction is just $\sim 30\%$, compared to $\sim 70\%$ for Milky Way-sized systems (Weinmann et al., 2006; van den Bosch et al., 2007; Ilbert et al., 2006; Choi et al., 2007; Park et al., 2007). The result presented in Figure 2.6 is perhaps surprising in light of this fact. Specifically, merger histories of galaxy halos are almost self-similar in M_0 when

this number of events is fairly typical of what we find based on ~ 2500 Milky Way-sized halos in Figure 2.4. However, it is also typical of a Milky Way-size halo to experience $1 - 2$ mergers more massive than any of these accretions.

the infalling mass m is selected to be a fixed fraction of M_0. For example, $\sim 18\%$ (70%) of $M_0 \simeq 10^{12}h^{-1}M_\odot$ halos have experienced an $m > 0.3M_0$ ($0.1M_0$) merger event in the last 10 Gyr. This fraction grows only marginally to $\sim 25\%$ (80%) for $M_0 \simeq 10^{13}h^{-1}M_\odot$ halos. The implication is that dark matter halo merger histories alone cannot explain the observed correlation between early-type fraction and halo mass. Specifically, baryon physics must play the primary role in setting the observed trend between galaxy morphology and halo mass.

2.5.4 Successive Minor Mergers

Recently, Bournaud et al. (2007) have used focused simulations to investigate the response of a very massive $\sim 2 \times 10^{11}M_\odot$ disk-dominated galaxy within a $\sim 10^{12}M_\odot$ halo to mergers with total mass *ratios* ranging from $m/M_z = 0.02$ to 1.0. Broadly speaking, they find that $m/M_z = 0.1$ merger ratio events can transform their disk galaxy to an S0, and that $m/M_z = 0.3$ ratio events produce ellipticals. It is unclear how these ratios would change for a smaller primary disk mass, considering that their disk mass is extremely massive for a halo of this size. In comparison, $\sim 95\%$ of our Milky Way-sized halos experience an event with a merger ratio of $m/M_z > 0.1$ (corresponding to $m \gtrsim 0.05\,M_0$, see Appendix) in the last 10 Gyr. Similarly, $\sim 60\%$ of our halos experience $m/M_z > 0.3$ events (See Figure 2.8). We note that the results of this type of simulation will be sensitive to the gas fractions and ISM model of the interacting galaxies (Robertson et al., 2006b).

Hayashi & Chiba (2006) have also investigated the response of a galactic disk to a succession of minor mergers of CDM subhalos. They find that subhalos more massive than 15% of the disk mass must not merge into the thin disk itself, or it will become thicker than the observed disk of the Milky Way. While our merger rates

are for subhalos entering the virial radius of the *halo*, not when it penetrates the disk, we expect the fraction of disk mergers involving objects of mass $6 \times 10^9 M_{odot}$ to be quite high. Recall that 95% of halos experience an accretion event larger than $5 \times 10^{10} M_{odot}$. Even if these halos lose 90% of their mass before disk impact (which seems unlikely) they still meet the Hayashi and Chiba criterion. Note, however, that a detailed thin/thick decomposition may be required in order to fully evaluate this limit (Kazantzidis et al., 2008). A more detailed study of large mergers, including the necessary baryon physics, is required to fully explore this issue.

2.5.5 Gas-rich Mergers

Many of our results provide qualitative support to the idea that cool gas-fractions play a fundamental role in governing the morphological outcome of large mergers (Robertson et al., 2006b; Brook et al., 2007a,b; Cox et al., 2008), with gas-rich mergers essential to the formation and survival of disk galaxies. While dark halo merger histories are approximately self-similar in M_0, gas fractions are known to decrease systematically with halo mass (at least at $z = 0$, see e.g. Geha et al., 2006; Kaufmann et al., 2007b, and references therein). This implies that gas-rich mergers should be more common in small halos than in large halos. If gas-rich mergers do allow for the formation or survival of disk galaxies, then the gas-fraction-mass trend may provide an important ingredient in explaining the observed morphology–mass trend. Specifically, small halos should experience more gas-rich mergers, while large halos should experience more gas-poor mergers. However, stars resulting from a gas-rich merger will be younger than the lookback time of the merger, suggesting that mergers of this type only serve as an adequate explanation for early mergers. Also, these gas-rich mergers would require sufficient angular momentum to keep the resulting disk from being too centrally concentrated.

2.5.6 Comparison to Previous Work

Semi-analytic models (e.g. Diaferio et al., 2001; Okamoto & Nagashima, 2001) and models based on cosmological SPH simulations (Maller et al., 2006) have demonstrated that many of the observed trends between galaxy morphology, density, and luminosity can be explained in ΛCDM-based models. However, these results rely on the ability to *choose* a characteristic galaxy mass ratio for morphological transformation $r_{\rm char}$ (usually $r_{\rm char} \sim 0.3$). The assumption is that that galaxy-galaxy mergers with $m_{\rm gal}/M_{\rm gal} \lesssim r_{\rm char}$ allow a disk to remain intact, while all larger mergers produce spheroids. In a recent investigation, Koda et al. (2009) have explored a two-parameter model, where stellar spheroid formation depends on both m/M_z and the absolute halo mass, M_z. Host halos with masses smaller than a critical M_z are assumed to have very low baryon content in this picture. Using the PINOCCHIO density-field algorithm (Monaco et al., 2002) to generate halo merger statistics, Koda et al. (2009) find that the fraction of disk-dominated galaxies can be explained if the only events that lead to central spheroid formation have $m/M_z > 0.3$ and $M_z \gtrsim 4 \times 10^{10} h^{-1} M_\odot$.

The goal of this work has not been to find a ratio that can explain morphological fractions. Rather, our aim has been to emphasize the relatively large number of more minor mergers that could potentially be ruinous to disk survival. As discussed in the Appendix, events with $m \simeq 0.1 M_0$ in galaxy halos typically have $m/M_z \simeq 0.2$ at the time of accretion. These $\sim 10^{11} h^{-1} M_\odot$ mergers would produce no morphological response in the primary disk under many standard treatments (e.g. Maller et al., 2006; Koda et al., 2009). For the sake of comparison, Figure 2.8 in the Appendix shows galaxy halo merger statistics for fixed m/M_z cuts. Our results are in good agreement with those derived by (Koda et al., 2009, Figure 4;) using the PINOCCHIO algorithm, and with those quoted by Wyse (2006) for an analysis made by L. Hebb using the GIF simulations.

Finally, we mention that Cole et al. (2008b) have used the large Millennium Simulation to investigate the progenitor mass functions of halos. In qualitative agreement with our findings, Cole et al. (2008b) find that the fraction of mass coming from halo progenitors is lower than expected from standard EPS treatments. Their approach was somewhat different than ours, as they focused on the full progenitor mass function, as opposed to the mass function of objects that merged into the main progenitor as we have here. They estimate that $\sim 14\%$ of a halo's progenitors are not accounted for in collapsed objects at any redshift. This may be compared to our estimate of $\sim 30 - 50\%$ for the fraction of mass not directly accreted in the form of virialized objects for $M_0 = 10^{13}$ to $10^{12} h^{-1} M_\odot$ halos. The differences between our numbers and theirs may come from the fact that we have actually measured slightly different quantities. We also used different halo-finding algorithms and halo mass definitions, and utilized different formulations to extrapolate the simulation results to unresolved masses (a peak heights formulation in their case, and a direct mass function formulation in our case). A more thorough investigation of the differences associated with halo-finding algorithms and mass definitions is reserved for future work. For the purposes of this work, it is useful to point out that while a direct comparison is difficult to make at this time, if anything, our results on overall merger counts seem *low* compared to the results given Cole et al. (2008b).

2.6 Conclusion

We have used a high-resolution ΛCDM N-body simulation to investigate the merger histories of $\sim 17,000$ galaxy dark matter halos with masses $M_0 = 10^{11-13} h^{-1} M_\odot$ at $z = 0$. Mergers with objects as small as $m = 10^{10} h^{-1} M_\odot$ were tracked. The principle goal has been to present the raw statistics necessary for tackling the issue

of thin disk survival in ΛCDM and for providing a cosmological context for more focused simulations aimed at understanding the role of mergers for processes like morphological transformation, star formation triggering, and AGN fueling.

Our main results may be summarized as follows:

1. Mass accretion into halos of mass M_0 at $z = 0$ is dominated by mergers with objects of mass $m \simeq (0.03 - 0.3)M_0$ (Figure 2.4). Typically, $\sim 1 - 4$ mergers of this size occur over a halo's history (Figure 2.3). Because these mergers tend to occur when the main progenitor's mass, M_z, was somewhat smaller than M_0, these dominant events have fairly large *merger ratios*, $m/M_z \simeq 0.1 - 0.6$ (see Appendix).

2. The mass accretion function, $n(m)$, of mergers larger than m accreted over a halo's history is well-described, on average, by a simple analytic form, $n(x \equiv m/M_0) = A\,x^{-\alpha}\,(0.5 - x)^{\beta}$, with $\alpha = 0.61$ and $\beta = 2.3$. The normalization increases as a function of the halo's mass at $z = 0$, M_0, as $A \simeq 0.47 \log_{10}(M_0) - 3.2$. By extrapolating this fit, we find that the total mass fraction accreted in objects of any mass ($m > 0$) does not asymptote to 1.0, but rather increases with M_0 from $\sim 50\%$ in $M_0 = 10^{11.5} h^{-1} M_\odot$ halos to $\sim 70\%$ in $M_0 = 10^{13} h^{-1} M_\odot$ halos. This suggests that a non-zero fraction of a halos mass may be accreted as truly "diffuse" material.

3. An overwhelming majority (95%) of Milky Way-sized halos with $M_0 \simeq 10^{12} h^{-1} M_\odot$ have accreted an object larger than the Milky Way's disk ($m \gtrsim 5 \times 10^{10} h^{-1} M_\odot$) in the last 10 Gyr. Approximately 70% have had accretions with $m > 10^{11} h^{-1} M_\odot$ objects over the same period, and 40% have had $m > 2 \times 10^{11} h^{-1} M_\odot$ events (Figure 2.5).

4. Halo merger histories are approximately self-similar in m/M_0 for halos with

masses in the range $M_0 = 10^{11} - 10^{13} h^{-1} M_\odot$ (Figure 2.6). This suggests that the empirical trend for late-type galaxies to be more common in smaller halos is not governed by differences in merger histories, but rather is associated with baryon physics.

5. Typically, a small fraction, $\sim 20 - 30\%$, of a halo's final mass M_0 is accreted *after* the most recent large merger with $m > (0.1 - 0.2)\, M_0$ objects (Figure 2.7). This suggests that the "regrowth" of a disk from newly accreted material after a large merger is unlikely. Note that this does not rule out the possibility that a disk reforms from gaseous material involved in the merger itself.

The relatively high fraction of halos with large $m \sim 0.1 M_0$ merger events raises concerns about the survival of thin disk galaxies within the current paradigm for galaxy formation in a ΛCDM universe. If we naively match percentages using Figure 2.5, we find that in order to achieve a $\sim 70\%$ disk-dominated fraction in $M_0 = 10^{12} h^{-1} M_\odot$ halos, then $m \simeq 0.2\, M_0 \simeq 2 \times 10^{11} h^{-1} M_\odot \simeq 3 \times 10^{11} M_\odot$ objects must not (always) destroy disks. Furthermore, since stars in the local thick disk and bulge are predominantly older than ~ 10 Gyr, this suggests that these mergers in the past ~ 10 Gyr must not drive gas towards the bulge or significantly thicken the disk. Note that the total mass in such an accreted object is ~ 10 times that of the Milky Way disk itself. Moreover halos typically do not accrete a significant fraction of their final mass after these mergers ($\sim 20\%$ on average). Finally, as noted in the Appendix, $m \sim 0.2\, M_0$ events typically have merger *ratios* of $m/M_z \simeq 0.4$ at the time of the merger. These numbers do not seem encouraging for disk survival, and may point to a serious problem with our current understanding of galaxy formation in a ΛCDM universe.

Our basic conclusion is unlikely to be sensitive to uncertain cosmological parameters. Note that the simulations considered here have a fairly high $\sigma_8 = 0.9$. At a fixed Ω_m,

a lower σ_8 will systematically produce slightly *more* recent merger events (e.g. Zentner & Bullock, 2003). However, given that the merger fractions measured using m/M_0 are approximately self-similar in M_0 (and therefore in $M_0/M_\star$), we expect that the overall merger fractions will be fairly insensitive to power-spectrum normalization.

As discussed in the introduction, a complete investigation into the issue of disk survival will require an understanding of the orbital evolution of objects once they have fallen within the main progenitor halo's virial radius and on the subsequent impact of interacting galaxies. Both of these outcomes will depend sensitively on the baryonic components in the main halo and in the smaller merging object. For this reason, the present work has focused on *halo mergers*, defined to occur when an infalling halo first crosses within the virial radius of the main progenitor halo. The merger statistics presented here are relatively devoid of uncertainties and can be used as a starting point for direct simulations of galaxy-galaxy encounters. Simulations of this kind will be essential to fully address the broader implications of these frequent, large mergers, which seem to pose a serious challenge to disk survival.

2.7 Corollary: Merger Mass Ratio Statistics

The bulk of the chapter focused on statistics of halo mergers at a fixed absolute mass threshold m on the merging objects. In this section we present statistics for m/M_z — the merger ratio relative to the main progenitor mass M_z at the redshift z prior to accretion. By definition, $M_z \leq M_0$, causing merger statistics to show larger accretions when presented in terms of m/M_z. For example, the merger ratio equivalent to Figure 2.3 (bottom panel) fits to $f(> x) = Ax^{-\alpha}(1-x)^{\beta}$ instead of Equation 2.3 (to better than 10% across mass range $10^{11.5} - 10^{13.5} M_\odot$), with parameters $A(M_0) \simeq 0.05 \log_{10}(M_0) - 0.2$, $\alpha = 0.04$, and $\beta = 2.0$, and M_0 in units of $M_\odot$. The m/M_z

equivalent for $n(>x)$ also fits to this equation (to better than 10% in the mass range $10^{12.0} - 10^{13.5} M_\odot$) with parameters $\alpha \simeq 0.4$, $\beta \simeq 2.0$, and $A(M_0) \simeq 2.0 \log_{10}(M_0) - 21.5$. Given that our simulation output has a fixed physical mass resolution, $m_{\rm res} = 10^{10} M_\odot$, and that halo main progenitor masses, M_z, vary as a function redshift, the completeness in m/M_z will, in principle, vary from halo to halo as a function of each particular mass accretion track and lookback time. We have accounted for this variable completeness limit in an average sense in what follows.

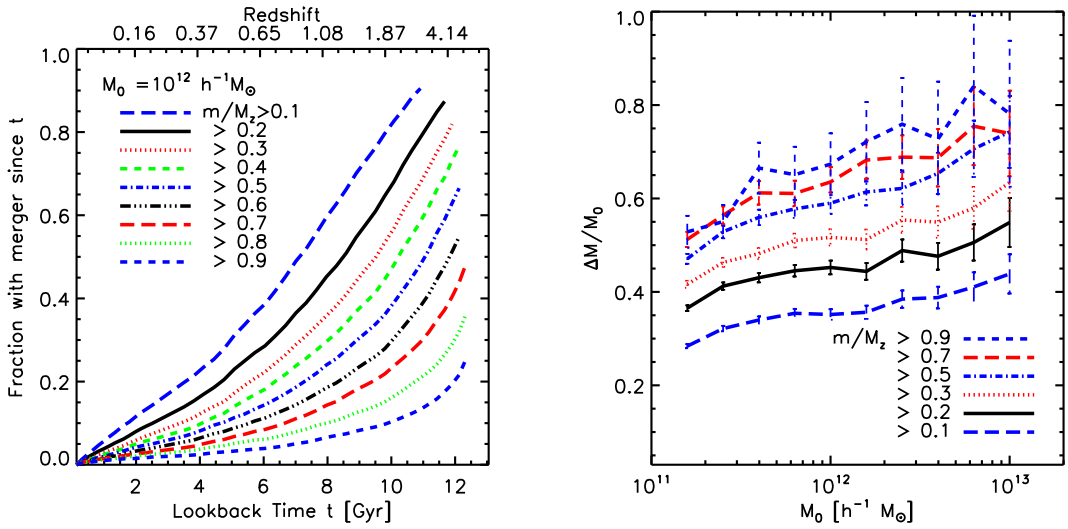

Figure 2.8: *Left:* The fraction of Milky Way-sized halos, $M_0 \simeq 10^{12} h^{-1} M_\odot$, that have experienced at least one merger larger than a given *ratio* m/M_z since lookback time t, where M_z is the main progenitor mass *at the time of accretion*. Lines are truncated at epochs where the mass resolution of the simulation limits our ability to resolve a given m/M_z ratio (*i.e.* when M_z gets so small that a quoted m/M_z ratio falls below the resolution with $m > 10^{10} h^{-1} M_\odot$). *Right:* The average change in mass $\Delta M/M_0$ that a halo experiences since its last major merger. Different lines show different "major merger" ratios, m/M_z, where the ratio is defined relative to the main progenitor mass *at the time of accretion*. Error bars show Poissonian $\sqrt{N}$ errors on the number of host halos averaged.

The *left* panel of Figure 2.8 shows the fraction of $M_0 = 10^{12} M_\odot$ halos that have experienced *at least one* merger larger than a given threshold ratio ($r_t = 0.1$, 0.2, ... 0.9) in m/M_z in the last t Gyr. This result may be compared to Figure 2.5, which shows the analogous fraction computed using fixed absolute m cuts relative

to M_0. In order to provide results that are robust to our completeness limit in m, for each threshold cut, r_t, the lines are truncated at the lookback time when the *average* $M_0 = 10^{12} M_\odot$ halo's mass falls below $M_z = m_{\rm res}/r_t$. We see that $\sim 50\%$ of halos have had a $m/M_z > 0.4$ event in the last ~ 10 Gyr, and that $\sim 10\%$ have experienced nearly equal-mass mergers, $m/M_z > 0.9$, in this time. These results are in good agreement with similar results quoted by Wyse (2006) for an analysis made by L. Hebb using the GIF simulations.

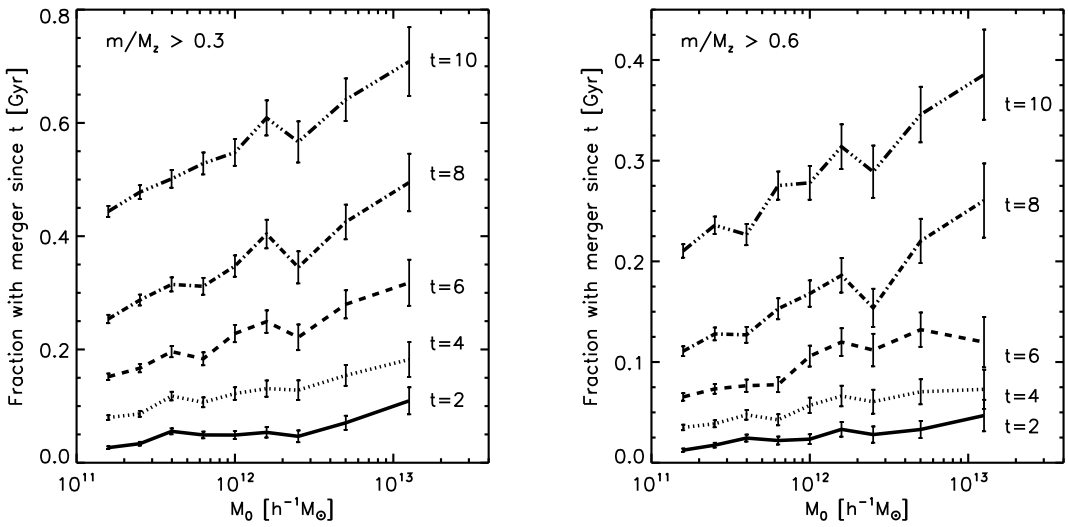

Figure 2.9: *Left:* The fraction of halos of mass M_0 at $z = 0$ that have experienced a merger ratio larger than $m/M_z = 0.3$ in the last t Gyr. The ratio is defined relative to the main progenitor mass at the time prior to accretion M_z. Error bars are Poissonian based on the number of halos used in each mass bin. Note the strong mass trend, in contrast to the results presented in Figure 2.6, where mergers were defined on a strict mass threshold, rather than merger ratio. *Right:* The fraction of halos of mass M_0 at $z = 0$ that have experienced a merger ratio larger than $m/M_z = 0.6$ in the last t Gyr. The ratio is defined relative to the main progenitor mass at the time prior to accretion M_z. Error bars are Poissonian based on the number of halos used in each mass bin. Note the strong mass trend, in contrast to the results presented in Figure 2.6, where mergers were defined on a strict mass threshold, rather than merger ratio.

The right panel of Figure 2.8 shows that, typically, the largest m/M_z events occur *before* most of the final halo mass M_0 is accreted. Specifically we show the fraction of mass $\Delta M/M_0$ accreted since the last major merger. Results for different major

merger ratio thresholds are shown as different line types. Each line presents the *average* $\Delta M/M_0$ at fixed M_0 and we only include halos that have actually had a merger of a given ratio (within the last ~ 11 Gyr) in this figure. Among halos that have had nearly equal-mass merger events, $m/M_z \gtrsim 0.9$, the fraction of mass that is accreted since that time is significant, with $\Delta M/M_0 \sim 70\%$ for $M_0 = 10^{12} M_\odot$ halos. If we associate post-merger accretion with the potential "regrowth" of a galactic disk, then, by comparison with Figure 2.7, high merger-ratio events are less of a concern for disk formation than high m/M_0 ratio events. Unlike most high m/M_z events, mergers that are large relative to M_0 typically have very little ($\lesssim 20\%$) fractional mass accretion after the merger.

The *left panel* of Figure 2.9 shows the fraction of halos that have had a merger larger than $m/M_z = 0.3$ within the last $t = 2$, 4, ... 10 Gyr, as a function of halo mass M_0. The *right panel* shows the same statistic computed for larger $m/M_z > 0.6$ mergers. Unlike the result shown in Figure 2.6, there is a fairly significant mass trend, with more massive halos more likely to have experienced a major merger at a fixed lookback time. Note, however, that most of these "major mergers" involve relatively small objects in an absolute sense. Much of this trend is driven by the fact that M_z falls off more rapidly with z for high M_0 halos compared to low M_0 halos.

The previous discussions lead to explore the relationship between an accreted halo's absolute mass m and the mass-ratio it had when it was accreted, m/M_z. The two panels of Figure 2.10 illustrate this relationship for objects accreted into $M_0 = 10^{12} M_\odot$ halos. The thick, solid line in the *left* panel shows the median merger ratio, m/M_z, that a halo of mass m/M_0 has when it was accreted. Specifically, we plot m/M_z *given* m/M_0 in this diagram. We see that typically $m/M_z \simeq 2\, m/M_0$, as shown by the dashed line in the figure. The dotted lines show the 68 % spread in the distribution of m/M_z given m/M_0. The opposite relationship is shown in the *right* panel of Figure

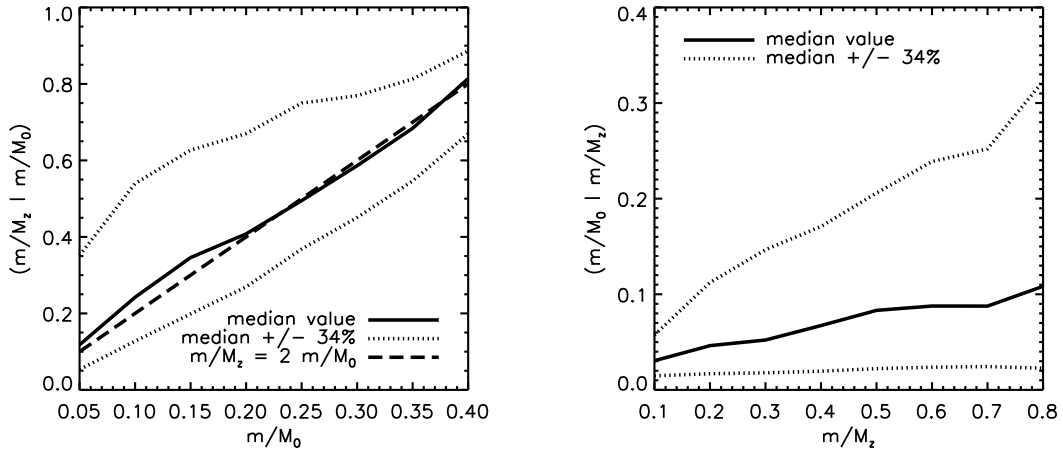

Figure 2.10: *Left:* An illustration of $P(m/M_z|m, M_0)$ — the distribution of merger ratio m/M_z *at the time of accretion* given a value of m for $M_0 = 10^{12}h^{-1}M_\odot$ halos. We plot m/M_z vs. m/M_0 for clarity. The solid line shows the median and the dotted lines show the 68% spread. *Right:* An illustration of $P(m/M_0|m/M_z)$ — the distribution of merging masses m *given* a merger ratio m/M_z. We see that the majority of high m/M_z events occur with M_z is small compared to the final halo mass M_0. Therefore most high-mass ratio mergers are small m mergers in an absolute sense.

2.10. Here, the thick, solid line shows the median m/M_0 value *given* a merger of mass ratio m/M_z. We see that the majority of high-ratio events involve objects that are small compared to the final halo mass M_0. Note that this result, and the associated distributions, are complete only to mergers that occur within the past ~ 11 Gyr. If we were able to track main progenitor masses M_z back to arbitrarily early times, we would expect a very larger number of high m/M_z events with small absolute m/M_0 values.

2.8 Acknowledgements

The contents of this chapter were previously published by Stewart, Bullock, Wechsler, Maller and Zentner (2008) in The Astrophysics Journal, August 2008 (v683, p597). The simulation used in this chapter was run on the Columbia machine at NASA

Ames. We would like to thank Anatoly Klypin for running the simulation and making it available to us. We are also indebted to Brandon Allgood for providing the merger trees. We thank Chris Brook, T. J. Cox, Fabio Governato, Christian Maulbetsch, Brant Robertson, Matias Steinmetz, Jerry Sellwood, and Rosemary Wyse for helpful comments on this work, and Onsi Fakhouri and Chung-Pei Ma for useful discussions about halo merger rates.

Chapter 3

Mergers in LCDM: Mass, Redshift, and Mass-Ratio Dependence

3.1 Chapter Abstract

We employ a high-resolution LCDM N-body simulation to present merger rate predictions for dark matter halos and investigate how common merger-related observables for galaxies—such as close pair counts, starburst counts, and the morphologically disturbed fraction—likely scale with luminosity, stellar mass, merger mass ratio, and redshift from $z = 0$ to $z = 4$. We investigate both rate at which subhalos first enter the virial radius of a larger halo (the "infall rate"), and the rate at which subhalos become destroyed, losing 90% of the mass they had at infall (the "destruction rate"). For both merger rate definitions, we provide a simple 'universal' fitting formula that describes our derived merger rates for dark matter halos a function of dark halo mass, merger mass ratio, and redshift, and go on to predict galaxy merger rates using number density-matching to associate halos with galaxies. For example, we find that the

instantaneous (destruction) merger rate of $m/M > 0.3$ mass ratio events into typical $L \gtrsim f\, L_*$ galaxies follows the simple relation $dN/dt \simeq 0.03(1+f)\,\mathrm{Gyr}^{-1}\,(1+z)^{2.1}$. Despite the rapid increase in merger rate with redshift, only a small fraction of $> 0.4L_*$ high-redshift galaxies ($\sim 3\%$ at $z = 2$) should have experienced a major merger ($m/M > 0.3$) in the very recent past ($t < 100$ Myr). This suggests that short-lived, merger-induced bursts of star formation should not contribute significantly to the global star formation rate at early times, in agreement with several observational indications. In contrast, a fairly high fraction ($\sim 20\%$) of those $z = 2$ galaxies should have experienced a morphologically transformative merger within a virial dynamical time (~ 500 Myr at $z = 2$). We compare our results to observational merger rate estimates from both morphological indicators and pair-fraction based determinations between $z = 0 - 2$ and show that they are consistent with our predictions. However, we emphasize that great care must be made in these comparisons because the predicted observables depend very sensitively on galaxy luminosity, redshift, overall mass ratio, and uncertain relaxation timescales for merger remnants. We show that the *majority* of bright galaxies at $z = 3$ should have undergone a major merger (> 0.3) in the previous 700 Myr and conclude that mergers almost certainly play an important role in delivering baryons and influencing the kinematic properties of Lyman Break Galaxies (LBGs).

3.2 Introduction

In the current theory of hierarchical structure formation (LCDM), dark matter halos and the galaxies within them are assembled from the continuous accretion of smaller objects (Peebles, 1982; Blumenthal et al., 1984; Davis et al., 1985; Wechsler et al., 2002; Fakhouri & Ma, 2008; Stewart et al., 2008; Cole et al., 2008a; Neistein & Dekel,

2008; Wetzel et al., 2009). It is well-established that galaxy and halo mergers should be more common at high redshift (e.g. Governato et al., 1999; Carlberg et al., 2000; Gottlöber et al., 2001; Patton et al., 2002; Berrier et al., 2006; Lin et al., 2008; Wetzel et al., 2009), but the precise evolution is expected to depend on details of the mergers considered. Moreover, it is unclear how these mergers manifest themselves in the observed properties of high-z galaxies and what role they play in setting the properties of galaxies in the local universe. Interestingly, there are indications that the familiar bimodality of galaxies as disks versus spheroids at $z = 0$ might be replaced by a categorization of disk-like versus merger-like at higher redshift (Förster Schreiber et al., 2006; Genzel et al., 2006; Law et al., 2007a; Kriek et al., 2008; Melbourne et al., 2008; Shapiro et al., 2008; Wright et al., 2009), although this shift in the dichotomy of galaxy morphologies is by no means robust and requires further study. In this chapter, we use N-body simulations to provide robust predictions and simple fitting functions for dark matter halo merger rates and merger fractions as a function of redshift, mass, and mass ratio. We use our predictions to address two observable consequences of galaxy mergers—merger-driven starbursts and morphological disturbances—and investigate their evolution with redshift.

The tidal interactions inherent in galaxy mergers produce concentrations of gas in the remnant centers. For major mergers ($m/M \gtrsim 0.3$), models predict that this effect results in a significant burst of increased star formation rate (SFR) compared to the central galaxy's past star formation history (e.g. Mihos & Hernquist, 1996; Cox et al., 2008). It is also likely to enable supermassive black hole growth and the fueling of AGN (e.g., Heckman et al., 1986; Springel et al., 2005a; Somerville et al., 2008). Cox et al. (2008) used Smooth Particle Hydrodynamical (SPH) simulations to show that the timescale over which merger-induced starbursts are active depends sensitively on the treatment of poorly-understood feedback and ISM physics; they demonstrate that future observational constraints on this timescale may provide a

means to constrain feedback models (Barton et al., 2007, and references therein). Historically, SPH simulations have treated star forming gas as isothermal, and this treatment results in starburst timescales in major mergers that are quite short-lived, with $t_* \sim 100$ Myr (e.g. Mihos & Hernquist, 1996; Cox et al., 2008). Recently, it has become popular in SPH simulations to impose a stiff equation of state for star-forming gas in order to mimic the effects of a multi-phase ISM and to suppress star formation and disk fragmentation (Yepes et al., 1997; Springel & Hernquist, 2003; Governato et al., 2007). Cox et al. (2008) showed that a stiff equation of state of this kind significantly lengthens the timescale for starburst activity in major mergers to $t_* \sim 500$ Myr. Below we investigate the evolution of merger fractions with 100 Myr and 500 Myr as a first-order means of addressing the differences between merger-induced starburst fractions in different feedback schemes.

A second observationally-relevant consequence of mergers is morphological disturbance. Very large mergers, especially those with moderately low gas fractions, likely play a role in transforming late type disk galaxies into ellipticals (e.g., Toomre & Toomre, 1972; Barnes & Hernquist, 1996; Robertson et al., 2006a,b; Burkert et al., 2008). If gas fractions are high in major mergers (as expected at high redshift) then they may play a role in building early disks (Robertson et al., 2006a; Hopkins et al., 2009a, 2008; Robertson & Bullock, 2008). More common are moderate-size ($m/M > 0.1$) dark matter halo mergers (Stewart et al., 2008), which can produce morphological signatures like disk flaring, disk thickening, and ring and bar-like structures in disk galaxies (Barnes & Hernquist, 1996; Kazantzidis et al., 2008; Younger et al., 2007; Villalobos & Helmi, 2008; Purcell et al., 2009) as well as tidal features seen in massive elliptical galaxies (Feldmann et al., 2008).

Below we explore two possibilities for the evolution of the morphological relaxation time with redshift. First, we explore a case where the remnant relaxation time scales

with redshift, approximated by the dark matter halo dynamical time ($\tau \propto (1+z)^{-\alpha}$, $\alpha \simeq 1.1 - 1.5$; see below), and second we investigate the possibility that relaxation times remain constant with redshift at $\tau \simeq 500$ Myr. The latter timescale is motivated by the results of Lotz et al. (2008b) who studied outputs from SPH merger simulations of $z = 0$ galaxies in great detail (see Cox et al., 2006b; Jonsson et al., 2006; Rocha et al., 2008; Cox et al., 2008, for additional descriptions of these simulations and their analysis). These choices bracket reasonable expectations and allow us to provide first-order estimates for the evolution in the morphologically disturbed fraction with redshift. More simulation work is needed to determine how the relaxation times of galaxy mergers should evolve with redshift, including an allowance for the evolution in approach speeds, galaxy densities, and orbital parameters (if any).

Though not discussed in detail here, a third consequence of mergers is the direct, cumulative deposition of cold baryons (gas and stars) into galaxies. For this question, one is interested in the full merger history of individual objects, rather than the instantaneous merger rate or recent merger fraction. Specifically, one may ask about the total mass that has been deposited by major mergers over a galaxy's history. We focus on this issue in Chapter 4.

In what follows we use a high-resolution dissipationless cosmological LCDM N-body simulation to investigate the merger rates and integrated merger fractions of galaxy dark matter halos of mass $M = 10^{11} - 10^{13} M_{\odot}$ from redshift $z = 0$ to 4. We adopt the simple technique of monotonic abundance-matching in order to associate dark matter halos with galaxies of a given luminosity or stellar mass (e.g., Kravtsov et al., 2004; Conroy et al., 2006; Berrier et al., 2006; Conroy & Wechsler, 2009a), and make predictions for the evolution of the galaxy merger rate with redshift.

The outline of this chapter is as follows. In §3.3 we discuss the numerical simulation used and the method of merger tree construction, while we present merger statistics

for dark matter halos in §3.4. In §3.5 we discuss the method of assigning galaxies to dark matter halos both as a function of stellar mass, and alternatively as a function of galaxy luminosity (compared to $L_*(z)$). In §3.6 we present our principle results, which characterize the merger rate of galaxies as a function of redshift, with comparison to observed properties of bright galaxies. We summarize our main conclusions in §3.7.

3.3 Simulation

We use a simulation containing 512^3 particles, each with mass $m_p = 3.16 \times 10^8 M_\odot$, evolved within a comoving cubic volume of $80h^{-1}$ Mpc on a side using the Adaptive Refinement Tree (ART) N-body code (Kravtsov et al., 1997, 2004). The simulation uses a flat, ΛCDM cosmology with parameters $\Omega_M = 1 - \Omega_\Lambda = 0.3$, $h = 0.7$, and $\sigma_8 = 0.9$. The simulation root computational grid consists of 512^3 cells, which are adaptively refined to a maximum of eight levels, resulting in a peak spatial resolution of $1.2h^{-1}$ kpc (comoving). Here we give a brief overview of the simulation and methods used to construct the merger trees. They have been discussed elsewhere in greater detail (Allgood et al., 2006; Wechsler et al., 2006; Stewart et al., 2008), as well as Chapter 2, and we refer the reader to those papers for a more complete discussion.

Field dark matter halos and subhalos are identified using a variant of the bound density maxima algorithm (Klypin et al., 1999a). A *subhalo* is defined as a dark matter halo whose center is positioned within the virial radius of a more massive halo. Conversely, a *field halo* is a dark matter halo that does not lie within the virial radius of a larger halo. The virial radius R and mass M are defined such that the average mass density within R is equal to $\Delta_{\rm vir}$ ($\simeq 337$ at $z = 0$) times the mean density of the universe at that redshift. Our halo catalogs are complete to a minimum halo mass of $M = 10^{10} M_\odot$, and our halo sample includes, for example,

$\sim 15,000(10,000)$ and $2,000(500)$ field halos at $z = 0(3)$ in the mass bins 10^{11-12} and $10^{12-13} M_{\odot}$, respectively.

We use the same merger trees described in Chapter 2 (Stewart et al., 2008), constructed using the techniques described in Wechsler et al. (2002) and Wechsler et al. (2006). Our algorithm uses 48 stored timesteps that are approximately equally spaced in expansion factor between $a = (1 + z)^{-1} = 1.0$ and $a = 0.0443$. We use standard terminologies for progenitor and descendant. Any halo at any timestep may have any number of progenitors, but a halo may have a single descendant — defined to be the halo in the next timestep that contains the majority of this halo's mass. The term *main progenitor* is used to reference the most massive progenitor of a given halo, tracked back in time.

Throughout this work we present results in terms of the *merger ratio* of an infalling object, m/M, where we always define m as the mass of the smaller object just *prior* to the merger and M is the mass *main progenitor* of the larger object at the same epoch. Specifically, M in the ratio does not incorporate the mass m and therefore m/M has a maximum value of 1.0. Except when explicitly stated otherwise, we always use dark matter halo masses to define the merger ratio of any given merger event, and we always define the merger ratio as the mass ratio just before the smaller halo falls into the virial radius of the larger one. Because there is not a simple linear relation between halo mass and galaxy stellar (or baryonic) mass, this is an important distinction. For example, our major mergers, defined by halo mass ratios, may not always correspond to major galaxy mergers as defined by stellar or baryonic mass ratios (see e.g. Stewart, 2009). We will discuss this in more detail in Chapter 5.

In what follows we investigate two types of mergers. The first and most robust of our predicted rates is the *infall rate*: the rate at which infalling halos become subhalos, as they first fall within the virial radius of the main progenitor. These are the results we

present in §3.4, which describes our 'universal' merger rate function for dark matter halos. The second rate is aimed more closely at confronting observations and is associated with central mergers between galaxies themselves. Specifically we define the *destruction rate* by counting instances when each infalling subhalo loses 90% of the mass it had prior to entering the virial radius of the larger halo. [1] We are unable to measure central crossings directly because the time resolution in our snapshot outputs (typically $\Delta t \simeq 250$ Myr) is comparable to a galaxy-galaxy crossing time at the centers of halos, however, for mergers with mass ratios $> 1/3(1/10)$, subhalo destruction typically takes place $\sim 2(3)$ Gyr after infall to the virial radius. Based on simulations of galaxy mergers, this definition leads to subhalo "destruction" sometime after its first pericenter (and likely after second pericenter), but probably before final coalescence (Boylan-Kolchin et al., 2008). Note that this second rate (destruction) is more uncertain than the first (infall) because, in principle, the orbital evolution of infalling galaxies will depend upon the baryonic composition of both the primary and secondary objects. Fortunately, as presented in detail below (see Table 3.1) for the relatively high mass-ratio merger events we consider, the merger rates (and their evolution with redshift) do not depend strongly on whether we define a merger to occur at halo infall or at this central mass-loss epoch.

3.4 Dark Matter Halo Merger Rates

We begin by investigating infall and destruction merger rates as a function of mass, merger ratio, and redshift. Merger rates are shown for several of these choices in the four panels of Figure 3.1. The upper panels show merger rates per unit time for $> m/M$ mass ratio objects falling into host halos of mass 10^{12} (black lines and

[1] Subhalo masses are defined to be the mass within a truncation radius R_t, which is set to be the minimum of the virial radius and the radius where the subhalo density profile begins to encounter the background halo density.

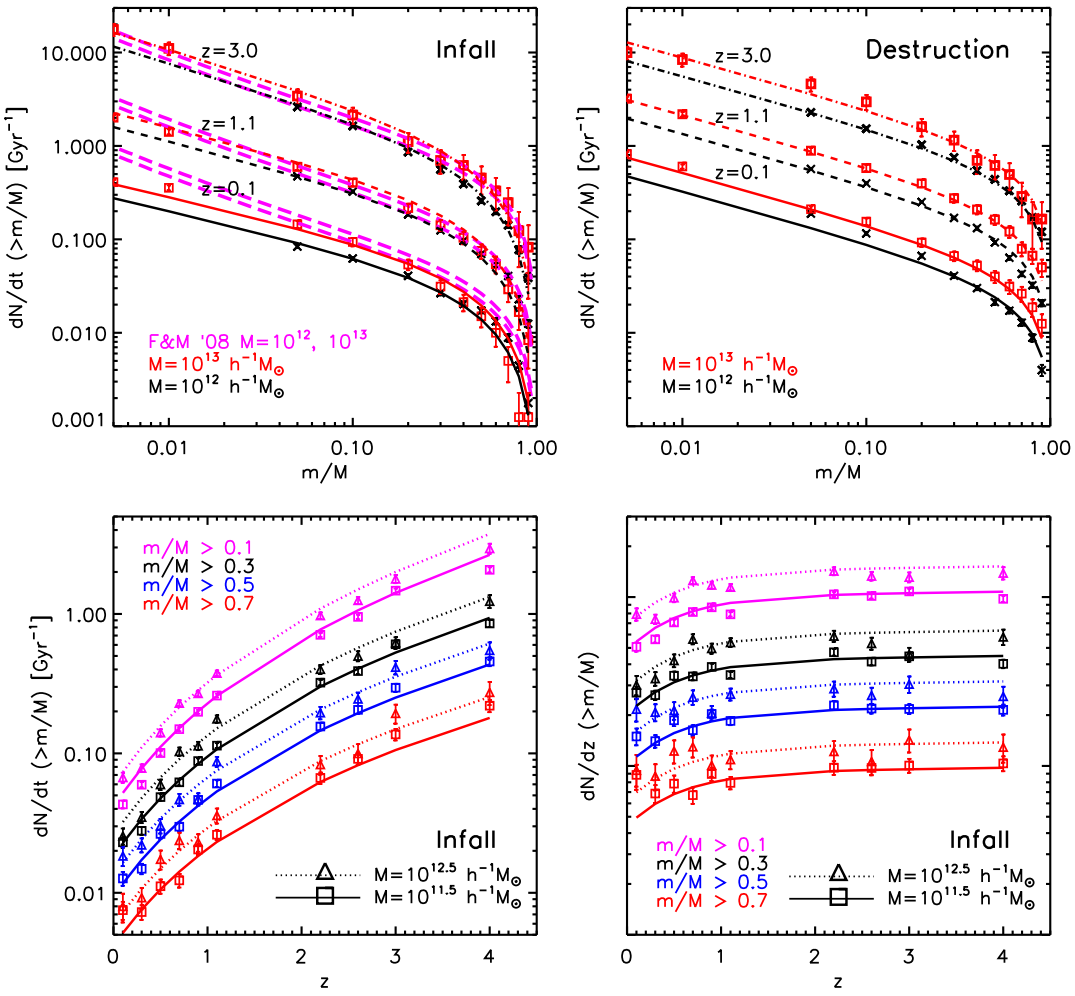

Figure 3.1: Dark matter halo infall and destruction rates (see §3.3) as a function of mass, merger-mass ratio, and redshift. Host halo mass bins span $\Delta \log_{10} M = 0.5$. *Top Left:* Infall rate per Gyr as a function of merger mass ratio. The dashed (pink) lines are a comparison to the results of Fakhouri & Ma (2008) for $M = 10^{12} M_{\odot}$ (lower) and $M = 10^{13} M_{\odot}$ (upper) halos. *Top Right:* Identical to top left, but for the destruction rate of halos instead of the infall rate. *Bottom Left:* Infall rate per Gyr as a function of redshift. *Bottom Right:* Infall rate per unit redshift, as a function of redshift. In the top panels, black and red lines correspond to different host halo masses (10^{12} and $10^{13} M_{\odot}$), while in the bottom panels, magenta, black, blue and red lines correspond to different merger ratios ($m/M > 0.1, 0.3, 0.5, 0.7$). In all panels, the mass ratio, m/M is defined prior to the infall of the smaller system. Error bars are Poissonian based on the number of host halos and the number of mergers. Horizontal error bars on the bottom figures have been omitted for clarity, but are identical to those in Figure 3.3.

Table 3.1: Merger Rate Fitting Function Parameters for Equations 3.1,3.2, and 3.3.

Dark Matter Halos: ($M = 10^{11.0-13.5} M_\odot$)	$A(z, M)^\dagger$	c	d
dN/dt: (INFALL) simple fit	$0.020\,(1+z)^{2.3}\,M_{12}^{0.15}$	0.50	1.30
dN/dt: (INFALL) complex fit	$0.020\,(1+z)^{2.3}\,M_{12}^{0.15}$	$0.4 + .05z$	1.30
dN/dz: (INFALL)	$0.27\,(d\delta_c/dz)^2\,M_{12}^{0.15}$	0.50	1.30
dN/dt: (DESTROYED)	$0.022\,(1+z)^{2.2}\,M_{12}^{0.2}$	0.54	0.72
dN/dz: (DESTROYED)	$0.32\,(d\delta_c/dz)\,M_{12}^{0.2}$	0.54	0.72
Galaxy Luminosity Cuts: ($L > fL_*$, $0.1 < f < 1.0$)	$A(z, f)^\dagger$	c	d
dN/dt:	$0.02\,(1+f)\,(1+z)^{2.1}$	0.54	0.72
Merger Fraction in past T Gyr: (Frac < 0.6, $T < 4$)	$0.02\,T\,(1+f)\,(1+z)^{2.0}$	0.54	0.72

Galaxy Stellar Mass Ranges: ($F(x) = F(m_*/M_*)$)	$A(z)^\dagger$	$c_*^\ddagger$	$d_*^\ddagger$
dN/dt ($10^{10.0} M_\odot < M_* < 10^{10.5} M_\odot$):	$0.015\,e^{1.0z}$	0.30	$1.1 - 0.2z$
dN/dt ($10^{10.5} M_\odot < M_* < 10^{11.0} M_\odot$):	$0.035\,e^{0.7z}$	0.25	$1.1 - 0.2z$
dN/dt ($10^{11.0} M_\odot < M_*$):	$0.070\,e^{1.0z}$	0.20	$1.0 - 0.3z$

†When not dimensionless, units are Gyr^{-1}.
‡Mass-ratio variable for galaxy stellar mass merger rates are identified with a *stellar mass* ratio, $r = m_*/M_*$.

crosses) and $10^{13} M_\odot$ (red lines and squares) at three different redshifts: $z = 0$ (solid), $z = 2$ (dashed), and $z = 3$ (dot-dashed). Host halo mass bins span $\Delta \log_{10} M = 0.5$, centered on the mass value listed. The upper left panel presents rates measured at subhalo infall — i.e., the merger rates of distinct halos — and the upper right panel presents rates of subhalo destruction (when the associated subhalo loses 90% of the mass it had prior to entering the virial radius of the larger halo), which we expect to more closely trace the galaxy merger rates. The lower left panel presents infall rates, now plotted at a fixed mass ratio ($> m/M = 0.1, ..., 0.7$ from top to bottom) and host mass ($M = 10^{12.5} M_\odot$, triangles; $M = 10^{11.5} M_\odot$, squares) as a function of redshift. The same information is presented in the lower right panel, but now presented as the rate per unit redshift instead of per unit time. We see that merger rates increase with increasing mass and decreasing mass ratio, and that the merger rate per unit time

increases with increasing redshift out to $z \sim 4$.

We quantify the measured dependencies using simple fitting functions. The merger rate (for both infall and destruction rates) per unit time for objects with mass ratios larger than m/M into halos of mass M at redshift z is fit using

$$\frac{dN}{dt}(> m/M) \quad = \quad A_t(z, M)\, F(m/M). \tag{3.1}$$

For the infall rate, we find that the normalization evolves with halo mass and redshift as $A_t(z, M) = 0.02\,\mathrm{Gyr}^{-1}\,(1+z)^{2.2}\,M_{12}^{b}$ with M_{12} the mass in units of $10^{12} M_{\odot}$ and $b = 0.15$. The merger mass ratio dependence is fit by

$$F(m/M) \equiv \left(\frac{M}{m}\right)^{c} \left(1 - \frac{m}{M}\right)^{d}, \tag{3.2}$$

with $c = 0.5$, and $d = 1.3$. A similar fit describes the destroyed rate, as summarized in Table 3.1. The fits are illustrated by solid lines that track the simulation points in each of the dN/dt panels in Figure 3.2.

The solid and dotted lines in the lower-right panel of Figure 3.2 show that the infall rate per unit redshift, dN/dz, is well described by the same mass-dependent function, but with a normalization that is only weakly dependent on redshift:

$$\frac{dN}{dz}(> m/M) = A_z(z, M)\, F(m/M), \tag{3.3}$$

where $A_z(z, M) = 0.27\,(d\delta_c/dz)^2\,M_{12}^{0.15}$ (for infall rate; see Table 3.1 for destruction rate). As discussed by Fakhouri & Ma (2008) (hereafter FM08), a redshift evolution

of this form is motivated by the expectations of Extended Press-Schechter theory. Note that since $d\delta_c/dz$ asymptotes to a constant ~ 1.3 for $z \gtrsim 1$ and evolves only mildly to ~ 0.9 at $z \simeq 0$, the overall redshift dependence is weak.

To a large extent, our results confirm and agree with those of FM08, who studied merger rates for halos in the Millennium simulation (Springel et al., 2005b) and presented a fitting function for the merger rate per unit redshift per unit mass-ratio for halos as a function of mass and redshift (the differential of our rate, dN/dz, with respect to the merger rate m/M), and concluded that it was nearly universal in form. For comparison, the pink dashed lines in the top left panel of Figure 3.2 show the implied expectations based on the FM08 fit for $M = 10^{12} M_\odot$ (lower lines for each pair) $M = 10^{12} M_\odot$ (upper lines) halos. [2] The agreement is quite remarkable, especially in light of the fact that the simulation, merger tree algorithm, and halo finder all differed substantially from our own. Note that the agreement is particularly good over the mass ratios $m/M \simeq 0.05 - 0.5$, that are likely the most important for galaxy formation (in terms of their potential for morphological transformation and overall mass deposition, see Chapter 2). We note however that our infall rate data are smaller than FM08 by a factor of ~ 1.5 for very large mass-ratio mergers $m/M \gtrsim 0.7$ and by a factor of ~ 2 for very small mass-ratio mergers $m/M \lesssim 0.01$ (this discrepancy for small mergers is slightly worse at low redshift, $z \lesssim 0.3$). In addition, we find a slightly stronger mass dependence, $dN/dt \propto M^{0.15}$ as opposed to $dN/dt \propto M^{0.1}$ as found by FM08.

It is interesting to note that in an independent analysis of the Millennium simulation, Genel et al. (2009) studied the (infall) merger rates of halos by defining halo masses and mergers in slightly different ways from FM08, in an effort to further remove artifacts of the halo-finding algorithm of the simulation. Among other results, their

[2] We use their fit for the 'stitching' merger rate, which corresponds most closely to our own definition for halo mergers.

findings suggested that the merger rates from FM08 are slightly too high (by $\lesssim 50\%$) for low redshift and for minor ($< 1/10$) mergers. This is qualitatively similar to the differences between FM08 and our own results, motivating the need for future study regarding the sensitivity of merger statistics from dark matter simulation on halo finding algorithms, as well as halo mass and merger definitions.

Our results also largely agree with an investigation of the major merger rate ($> 1/3$ mergers) of halos and subhalos by Wetzel et al. (2009). They found that the infall rate for halos ($M = 10^{11} - 10^{13} M_{\odot}$) evolves with redshift as $dN/dt = A(1+z)^{\alpha}$ (with $A \sim 0.03$ and $\alpha = 2.0 - 2.3$) from $z = 0.6 - 5$, in good agreement with our infall rates both in slope and in normalization (see Table 3.1). Wetzel et al. (2009) also reported on the subhalo merger rate in their simulations (the rate at which satellite subhalos finally merge with the central subhalo) and found similar behavior as field halos for low redshift ($A \sim .02$ and $\alpha \sim 2.3$ for $z = 0.6 - 1.6$, in good agreement with our destruction rates) but with a significantly flatter slope for high redshift ($A \sim 0.08$ and $\alpha = 1.1$ for $z = 2.5 - 5$, a factor of $2 - 3$ lower than our results, with a significantly flatter slope). Even though our destruction rate attempts to track a similar physical phenomenon as their subhalo merger rate—the rate of impact of satellite galaxies onto central galaxies—we find destruction rates to show qualitatively similar behavior to infall rates at *all* redshifts.

We speculate that the discrepancy between their results and ours may be due primarily to differences in definition. For example, we define an infalling halo to be "destroyed" once it loses 90% of its infall mass (see §3.3). Wetzel et al. (2009) defines subhalo mergers by tracking the evolution of the subhalo's 20 most-bound particles, resulting in a much more stringent definition of a merger, and increasing the time delay between infall to the virial radius ($t_{\rm inf}$) and the time at which the satellite is destroyed ($t_{\rm merge}$). More importantly, we define the merger mass ratio by the halo

masses when the satellite halo first falls into the virial radius of the host, $m_{\rm inf}/M_{\rm inf}$. Although we track the subhalo until it has lost 90% of its mass in order to assign a proper *time* that the merger takes place, we do not redefine this merger ratio based on any subsequent growth or decay of either halo. Although Wetzel et al. (2009) defines the satellite halo's mass in an identical fashion, they allow for the growth of the central halo during the decay time of the subhalo. Once the subhalo is destroyed, they use the host halo mass at *this* time (minus the mass of the subhalo, so that $m/M < 1$) and thus define the merger ratio as $m_{\rm inf}/M_{\rm merge}$. As a consequence, the host halo has a significant time period ($t_{\rm merge} - t_{\rm inf}$) to grow in mass, leading to smaller mass ratio definitions for identical merger events, as compared to our definition. This effect is likely negligible at late times, when halos do not grow significantly over the ~ 2 Gyr decay timescales typical for major mergers. This may be why the two studies agree rather well for $z < 1.6$. However, the central halo's mass growth on these timescales becomes increasingly important at high redshift, possibly explaining the flattening of α reported by Wetzel et al. (2009), as compared to our own results.

Fakhouri & Ma (2009) investigates this issue to some degree by studying the subhalo merger rate in the Millennium simulation using differing mass ratio definitions. Whether they implement a merger ratio definition similar to our destruction rate, or one more similar to that of Wetzel et al. (2009), their merger rates remain well-fit to a power law in $(1 + z)$, in line with our results. In this case, the underlying cause of the discrepancy between our merger rates (and those of Fakhouri & Ma (2009)) and the subhalo merger rates reported by Wetzel et al. (2009) remains uncertain. Such comparisons between our respective results highlight the differences that are manifest in defining mergers. When including baryons, properly defining mergers and merger mass ratios becomes even more complicated (e.g. Chapter 5), but even between dark matter structures, differences such as those found between our work, Wetzel et al. (2009) and Fakhouri & Ma (2009) further motivate the need for focused simulations

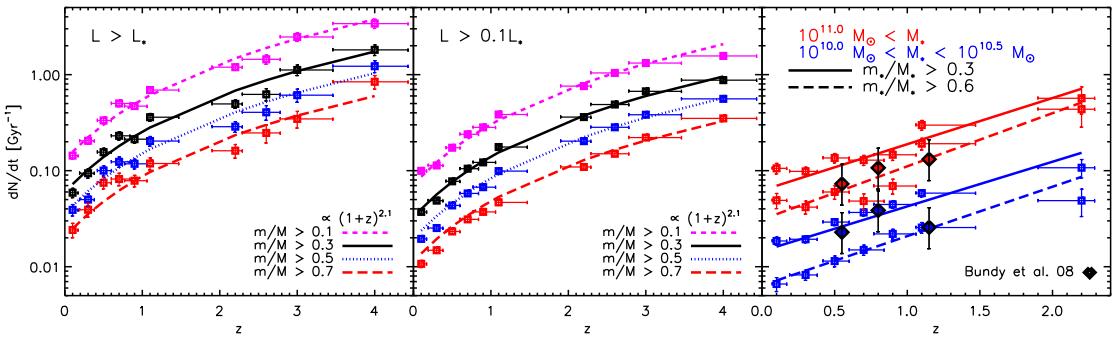

Figure 3.2: Expected merger rates per Gyr for galaxies of an indicated type as a function of redshift. The vertical error bars show Poisson errors on both the number of main halos and the total number of mergers averaged over per redshift bin while the horizontal error bars show the redshift bins used to compute the merger rate at each redshift. The error bars do not include uncertainties in the mapping of mass to luminosity or stellar mass. *Left:* Merger rate into galaxies with $L > L_*$ involving objects with *total* mass ratios $m/M > 0.1, ..., 0.7$ as indicated. *Middle:* Merger rate into galaxies with $L > 0.1L_*$. *Right:* Merger rates for galaxies of a given *stellar* mass involving objects with *stellar mass ratios* $m_*/M_* > 0.3$ and 0.6 as a function of redshift. (Note that the redshift range in this panel only goes to $z = 2$.) We include two different stellar mass cuts in this panel, represented by the red and blue lines. The dotted lines in this panel show an extrapolation out to $z \sim 4$, based on our fit to the $z < 2$ simulation data. The filled diamonds show observational results for the same stellar mass cuts from Bundy et al. (2009).

in order to determine the timescales and observational consequences associated with the much more cleanly defined rate with which dark matter subhalos first fall within the virial radii of their hosts.

3.5 Associating Halos with Galaxies

While dark matter halo merger rates at a given mass are theoretically robust quantities to compute in our simulation, they are difficult to compare directly with observations. One particularly simple, yet surprisingly successful approach is to assume a monotonic mapping between dark matter halo mass M (or similarly the halo maximum circular velocity) and galaxy luminosity L (Kravtsov et al., 2004;

Tasitsiomi et al., 2004; Vale & Ostriker, 2004; Conroy et al., 2006; Berrier et al., 2006; Purcell et al., 2007; Marín et al., 2008; Conroy & Wechsler, 2009a). With this assumption, provided that we know the cumulative number density of galaxies brighter than a given luminosity, $n_g(> L)$, we may determine the associated halo population by finding the mass $M(L)$ above which the number density of halos (including subhalos) matches that of the galaxy population $n_h(> M_{\rm DM}) = n_g(> L)$. Table 3.2 shows the number densities of various galaxy populations from redshifts $z = 0.1 - 4$ obtained using a variety of surveys for galaxies brighter than $L = f\,L_*$, where $f = 0.1, 0.4$, and 1.0. We list the associated number-density matched minimum dark matter halo mass in each case, $M_{\rm DM}$, and we use this association to identify halos with galaxies below. For example, from the top left entry of this table, we see that $n_h(> 10^{11.2} M_\odot) = n_g(> 0.1 L_*)$ at $z = 0.1$.

Table 3.2: Dark Matter–Luminosity Relationship by Number Density Matching.

z	Source	$> 0.1L_*$		$> 0.4L_*$		$> L_*$		$\tau(z)$
		$n_g^\dagger$	$M_{DM}^\ddagger$	$n_g^\dagger$	$M_{DM}^\ddagger$	$n_g^\dagger$	$M_{DM}^\ddagger$	[Gyr]
0.1	SDSS [1]	29	$10^{11.2}$	10	$10^{11.7}$	3.2	$10^{12.3}$	1.79
0.3	COMBO-17/DEEP2 [2]	20	$10^{11.4}$	5.8	$10^{12.0}$	1.5	$10^{12.6}$	1.50
0.5	COMBO-17/DEEP2 [2]	24	$10^{11.3}$	7.0	$10^{11.9}$	1.8	$10^{12.5}$	1.28
0.7	COMBO-17/DEEP2 [2]	20	$10^{11.4}$	5.8	$10^{12.0}$	1.5	$10^{12.6}$	1.09
0.9	COMBO-17/DEEP2 [2]	25	$10^{11.3}$	7.3	$10^{11.9}$	1.9	$10^{12.5}$	0.95
1.1	COMBO-17/DEEP2 [2]	19	$10^{11.4}$	5.5	$10^{12.0}$	1.4	$10^{12.5}$	0.81
2.2	Keck Deep Fields [3]	20	$10^{11.3}$	6.4	$10^{11.7}$	1.8	$10^{12.2}$	0.49
2.6	Extrapolation	~ 18	$10^{11.3}$	~ 5.2	$10^{11.8}$	~ 1.2	$10^{12.3}$	0.40
3	Keck Deep Fields [3]	15	$10^{11.2}$	3.8	$10^{11.7}$	0.90	$10^{12.2}$	0.32
3	LBGs [4]	NA	NA	5.0	$10^{11.7}$	0.82	$10^{12.2}$	0.32
4	HUDF, HST ACS [5]	18	$10^{11.0}$	3.2	$10^{11.6}$	0.61	$10^{12.0}$	0.25

$^\dagger 10^{-3}\ h^3\ {\rm Mpc}^{-3}$

$^\ddagger M_\odot$

[1]Blanton et al. (2003) ($r^{0.1}$-band)

[2]Faber et al. (2007) with DEEP2 optimal weights (B-band)

[3]Sawicki & Thompson (2006) (UV)

[4]Shapley et al. (2001) (V-band) – note that rest-frame V number densities match well with $> 0.4L_*$ and $> L_*$ values in rest-UV at $z = 3$.

[5]Bouwens et al. (2007) (UV)

One important point of caution is that the luminosity functions used to make these assignments at different redshifts vary in rest-frame band, as indicated in Column 2. Specifically, one concern might be that UV luminosity at low redshift is not strongly correlated with dark matter halo mass, so assuming such a correlation for high redshift galaxies is not valid. Unlike their low redshift counterparts, however, there is a strong correlation in high redshift ($z > 2$) galaxies between star formation and total baryonic mass, as well as a trend for more UV luminous galaxies to be more strongly clustered, suggesting that connecting UV luminosity to halo mass at these redshifts is a valid technique (see discussion in Conroy et al., 2008, and references therein). Encouragingly, as shown in the two $z = 3$ rows, the number density of $f\,L_*$ galaxies from Sawicki & Thompson (2006; rest-frame UV) and Shapley et al. (2001; rest-frame V) are quite similar.

We also note that the data from these various sources will contain uncertainties in the number counts of galaxies from, e.g. cosmic variance. For example, the COMBO17/DEEP2 data fluctuates about a nearly constant value ($\sim 0.02{-}0.03h^3\mathrm{Mpc}^{-3}$) from $z = 0.3 - 1.1$, suggesting a $\sim 30\%$ uncertainty in these values. We find that a 30% error in the observed number density typically translates into a similar 30% error in the assigned minimum halo mass in our simulation. Since dark matter halo merger rates are only weakly dependent on halo mass ($\propto M_{\mathrm{DM}}^{0.2}$), this should result in only a $\sim 10\%$ uncertainty in our merger rates. Thus, the merger rates we present here should be relatively robust to small errors in observational uncertainties. For example, if we adopt minimum halo masses (regardless of redshift) of $M_{\mathrm{DM}} = 10^{11.2}, 10^{11.7}, 10^{12.3} M_\odot$ as corresponding to $> 0.1, 0.4, 1.0 L_*$ galaxies, respectively, our resulting merger rates change by $< 25\%$ (typically $5 - 15\%$).

A related approach is to use observationally-derived stellar mass functions and to assume a monotonic relationship between halo mass and stellar mass M_*. Though a

monotonic relationship between total stellar mass and dark matter mass avoids the issue of color band that arises in luminosity mapping, we cannot use it explore merger rates as a function of stellar mass above $z \sim 2$ because the stellar mass function is poorly constrained beyond moderate redshifts. For our analysis, we will adopt the relation advocated by Conroy & Wechsler (2009a, hereafter CW09; interpolated from the data shown in their Figure 2). For example, CW09 find that the halo mass M associated with stellar masses of $M_* = (1, 3, 10) \times 10^{10} M_\odot$ at $z = 0, 1, 2$ are $M(z = 0) \simeq (2.5, 7.0, 47) \times 10^{11} M_\odot$; $M(z = 1) = (4.0, 9.6, 41) \times 10^{11}$; and $M(z = 2) = (2.1, 3.9, 10) \times 10^{12} M_\odot$. We note that because this mapping between stellar mass and halo mass is not well fit by a constant ratio, $M_* = f M_{\rm DM}$, merger rates in terms of *stellar* mass ratios show qualitatively different evolution with redshift (see §3.6.1). This is primarily because mergers of a fixed dark matter mass ratio do *not* typically correspond to the same stellar mass ratio (Stewart, 2009).

Note that while the dark matter halo merger rates presented in §3.4 give robust theoretical predictions, the merger rates we will present in terms of luminosity (or stellar mass) are sensitive to these mappings between halo mass and L (or M_*). In addition, it is difficult to perform a detailed investigation into the errors associated with these mappings, as there are inherent uncertainties in the luminosity and stellar mass functions, especially at $z > 1$. It is also possible that the monotonic mapping between halo mass and L (or M_*) may break down at $z > 1$ (see discussion in CW09). These uncertainties must be kept in mind when comparing our predicted merger rates (in terms of L or M_*) to observations, especially at high redshift. Nevertheless, the halo masses we have associated with a given relative brightness should be indicative.

3.6 Galaxy Merger Predictions

3.6.1 Merger Rates

Our predicted merger rates (per galaxy, per Gyr) and their evolution with redshift, averaged over $L > L_*$ and $L > 0.1\,L_*$ galaxy populations, are illustrated in the left and middle panels of Figure 3.3. Rates are presented for a few selected *dark matter halo* mass ratio cuts $m/M > 0.1$, 0.3, 0.5, and 0.7. Here, galaxy merger rates are defined using the *destruction rate*, when the infalling subhalo is identified as destroyed in the simulation (see §3.3). The solid lines correspond to a fit in the form of Equation 3.1, with the normalization evolving as $A_t(z, f) \propto (1 + f)\,(1 + z)^{2.1}$ for $L > fL_*$ galaxies. The explicit best-fit parameters for the merger rate as a function of luminosity cut are given in Table 3.1.

For comparison, the right panel in Figure 3.3 shows the predicted evolution in the merger rates per galaxy for two bins of stellar mass, according to the CW09 mapping described above: $10^{10.0} M_\odot < M_* < 10^{10.5} M_\odot$ (lower, blue) and $M_* > 10^{11} M_\odot$ (upper, red). Shown are merger rates for two choices of *stellar mass* ratio mergers, $(m_*/M_*) > 0.3$, 0.6 (solid and dashed lines respectively). The solid and dashed lines correspond to fits to our simulation results in the form of Equation 3.1, with $A_t(z) \propto e^{1.2z}$. The explicit best-fit parameters for these two stellar mass bins (as well as an intermediate bin, $10^{10.5} M_\odot < M_* < 10^{11.0} M_\odot$) can be found in Table 3.1. Table 3.1 also provides best fit parameters for the function $F(r)$ (Equation 3.2) where now we associate the ratio r with the stellar mass ratio $r = m_*/M_*$. Note that we only show our simulation points for $z \lesssim 2$ in this panel, due to uncertainties in the stellar mass function at high redshift.

While the galaxy merger rate cannot be observed directly, it can be inferred using

a number of different techniques. Mergers that are about to occur may be forecast by counting galaxy close pairs, and close pair fractions are often used as a proxy for the merger rate. The filled diamonds in the right panel of Figure 3.3 are recent merger-rate estimates from the pair count study of Bundy et al. (2009), for the same two stellar mass bins shown in the simulations (blue for the lower mass bin, red for the upper mass bin). Bundy et al. (2009) have used the simulation results of Kitzbichler & White (2008) to derive merger rates from the observed pair fraction. Overall, the trends with mass and redshift are quite similar and this is encouraging. However, the Bundy et al. (2009) results correspond to mergers with stellar mass-ratios larger than $m_*/M_* \gtrsim 0.25$. Our normalization is a factor of ~ 2 too high compared to this, and only matches if we use larger merger-ratios $m_*/M_* \gtrsim 0.5$. It is possible that this mismatch is associated with the difficulty in assigning merger timescales to projected pairs (Berrier et al., 2006, see, e.g.). It may also be traced back to uncertainties in assigning stellar masses to dark matter halo masses, however, since merger rates have relatively weak dependence on halo mass, it would require increasing our assigned stellar masses by a factor of ~ 3 in order to account for this discrepancy solely by errors in assigning stellar mass (such an increase in stellar mass would result in unphysical baryonic content for dark matter halos: e.g., $10^{12} M_\odot$ halo containing $M_* > 10^{11} M_\odot$).

There are a number of other observational estimates of the merger rate based on pair counts of galaxies (e.g., Patton et al., 2002; Lin et al., 2004; Bell et al., 2006; Kartaltepe et al., 2007; Kampczyk et al., 2007; de Ravel et al., 2009; Lin et al., 2008; McIntosh et al., 2008; Patton & Atfield, 2008; Ryan et al., 2008). We choose to compare our results to Bundy et al. (2009) as a recent representative of such work, primarily because it is more straightforward for us to compare to samples that are defined at a fixed stellar mass and stellar mass ratio. It is also difficult to compare to many different observational results on the same figure self-consistently,

because different groups adopt slightly different cuts on stellar mass (or luminosity) and on mass ratios for pairs. We note that if we were to extrapolate our best-fit curves to higher redshift than our data ($z \sim 4$), we find good agreement between our simulation data and the merger rate estimates using CAS (concentration, asymmetry, clumpiness) morphological classifications from Conselice et al. (2003) for galaxies with $M_* > 10^{10} M_\odot$. However, the mapping between stellar mass and halo mass adopted from Conroy & Wechsler (2009a) is only valid to $z = 2$ (and most robust for $z < 1$), so extrapolating these fits to $z \sim 4$ is only a first-order check, and should not be considered a reliable prediction.

3.6.2 Merger Fractions

Another approach in measuring galaxy merger rates is to count galaxies that show observational signatures of past merging events such as enhanced star formation, AGN activity, and morphological disturbances. Unfortunately, the timescale over which any individual signature will be observable is often extremely uncertain, and will depend on the total mass and baryonic makeup of the galaxies involved as well as many uncertain aspects of the physics of galaxy formation (e.g. Berrier et al., 2006; Cox et al., 2008; Lotz et al., 2008b; Kitzbichler & White, 2008). In order to avoid these uncertainties, we present results for merger fractions using several choices for lookback timescale here.

The three panels of Figure 3.3 show the predicted evolution of the merger fraction in galaxies brighter than $0.4L_*$ for three different choices of merger lookback time and for various choices for the total mass merger fraction $m/M > 0.1, ..., 0.7$. The horizontal error bars on this figure show the *actual* redshift bins used to compute the merger fractions. The left and right panels show the merger fraction within 100 Myr

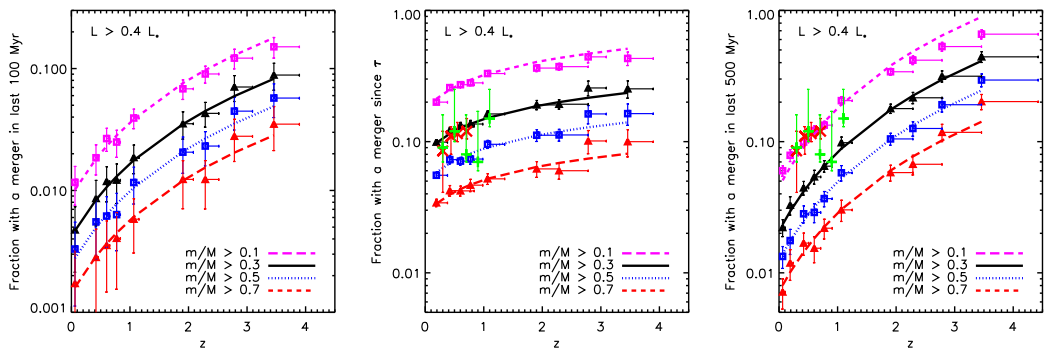

Figure 3.3: The fraction of halos that experience at least one merger larger than m/M in the past 100 Myr (left), halo dynamical time τ (middle), or 500 Myr (right), as a function of z. Error bars show the Poisson $\sqrt{N}$ error based on the both the number of main halos and the total number of mergers averaged over, while the horizontal error bars show the redshift bins used to compute the merger rate at each redshift. The error bars do not include uncertainties in the mapping of mass to luminosity. The symbols represent estimates of the observed merger fraction at various redshifts, based on Jogee et. al (2008, red crosses) and Lotz et al. (2008a, green plus signs), respectively.

and 500 Myr, respectively [3], and the middle panel shows the fraction of galaxies that have had a merger within the past halo dynamical time [4] $\tau(z)$, where $\tau(z) \simeq 2.0$ Gyr $(1+z)^{-1.15}$ for $z \leq 1$ and $\tau(z) \simeq 2.6$ Gyr $(1+z)^{-1.5}$ for $z > 1$.

3.6.3 Merger-driven starbursts

Several recent studies of star formation rates in galaxies at $z = 0 - 1$ suggest that the cosmic SFR density is not dominated by strongly disturbed systems with brief periods of intense star formation, as might be expected if merger-driven starbursts are common. Instead, the SFR density appears to be dominated by normal, non-merging galaxies (Wolf et al., 2005; Bell et al., 2005; Jogee et. al, 2008; Noeske et al.,

[3] In most cases, the available timesteps ($\Delta t \simeq 250$ Myr) are too widely spaced to directly measure fractions within 100 Myr. For this reason, the left panel is actually the merger fraction within the last Δt timestep, scaled down by a factor of $(\Delta t/100\text{Myr}) \simeq 2.5$.

[4] We use $\tau = R/V \propto (\Delta_v(z)\,\rho_u(z))^{-1/2}$, such that the halo dynamical time is independent of halo mass.

2007). That is, $< 30\%$ of the instantaneous SFR density at a given redshift (from $z = 0-1$) is derived from morphologically disturbed galaxies, which may be currently undergoing a merger-induced starburst. Even at high redshift ($z \sim 2$), a comparison of the clustering of star-forming galaxies to that of dark matter halos suggests that these galaxies are consistent with massive galaxies (in massive DM halos) quiescently forming stars, as opposed to less massive galaxies (less massive DM halos) in the midst of merger-induced starbursts (Conroy et al., 2008). However, this conclusion is based on the assumption that UV-bright galaxies at this redshift comprise a representative sample of star-forming galaxies.

As discussed in the introduction, the briefest timescales we expect for merger-triggered starbursts is ~ 100 Myr (Mihos & Hernquist, 1996; Cox et al., 2008), and for these models we expect the SFR to increase to ~ 20 times the isolated value for $m/M \gtrsim 0.3$ events (Cox et al., 2008). (While we adopt these timescales as "typical" of galaxy mergers, it is important to keep in mind that Cox et al. (2008) focuses on $z = 0$ galaxies. High redshift galaxies should typically contain higher gas fractions, which may impact the properties of merger-induced starbursts at these epochs.) As we see from the left-panel of Figure 3.3, the fraction of galaxies that have a merger large enough ($m/M > 0.3$) to trigger such a burst is quite small, $\lesssim 1\%$ for $z \lesssim 1$. It is therefore not surprising that stochastic starbursts of this kind do not dominate the SFR density at moderate to low redshifts. Even at at higher redshift ($z = 3 - 4$), the fraction of galaxies with major mergers on these timescales is less than $\sim 6\%$ of the total bright galaxy population (consistent with the results presented in Somerville et al. (2008), for their semi-analytic model). However, galaxy gas fractions are expected to increase with redshift (Erb et al., 2006), which could presumably result in significant starburst activity from more minor mergers (as well as providing fresh gas accretion in a more cumulative sense, see Chapter 4). A higher fraction of galaxies have experienced such minor ($> 1/10$) mergers on these timescales at

$z = 3 - 4$ ($\sim 15\%$).

Alternatively, if merger-driven starbursts remain active for ~ 500 Myr, as other models suggest, then their enhancements are expected to be less pronounced (with an SFR ~ 5 times isolated; Cox et al. 2008). In this case, the right panel of Figure 3.3 is the relevant prediction, and we see that (at most) $\sim 3 - 9\%$ of bright galaxies could exhibit signs of such elevated SFR activity between $z = 0$ and $z = 1$. It seems that in either case, we would not expect merger-triggered activity to play a major role in driving the integrated star formation rate at these epochs. Only at the highest redshifts $z \gtrsim 3$ would this seem possible. However, we once again point out that the detailed study of Cox et al. 2008, which we have quoted here, focuses on low redshift galaxies, with gas fractions $< 30\%$. If minor mergers with very high gas fractions ($> 50\%$) are capable of triggering starbursts, then over half of all bright galaxies at $z > 2$ (where such high gas fractions are more common) may be in the process of starbursting.

Under the presumption that only major mergers trigger starbursts, we note that our numbers are an upper limit on the fraction of bright galaxies that could be experiencing merger-induced starbursts, because moderately high gas fractions are also necessary. For example, a study of 216 galaxies at $z \sim 2-3$ by Law et al. (2007b) found that galaxy morphology (in rest-frame UV) was not necessarily correlated with star formation rate, and in a recent examination of two Chandra Deep Field South sources using adaptive optics, Melbourne et al. (2005) found an example of a merger of two evolved stellar populations, in which the major merger signature was not accompanied by a burst of star formation, presumably because both galaxies were gas-poor. Lin et al. (2008) finds that $\sim 8\%$ (25%) of mergers at $z \sim 1.1$ (0.1) are gas-poor, suggesting that this issue, while less dominant at high redshift, is a significant effect and must be taken into consideration.

We note that we have focused on galaxies which are in the *midst* of a merger-induced starburst. The lingering impact these bursts will have on the cumulative star formation histories (SFH) of galaxies in a separate issue entirely. A recent study by Cowie & Barger (2008) traced recent star formation in > 2000 galaxies from $z = .05 - 1.5$ and found that roughly a quarter of these galaxies showed color indications (AB3400-AB8140 vs. EW in Hβ) indicative of starbursts in the past $0.3 - 1.0$ Gyr. Once again, we find our predictions to be broadly consistent with this result, with $\sim 20\%$ of bright galaxies ($> 0.4L_*$) having experienced a major merger in the past Gyr at $z \sim 1$. With this study of individual galaxies' star formation histories emphasizing the importance of starbursts, and the previously mentioned studies of the global SFR density emphasizing the importance of star formation in normal, non-merging systems, we find that our predicted merger rates are broadly consistent with both results, suggesting that while starbursts may not be the globally dominant form of star formation in the Universe, they still play an important role in the star formation histories of galaxies. Detailed progress in understanding the full importance of merger-induced starbursts on the global SFR density of the Universe will require a better understanding of the timescales and signatures associated with galaxy mergers and merger-induced starbursts.

3.6.4 Morphological signatures

Even if the contribution to the overall SFR due to very recent mergers remains low, this does not necessarily imply that there would be a lack of morphological signature. The timescale for morphological relaxation may be significantly longer than starburst activity. Though the precise timescales for relaxation are uncertain, the middle and right panels of Figure 3.3 explore merger fractions for two reasonable choices: a fixed 500 Myr timescale and a redshift-dependent halo dynamical time τ.

Lotz et al. (2008a) used AEGIS survey data to study the morphological evolution and implied galaxy merger fraction from redshift $z = 0.2$ to 1.2. The merger fraction results for $> 0.4L_*$ galaxies from Lotz et al. (2008a) are shown by the green pluses in the middle and right panels of Figure 3.3. In a similar investigation, Jogee et. al (2008) study $z = 0.2 - 0.8$ galaxies using a combination of HST, ACS, Combo-17, and Spitzer 24 μm data to estimate the fraction of "strongly disturbed" galaxies. Their results [5] are shown by the red crosses in Figure 3.3, and are in reasonably good agreement with the points from Lotz et al. (2008a). We note that the data from these very recent works seem to be in good agreement with the $m/M > 0.3$ merger fraction if the relaxation time is close to τ. This case in particular has a fairly weak evolution because τ is decreasing with time. Interestingly, however, due to the rather large measurement uncertainties, the data are also in reasonable agreement with the fixed relaxation timescale case of 500 Myr (which has a steeper evolution with z), as long as more minor mergers ($m/M > 0.1$) can trigger the observed activity. The fact that the data matches both the predictions in the middle panel and right panel of Figure 3.3 draws attention to the inherent degeneracies in this comparison. The same merger fractions are obtained with high-mass ratio merger events and lookback times or with lower mass ratio mergers with slightly shorter lookback times.

We may also compare our predictions with the results of Melbourne et al. (2008), who imaged 15 $z \sim 0.8$ luminous infrared galaxies (LIRGs) with the Keck Laser Guide Star (LGS) AO facility, and found that 3/15 of the galaxies showed evidence for a *minor* merger, while only 1/15 was consistent with a major merger. These results match our expectations for major ($m/M > 0.3$) and minor ($m/M > 0.1$) merger fractions at $z \sim 0.8$ fairly well, considering the small number statistics. Similarly, Shapiro et al. (2008) study 11 rest-frame UV/optical-selected z$\sim$2 galaxies with spectroscopic

[5]The data from Jogee et. al (2008) correspond to a fixed stellar mass cut at $M_* \sim 2.5 \times 10^{10} M_\odot$, but the associated dark matter halo mappings from CW09 are close to those for galaxies with $> 0.4L_*$ (see Table 3.1 and our discussion in §3.5).

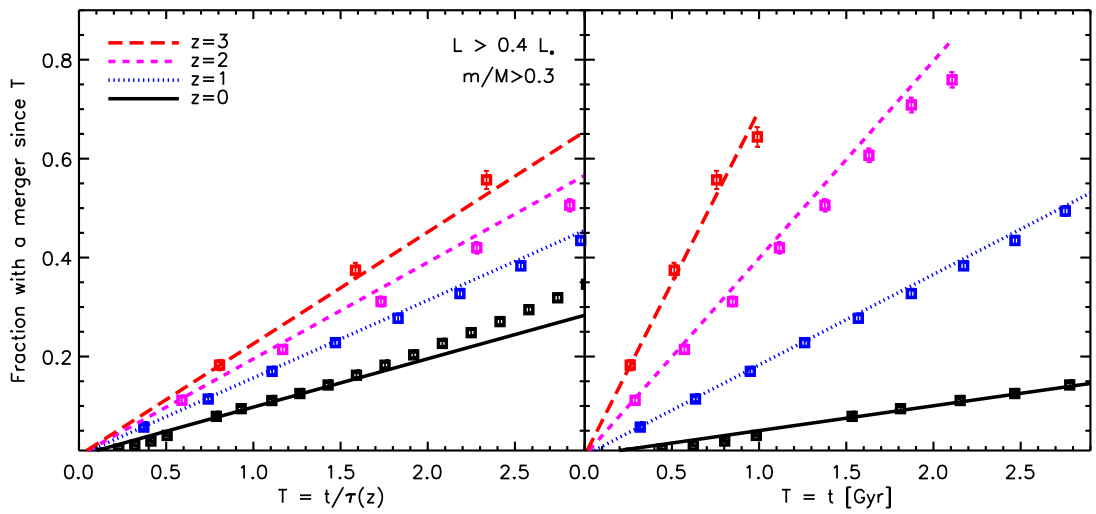

Figure 3.4: The fraction $> 0.4L_*$ galaxies at $z \sim 0, 1, 2, 3$ (black solid to red dashed lines) that have experienced a major merger ($m/M > 0.3$) over a given time period. Symbols show the simulation data, while the lines are given by the fit in Table 3.1. *Left:* Merger fraction since t, normalized by the halo dynamical time at each redshift, $\tau(z = 0, 1, 2, 3) \simeq 1.95, 0.92, 0.49, 0.32$ Gyr. *Right:* Merger fraction in the past t Gyr. Error bars show the Poisson $\sqrt{N}$ error based on the total number of mergers, and are comparable to the symbol sizes. The error bars do not take uncertainties in the mapping of mass to luminosity into account.

data from SINFONI on the VLT, and estimate that ∼25% of these systems are likely undergoing a major (mass ratio $\leq$ 3:1) merger. Again, our expectations as shown in the middle and right panels of Figure 3.3 are consistent with these numbers.

The above discussion makes it clear that meaningful comparisons between observed morphologically disturbed fractions and predicted merger fractions rely fundamentally on understanding how the mass ratio involved affects the morphological indicator and on the associated relaxation timescales of the associated remnants. In addition, merger rates are expected to depend sensitively on the galaxy luminosity and redshift (see Table 3.1). Comparisons between observational results and theory therefore require great care, especially as it concerns the evolution of the merger rate. If, for example, higher redshift measurements are biased to contain brighter galaxies than lower redshift measurements, then the redshift evolution will likely be steeper than

the underling halo merger rate at fixed mass. Or, if higher redshift measurements are sensitive to only the most massive mergers, while lower redshift measurements detect more subtle effects, then the evolution in the merger rate will be biased accordingly.

3.6.5 High Redshift Expectations

As seen clearly in Figures 3.2 and 3.3, the merger rate per galaxy and the corresponding merger fraction at a fixed time are expected to rise steadily towards high redshift. Even after normalizing by the halo dynamical time, which decreases with redshift, this evolution with redshift persists, as seen in Figure 3.3 (middle). This point is emphasized in Figure 3.4, which shows the fraction of $L > 0.4L_*$ galaxies that have had a merger larger than $m/M = 0.3$ within the last t Gyr (right) and within the last $t/\tau(z)$ (left). The left-hand panel scales out the evolution in the halo dynamical time. We see that $\sim 50\%$ of z=3 galaxies are expected to have had a major merger in the last 700 Myr, and that these galaxies are ~ 4 times as likely to have had a significant merger in the last dynamical time than bright galaxies at z=0. It would be surprising then if mergers did not play an important role in setting the the properties of most $z = 3$ galaxies like Lyman Break Galaxies (LBGs). These major mergers should (at least) deliver a significant amount of gas to fuel star formation, affect LBG dynamics, and perhaps trigger starburst activity. If LBGs represent a biased sample at $z = 3$ (of unusually bright galaxies, more likely to have recently undergone a merger-induced starburst) [6] then it may be possible that the merger fraction in LBGs is even higher than the global merger fraction for $> 0.4L_*$ galaxies.

At higher redshifts, $z > 3$, we expect major mergers to become increasingly common. The brightest galaxies $L > 0.4L_*$ should be undergoing mergers frequently, with an

[6] It is estimated that $\sim 75\%$ of all bright galaxies at $z \sim 3$ are LBGs (Marchesini et al., 2007; Quadri et al., 2007).

overwhelming majority of $z = 4$ galaxies having experienced some significant merger activity in the last ~ 500 Myr.

3.7 Conclusion

We have used a high-resolution ΛCDM N-body simulation to investigate the instantaneous merger rate of dark matter halos as a function of redshift (from $z = 0 - 4$), merger mass ratio, and host halo mass from $M = 10^{11}$ to $10^{13} M_{\odot}$. Merging companions as small as $m = 10^{10} M_{\odot}$ were tracked. We use number density matching to associate galaxies with dark matter halos and present predictions for the merger rate and merger fraction as a function of galaxy luminosity and stellar mass. The principle goal has been to present raw merger statistics that can be compared directly to observations of galaxies to high redshift. Fitting functions that describe our results as a function of luminosity, mass, mass-ratio, and redshift are provided in Table 3.1.

Our main results may be summarized as follows:

1. A simple fitting function describes the accretion rate of small dark matter halos of mass m into larger dark matter halos of mass M as a function redshift: $dN/dt = A(z, M)\, F(m/M)$, where typically $A(z, M) \propto (1 + z)^{2.2} M^{0.15}$ and $F(m/M) = (M/m)^{c}(1 - m/M)^{d}$. Fit parameters for merger rates in terms of dark halo mass, luminosity, or stellar mass are given in Table 3.1.

2. The merger rate of galaxies of luminosities $L > f L_{*}$ should evolve in a similar manner, with a redshift and luminosity dependence that follows $A(z, f) \propto (1 + f)\,(1 + z)^{2.1}$.

3. Only a small fraction (0.5% at $z = 0$, 10% at $z = 4$) of bright ($> 0.4 L_{*}$) galaxies should have experienced a major (> 0.3) merger in their very recent history

(100 Myr, Figure 3.3 left panel). Even if mergers trigger the kind of short-lived, highly-efficient star formation bursts that are expected in some models, they cannot contribute significantly to the overall distribution of star formation rates at any given epoch.

4. The predicted fraction of galaxies with a merger in the past 500 Myr, or alternatively within a past halo dynamical time, are in reasonable agreement with the fraction of galaxies that show observational signs of morphological disturbance between redshifts $z = 0 - 2$ (Figure 3.3, middle and left panels). We emphasize, however, that comparisons between theory and observations suffer from significant uncertainties associated with mass-ratio dependencies and relaxation timescales.

5. Galaxy merger rates should depend on at least three parameters: mass (or luminosity), merger mass ratio, and redshift (see Table 3.1). Therefore any attempt to compare two observational indicators of the merger rate or to relate specific observations to theoretical predictions must take great care in the respective comparisons.

6. Mergers must become increasingly important in shaping galaxy properties at $z > 3$. At $z = 3$, the fraction of galaxies with a merger in the past dynamical time is ~ 4 times higher than at $z = 0$. We expect $\sim 30\%$ (60%) of $> 0.4L_*$ galaxies to have experienced a $m/M > 0.3$ major ($m/M > 0.1$ minor) merger in the past 500 Myr at $z = 3$. Though it is unlikely that short-lived starbursts associated with these mergers drive the increase in the global star formation rate of galaxies with redshift, the broader implications of these mergers (fresh supply of gas brought in to the central galaxy through accreted satellites, etc.) are undoubtedly linked to star formation and the general growth of galaxies on longer timescales.

3.8 Acknowledgements

The contents of this chapter were previously published by Stewart, Bullock, Barton and Wechsler (2009) in The Astrophysics Journal, September 2009 (v702, p1005). The simulation used in this chapter was run on the Columbia machine at NASA Ames. We would like to thank Anatoly Klypin for running the simulation and making it available to us. We are also indebted to Brandon Allgood for providing the merger trees. We thank Charlie Conroy for providing us the abundance matching data from CW09, and Kevin Bundy for providing us with an advance copy of his paper before publication. We thank Jeff Cooke, David Law, Lihwai Lin, Ari Maller, David Patton, Brant Robertson, and Andrew Wetzel for useful discussions.

Chapter 4

Gas-Rich Mergers and Disk Survivability

4.1 Chapter Abstract

We use N-body simulations and observationally-normalized relations between dark matter halo mass, stellar mass, and cold gas mass to derive robust expectations about the baryonic content of major mergers out to redshift $z \sim 2$. First, we find that the majority of major mergers ($m/M > 0.3$) experienced by Milky Way size dark matter halos should have been gas-rich, and that gas-rich mergers are increasingly common at high redshift. Though the frequency of major mergers into galaxy halos in our simulations greatly exceeds the observed early-type galaxy fraction, the frequency of *gas-poor* major mergers is consistent with the observed fraction of bulge-dominated galaxies across the halo mass range $M_{\rm DM} \sim 10^{11} - 10^{13} M_{\odot}$. These results lend support to the conjecture that mergers with high baryonic gas fractions play an important role in building and/or preserving disk galaxies in the universe. Secondly,

we find that there is a transition mass below which a galaxy's past major mergers were primarily gas-rich and above which they were gas poor. The associated stellar mass scale corresponds closely to that marking the observed bimodal division between blue, star-forming, disk-dominated systems and red, bulge-dominated systems with old populations. Finally, we find that the overall fraction of a galaxy's cold baryons deposited directly via major mergers is significant. Approximately $\sim 20-30\%$ of the cold baryonic material in $M_{\rm star} \sim 10^{10.5} M_{\odot}$ ($M_{\rm DM} \sim 10^{12} M_{\odot}$) galaxies is accreted as cold gas or stars via major mergers since $z = 2$, with most of this accretion in the form of cold gas. For more massive galaxies with $M_{\rm star} \sim 10^{11} M_{\odot}$ ($M_{\rm DM} \sim 10^{13} M_{\odot}$) the fraction of baryons amassed in mergers since $z = 2$ is even higher, $\sim 40\%$, but most of these accreted baryons are delivered directly in the form of stars. This baryonic mass deposition is almost unavoidable, and provides a limit on the fraction of a galaxy's cold baryons that can originate in cold flows or from hot halo cooling.

4.2 Introduction

In the cold dark matter (CDM) model of structure formation, major galaxy mergers are believed to play an important role in determining a galaxy's morphology (e.g. Toomre & Toomre, 1972; Barnes & Hernquist, 1996; Robertson et al., 2006a,b; Burkert et al., 2008), as well as triggering star formation and AGN activity (e.g. Mihos & Hernquist, 1996; Heckman et al., 1986; Springel et al., 2005a; Cox et al., 2008), while minor mergers may help explain the origin of thick disks and extended diffuse light components around galaxies (Barnes & Hernquist, 1996; Kazantzidis et al., 2008; Purcell et al., 2007; Younger et al., 2007; Purcell et al., 2008; Villalobos & Helmi, 2008; Kazantzidis et al., 2009). More than simply triggering star formation in existing gas and altering existing galaxy morphologies, mergers deliver new stars and additional

fuel for star formation, and thereby contribute to baryonic acquisition of galaxies over their histories. That mergers contribute significantly to many aspects of galaxy formation is now fairly well accepted, however there are lingering concerns that mergers are too common in CDM to explain the prominence of thin disk-dominated galaxies in the local universe (e.g. Toth & Ostriker, 1992; Walker et al., 1996; Stewart et al., 2008; Purcell et al., 2009; Bullock et al., 2009b, and references therein). Here we explore the baryonic content of these predicted mergers and the potential ramifications of gas-rich and gas-poor mergers on galactic morphological evolution.

The baryonic delivery of material into galaxies via major mergers touches on a broader question in galaxy formation: how do galaxies get their baryons? In recent years, studies motivated by hydrodynamic simulations have placed a growing emphasis on the importance of smooth gas accretion via "cold flows." These cold flows constitute streams of cold gas flowing along filamentary structures (particularly at high redshift) with sufficiently high densities to penetrate into a halo's central region without heating the gas to the virial temperature (e.g. Birnboim & Dekel, 2003; Kereš et al., 2005; Dekel & Birnboim, 2006; Kereš et al., 2009; Dekel et al., 2009; Brooks et al., 2009; Agertz et al., 2009). These simulations demonstrate a characteristic halo mass scale ($\sim 10^{12} M_{\odot}$) below which cold streams are the dominant mode of gas accretion, and above which gas cooling directly from shock-heated (hot mode) material dominates.

Though there has yet to be any observational evidence that cold flows actually occur in nature, the possibility is well motivated by theory and is suggestive of a number of interesting scenarios for galaxy assembly. One particularly interesting idea is that flows of cold gas are vital to the formation of disk galaxies at high redshift $z \gtrsim 1$ (Dekel et al., 2009). Still, even if disks were built at high redshift via streams of cold gas, we can return to the issue of disk *survival* raised above. How do observed populations of disk galaxies at high redshift (e.g. Wright et al., 2009, at $z \sim 1.6$)

survive subsequent mergers and remain disk-dominated by $z = 0$?

In Chapter 2 we studied the merger histories of Milky Way-size dark matter halos within a cosmological N-body simulation and found that approximately 70% should have accreted an object with more than twice the mass of the Milky Way disk ($m > 10^{11} M_{\odot}$) in the last 10 Gyr. In order to achieve the $\sim 70\%$ disk-dominated fraction that has been observed in Milky Way-sized halos (Weinmann et al., 2006; Park et al., 2007; Choi et al., 2007; Weinmann et al., 2009), mergers involving $> 1/3$ mass-ratio events must *not always* destroy disks. Adding to the associated concern, Purcell, Kazantzidis, and Bullock (2008b) performed focused numerical experiments to study the impact of $m = 10^{11} M_{\odot}$ encounters onto fully-formed Milky-Way type thin *stellar* disks and concluded that *thin* (~ 400 pc) dissipationless stellar disks do not survive these (presumably common) encounters.

One possible solution appeals to the role of cold gas in mergers. Focused merger simulations in the past few years have begun to suggest that sufficiently gas-rich mergers may help build angular momentum in the central galaxy, while feedback physics prevents the gas from forming stars too quickly, resulting in a disk-dominated merger remnant (Barnes, 2002; Springel & Hernquist, 2005; Robertson et al., 2006a; Brook et al., 2007b; Hopkins et al., 2009a; Robertson & Bullock, 2008). Encouragingly, cosmological simulations that have been successful in reproducing disk galaxies have also shown that gas-rich mergers have played an important role in the disk's creation (e.g. Brook et al., 2004; Governato et al., 2007, 2009), and there have been recent observations of late-type galaxies that may be in the process of reforming after a recent gas-rich major merger (e.g. Hammer et al., 2009b). Robertson & Bullock (2008) also showed that the disk-like merger remnants from gas-rich mergers are similar to the kinematically hot disks that have been observed at $z \sim 2$ (Förster Schreiber et al., 2006; Genzel et al., 2006; Shapiro et al., 2008).

Our goal in this work is to provide an empirically-motivated accounting for the expected gas and stellar content of mergers by relying on robustly determined dark matter halo merger rates. We aim first to determine whether gas-rich mergers are common enough to significantly alleviate the disk formation problem (a necessary but not sufficient condition in evaluating this scenario). We also aim to investigate the overall importance that mergers play in the acquisition of a galaxy's cold baryons.

While the merger histories of the dark matter halos are predicted accurately in dissipationless N-body simulations, the baryonic content of these mergers are much more difficult to predict from first principles. Indeed, an accurate *ab initio* accounting of the baryonic content of dark matter halos would require an overarching theory that solved all of the major problems in galaxy formation, including star formation, feedback, and the complicated interplay between mergers and galaxy assembly. In this work we chose to avoid the issues of galaxy formation physics entirely. Instead we adopt a semi-empirical approach that forces our model to match observations at various redshifts. First, we adopt the technique of monotonic abundance matching to assign stellar masses to dark matter halos (specifically following Conroy & Wechsler, 2009a). Second, we use observational relations between stellar mass and gas mass (e.g. McGaugh, 2005; Erb et al., 2006) to assign gas masses to our halos. We then combine these relations with the N-body halo merger histories described in Chapters 2 and 3 in order to determine the baryonic properties of mergers back to redshift $z \sim 2$. In §4.3 we discuss the details of our method. We present our primary results and discuss the implications for disk survival and the baryonic assembly of galaxies via mergers in §4.4. We summarize our main conclusions in §4.5.

4.3 Method

4.3.1 The Simulation

Our simulation contains 512^3 particles, each with mass $m_p = 3.16 \times 10^8 M_\odot$, evolved within a comoving cubic volume of $80h^{-1}$ Mpc on a side using the Adaptive Refinement Tree (ART) N-body code (Kravtsov et al., 1997, 2004). We assume LCDM cosmological parameters: $\Omega_M = 1 - \Omega_\Lambda = 0.3$, $h = 0.7$, and $\sigma_8 = 0.9$. The simulation root computational grid consists of 512^3 cells, which are adaptively refined to a maximum of eight levels, resulting in a peak spatial resolution of $1.2h^{-1}$ kpc (comoving). We give only a brief overview of the simulation here, as it has been reviewed more extensively in previous works. We refer the reader to Chapter 2, and references therein, for a more complete discussion.

Field dark matter halos and subhalos are identified using a variant of the bound density maxima algorithm (Klypin et al., 1999a). A *subhalo* is defined as a dark matter halo whose center is positioned within the virial radius of a more massive halo, whereas a *field halo* does not. The virial radius is defined as the radius of a collapsed self gravitating dark matter halo within which the average density is $\Delta_{\rm vir}$ times the mean density of the universe. Under comparison to constructed mass functions, we have determined that our halo catalogs are complete to a minimum mass of $10^{10} M_\odot$, and our sample includes $\sim 17,000$ field halos at $z = 0$ in the mass range $M = 10^{11.2-13.2} M_\odot$. We use the same merger trees described in Chapter 2, constructed using the techniques described in Wechsler et al. (2002, 2006).

We present our results primarily in terms of the dark matter mass ratio between the two halos that are undergoing a merger, $(m/M)_{\rm DM}$, where we always define $m_{\rm DM}$ as the mass of the smaller dark matter halo (which we will sometimes refer to as the

satellite halo) just *prior* to entering the virial radius of the larger one, and $M_{\rm DM}$ is the mass of the larger dark matter halo (also referred to as the *host* halo) at this infall epoch. Thus, $M_{\rm DM}$ does not incorporate the mass $m_{\rm DM}$, and $(m/M)_{\rm DM}$ has a maximum value of 1.0. However, we also present results in terms of the *stellar* mass ratio of the central galaxies within merging halos, or the mass ratio between the *total* baryonic mass of these central galaxies (stellar mass plus gas mass). We refer to the dark matter, stellar, and galaxy (baryonic) mass ratios as $(m/M)_{\rm DM}, (m/M)_{\rm star}, (m/M)_{\rm gal}$, respectively. Independent of the mass ratio definitions above, we always refer to a merger ratio of $m/M > 0.3$ as a *major merger*. For the sake of comparison to our past work, we emphasize that in Chapter 2, we considered two definitions of merger ratio. The first (written as m/M_0 in that chapter) referred to the ratio of the satellite mass at infall m to the final dark matter halo mass M_0 at $z = 0$. This is *not* the ratio we are using here. The mass ratio definition we adopt here is more standard and refers always to the mass ratio at the redshift z of accretion (m/M_z in the notation of Stewart et al. 2008).

In order to provide robust results, we define a merger to occur once the smaller halo crosses within the virial radius of the larger halo and becomes a subhalo, as the subsequent orbital evolution of each subhalo will depend on the baryonic distribution within both halos. We emphasize that for the major mergers we consider in this chapter, the dynamical friction decay timescales are expected to be short (comparable to the halo dynamical timescale) for typical orbital parameters (Boylan-Kolchin et al., 2008). Since only $\sim 5\%$ of $10^{12} M_{\odot}$ halos have experienced a major merger in the past halo dynamical time at $z = 0$ (see Figure 4.4), most of these major mergers into the virial radius have had adequate time to impact the central galaxy and do not survive as distinct substructure by $z = 0$. For a more in-depth comparison between merger rates into the virial radius and the rate at which accreted satellites are "destroyed" in this simulation (i.e. once they lose 90% of their infall mass) we refer the reader to

4.3.2 Assigning Stars

One particularly simple, yet surprisingly successful approach for assigning galaxies to dark matter halos is to assume a monotonic mapping between dark matter halo mass $M_{\rm DM}$ and galaxy luminosity L (Kravtsov et al., 2004; Tasitsiomi et al., 2004; Vale & Ostriker, 2004; Conroy et al., 2006; Berrier et al., 2006; Purcell et al., 2007; Marín et al., 2008). Using this technique, provided we know $n_g(> L)$ (the cumulative number density of galaxies brighter than L) we may determine the associated dark matter halo population by finding the halo mass above which the number density of halos (including subhalos) matches that of the galaxy population, $n_h(> M_{\rm DM}) = n_g(> L)$.

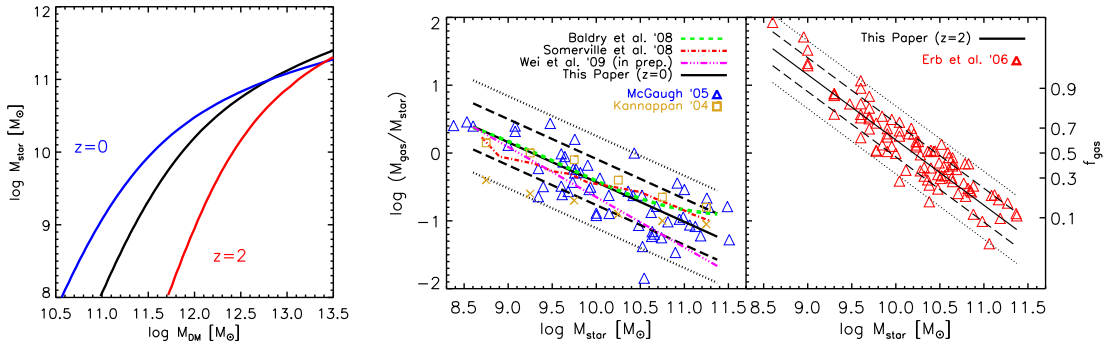

Figure 4.1: Two step method for assigning baryons to dark matter halos. *Left:* Stellar mass $M_{\rm star}$ versus dark matter halo mass $M_{\rm DM}$, for $z = 0, 1, 2$, based on abundance matching (Conroy & Wechsler, 2009a). *Middle(Right):* Power law fits to $M_{\rm gas}/M_{\rm star}$ as a function of stellar mass at $z = 0(2)$, with the corresponding gas fraction $f_{\rm gas} = M_{\rm gas}/(M_{\rm gas} + M_{\rm star})$ shown on the right axis. The symbols represent observational estimates from McGaugh, 2005 (entire sample: blue triangles), Kannappan, 2004 (average of blue galaxy sample, gold squares; average of red galaxy sample, gold X's), Baldry et al., 2008 (average: green short-dashed line), Somerville et al., 2008 (average: red dot-dashed line), Wei et al., 2009 (best fit to total sample: magenta dot-dot-dot-dashed line) and Erb et al., 2006 (entire sample: red triangles). The solid (black) line in each panel is the best-fit relation (Equation 4.1), while the long-dashed and dotted (black) lines represent the 1σ and 2σ scatter, respectively.

We use a similar approach, and instead assume a monotonic relationship between halo mass and stellar mass $M_{\rm star}$. Specifically, we adopt the relation found by Conroy & Wechsler (2009a) (hereafter CW08; interpolated from their data as shown in their Figure 2). Figure 4.1 (left panel) shows the resulting relation between stellar mass and dark matter halo mass for $z = 0, 1, 2$ (upper blue, middle black, lower red curves respectively) where $M_{\rm star}$ is the stellar mass of the central galaxy residing within a dark matter halo of mass $M_{\rm DM}$. We ignore scatter in this relationship for the results that follow, but we find that including a Gaussian scatter of 0.1 dex has no substantive effect our results.

Of course, a simple relation of this kind cannot be correct in detail, however, in an average sense, it provides a good characterization of the relationship between halo mass and galaxy stellar mass that must hold in order for LCDM to reproduce the observed universe. Moreover, by adopting it we insure that our model self-consistently reproduces the observed stellar mass function of galaxies out to $z \sim 2$. We cannot use this method to explore merger rates as a function of stellar mass beyond $z \sim 2$ because the stellar mass function is poorly constrained at higher redshifts. We refer the reader to Marchesini et al. (2009) for a detailed investigation of random and systematic uncertainties in computing the stellar mass function at $1.3 < z < 4.0$ (e.g. the impact of different SED-modeling assumptions, cosmic variance, and photometric redshift errors).

4.3.3 Assigning Gas

In order to reasonably assign gas to the central galaxies within our halos, we quantify observationally-inferred relations between the ratio of cold gas mass to stellar mass ($M_{\rm gas}/M_{\rm star}$) as a function of stellar mass using the empirical results of McGaugh,

2005 (blue triangles, for disk-dominated galaxies at $z = 0$) and Erb et al., 2006 (red triangles, for UV-selected galaxies at $z \sim 2$), as shown in the middle and right panels of Figure 4.1. Though both of these samples are biased with respect to blue (gas-rich) galaxies, we argue below that by adopting these relations we are not strongly biasing our overall results.

As shown by the black solid lines in the right panels of Figure 4.1, the $z \sim 0$ and $z \sim 2$ cold gas fraction data can be characterized by a relatively simple function of stellar mass and redshift:

$$\frac{M_{\rm gas}}{M_{\rm star}} = 0.04 \left(\frac{M_{\rm star}}{4.5 \times 10^{11} M_{\odot}} \right)^{-\alpha(z)}, \tag{4.1}$$

where the gas fraction relation evolves and steepens with redshift as $\alpha(z) = 0.59(1 + z)^{0.45}$. Assuming a Gaussian scatter about the best-fit lines (independent of mass), we find that the scatter evolves with redshift as $\log_{10}[\sigma(z)] = 0.34 - 0.19 \log_{10}(1 + z)$, such that the correlation between the cold gas fraction and stellar mass is tighter at $z \sim 2$ than it is at $z = 0$. The black long-dashed and dotted lines in the right panels of Figure 4.1 demonstrate the 1σ and 2σ scatter, respectively. In order to assign gas content to our halos as a function of stellar mass, we draw randomly from a Gaussian distribution with the average value and standard deviation given by the above analytic characterizations of $M_{\rm star}(M_{\rm gas})$.

For comparison, the middle panel of Figure 4.1 also shows several additional observational estimates for the gas-fraction relation as a function of stellar mass. The gold squares and gold X's present the average relation measured by Kannappan (2004) for blue galaxies and red galaxies, respectively. The green short-dashed line shows the average (statistical) relation derived using a combination of published galaxy stellar mass functions and the observed stellar mass-metallicity relation by Baldry et al.

(2008), who used robust chemical evolution arguments to derive implied gas fractions as a function of stellar mass. Finally, the average results from direct measurements by (Wei et al., 2009, in preparation) are shown by the magenta dot-dot-dot-dashed line. For the sake of comparison, we show the *predicted* relation from the semi-analytic model of Somerville et al., 2008 (red dot-dashed line). While we do not utilize these additional data sets in *constructing* our fitting function, they conform well to our average relation and certainly lie within the 1σ scatter of our fit to the McGaugh (2005) data (with the exception of low-mass red galaxies from Kannappan, 2004; see discussion below). We also note that the cold gas fractions derived by Wright et al. (2009) for six galaxies at $z \sim 1.6$ are also consistent with the evolution in our fit, with every galaxy in their sample falling within our 2σ scatter. Their sample does have a slightly higher average gas fractions at fixed $M_{\rm star}$ than our adopted relation, but the discrepancy is not significant given the small-number statistics. We have also compared our fit to the 34 galaxies at $z \simeq 0.6$ studied in Hammer et al. (2009a), in which the authors use K-band magnitudes to estimate total stellar mass via the methodology of Bell et al. (2003), and assume the Schmidt-Kennicutt law to derive gas masses from star formation rates. Encouragingly, 26 of their galaxies ($\sim 75\%$) fall within the 1σ contours of our best-fit at this redshift, with all 34 of them within 2σ.

The fact that we have fit our $z = 0$ relation to disk-dominated galaxies introduces a potential worry about applying the relation to every galaxy halo in our simulation, including ones that presumably host massive (spheroidal) galaxies. However, it is unlikely that this bias will drastically affect our results, primarily because the gas fractions in the adopted relation are only appreciable ($\gtrsim 0.5$), in the smallest galaxies (at $z = 0$) with $M_{\rm star} \lesssim 10^{10.5} M_{\odot}$ – the stellar mass regime that is known to be dominated by disk-dominated galaxies (see, e.g., the left panel of Figure 4.2). For larger galaxies, it is reassuring to note that the average relation for the red galaxy

sample from Kannappan (2004) lies within our adopted σ scatter and is in relatively good agreement with the other (disk-selected) observations. It is only for *less* massive galaxies (a regime where blue disk galaxies dominate the total population anyway) where the red galaxy sample of Kannappan (2004) becomes significantly discrepant from our fiducial relation. Finally, even if our fiducial relation is biased to be slightly high for massive galaxies, the gas fractions are already small enough that we would never classify them as "gas-rich" in our discussions below.

A similar point of concern may be applied to the Erb et al. (2006) data at $z \sim 2$. These galaxies were selected based on UV luminosity and thus constitute an actively star-forming population. However, there is a good deal of evidence that UV luminosity is tightly correlated with total stellar mass (or halo mass) at $z \gtrsim 2$ (see e.g., discussion in Conroy et al., 2008, and references therein). For example, galaxies with higher UV luminosities at $z \sim 2$ are more strongly clustered (Adelberger et al., 2005), suggesting that they reside within more massive dark matter halos. In addition, the UV and V-band luminosity functions of galaxies at $z \sim 3$ are in relative agreement, producing similar number densities for $\sim L^*$ galaxies (Shapley et al., 2001; Sawicki & Thompson, 2006; also see Table 3.2, and discussion, in Chapter 3). As such, it is reasonable to consider a galaxy sample selected on UV luminosity to contain a fairly representative sample of bright galaxies at $z \sim 2$.

We also note that the gas estimates we adopt from Erb et al. (2006) assume the global Schmidt law of Kennicutt (1998): $\Sigma_{\rm SFR} \propto \Sigma_{\rm gas}^{1.4}$. Both observations and recent hydrodynamic simulations have suggested that while this relation is tightly correlated for *molecular* gas, it may underestimate the *total* gas content, especially for galaxies where the fraction of gas in molecular form is not uniform (e.g. Wong & Blitz, 2002; Robertson & Kravtsov, 2008; Gnedin et al., 2009). As a consequence, the gas fraction estimates from Erb et al. (2006) may represent a lower limit, such that the evolution

of gas fraction with redshift may actually be *steeper* than our adopted relation. Insofar as issues of gas accretion and disk survival are concerned, our relation may be considered a conservative lower limit on the estimated gas content of our galaxies.

Finally, there has been some discussion in the literature that the stellar initial mass function (IMF) may evolve systematically to become more top heavy at high redshift in galaxies with extremely low metallicities (e.g. Lucatello et al., 2005; Tumlinson, 2007; van Dokkum, 2008; Komiya et al., 2008). This evolution in the IMF has not been corrected for in our adopted mapping between halo mass and stellar mass. While we do not expect this to significantly affect our results, including this evolution of the IMF would decrease our stellar mass estimates at fixed halo mass—which would, in turn, *increase* our estimated gas fractions. As such, so far as issues of gas accretion and disk survival are concerned, the results we present are a conservative lower limit.

With the above qualifications in mind, we now turn to the implications of this empirically-motivated stellar mass and gas mass assignment prescription.

4.4 Results and Implications

4.4.1 Galaxy Morphology

We start by investigating the merger histories of $z = 0$ dark matter halos. The solid black line in the left panel of Figure 4.2 shows the fraction of dark matter halos that have experienced at least one major dark matter merger with $(m/M)_{\rm DM} > 0.3$ since $z = 2$ as a function of dark matter halo mass (lower axis label). Equivalently, the merger fraction as a function of galaxy stellar mass can be seen by focusing on the upper axis label. Compare this result to the black squares, which show the early-type

fraction for SDSS galaxies as a function of central halo mass as derived by Weinmann et al. (2006; with "early-type" based on galaxy color and specific star formation rate) [1]. Also compare to the early-type fraction for SDSS galaxies as a function of halo mass, where "early-type" is defined by the concentration parameter ($C > 3$), shown as the black crosses, from Weinmann et al. (2009) (We will refer to these two results as W06 and W09, respectively). Clearly the fraction of halos with major mergers greatly exceeds the early-type fraction at low masses.

Consider now the likely baryonic makeup of these mergers. The (blue) dotted line shows the fraction of halos that have experienced a *gas-rich* major merger since $z = 2$ and the (red) dashed line shows the fraction of halos with at least one *gas-poor* merger. In our fiducial case, we define a merger to be gas-rich if both the central galaxy *and* the infalling satellite galaxy have more baryonic mass in the form of gas than in stars: $f_g \equiv M_{\rm gas}/(M_{\rm gas} + M_{\rm star}) > 50\%$. Similarly, gas-poor mergers are defined such that each of the progenitors has $f_g < 50\%$. The shading of the red and blue bands correspond to varying the definition of gas-rich from $f_g > 30\%$ to $f_g > 70\%$. [2]

Remarkably, if one makes the simplistic assumption that only gas-poor mergers generate early-type galaxies (red dashed line) and gas-rich mergers preserve disks, then the observed SDSS relation from W06 and W09 is reproduced fairly well. Specifically,

[1] Note that in W06, they divide galaxies into three categories instead of two; early-type, late-type and intermediate-type. In order to compare our simple bimodal model to their findings, we count half of their intermediate-types as early-type, and half as late-type.

[2] Because the morphological impact of a mixed merger (where one galaxy is gas-rich and one is gas-poor) is largely unclear, we choose to focus on the extreme cases where both are either gas-rich or gas poor, and to leave a more detailed exploration of mixed mergers for future work. This means that the combined gas-rich fractions and gas-poor fractions in Figure 4.2 need *not* equal the total merger fraction, which includes all major mergers regardless of baryonic content. However, because a galaxy's gas fraction is a strong function of halo mass at fixed redshift (and because we define a strict cutoff between gas-rich and gas-poor based on gas fraction) we find that mixed mergers are less frequent than mergers between two gas-poor or two gas-rich systems. If the larger galaxy in a major merger is gas-rich (by our definition), then the smaller galaxy is most likely gas-rich as well. Conversely, if the smaller galaxy in a major merger is gas-poor, then the larger galaxy is most likely also gas-poor. While there does exist a characteristic mass scale for which mixed mergers become a significant portion of the overall merger fraction, even at this special mass scale they still only constitute about half of all mergers (see Figure 4.4, discussion in §4.4.3).

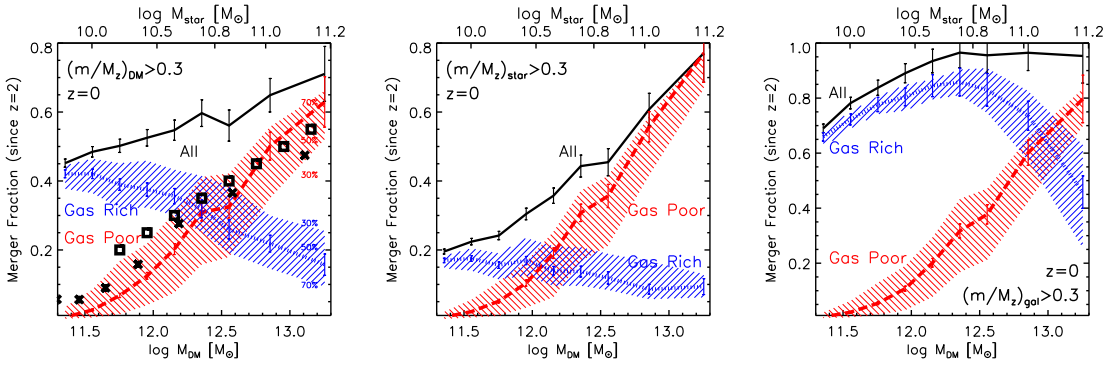

Figure 4.2: Fraction of dark matter halos with at least one major merger since $z = 2$, as a function of host halo mass $M_{\rm DM}$ (lower axis) and stellar mass $M_{\rm star}$(upper axis), for varying definitions of 'major merger.' *Left:* Major merger defined by the ratio of dark matter halo masses, $(m/M)_{\rm DM}$. The black squares and crosses in this figure show the observed early-type fraction as a function of halo mass from Weinmann et al. (2006, 2009). *Middle:* Major merger defined by the ratio of the stellar masses in each central galaxy, $(m/M)_{\rm star}$. *Right:* Major merger defined by ratio of the total baryonic mass of the central galaxies, $(m/M)_{\rm gal}$. In each panel, the solid (black) line shows the total merger fraction. The dashed (red) line shows the merger fraction while *only* considering mergers between two halos that *both* contain gas-poor central galaxies ($f_g < 50\%$). The dotted (blue) line shows only mergers for which both galaxies are gas-rich ($f_g > 50\%$). The shaded regions surrounding the red and blue lines represent the impact of varying our distinction between gas-rich and gas-poor from 30% to 70%. The bottom axis shows the same range in halo mass in each panel, while the corresponding stellar (or baryonic) mass of the central galaxy is shown on the top axis. Note that the range in y-values in the right panel is larger than the left and middle panels. Error bars are Poissonian based on the number of host halos and the total number of mergers, and do not include possible errors in assigning stars and gas to halos (though we do account for *scatter* in the $M_{\rm star}(M_{\rm gas})$ relation, see §4.3.2, 4.3.3).

we find that the fraction of halos with a disk-destructive merger increases from only $\sim 15\%$ at $10^{12} M_\odot$ to $\sim 55\%$ at $10^{13} M_\odot$, in remarkably good agreement with W06 and W09. Not only does this agreement provide a possible solution to disk survivability within Milky Way-sized halos, but it also implies that the gas-poor merger history of a dark matter halo may be closely tied to the halo mass–morphology relation (across this range in halo mass). Although halo merger rates have been shown to depend strongly on environment (Fakhouri & Ma, 2009), suggesting a possible connection to the morphology–density relation of galaxies, we see in Figure 4.2 that the overall halo

major merger rate (solid black line) is *not* steep enough to account for the observed change in morphological fraction with halo mass.

It is also worth mentioning that the implied transition between mostly gas-rich and mostly gas-poor mergers occurs at a characteristic mass $M_{\rm star} \simeq 5 \times 10^{10} M_{\odot}$ (or equivalently $M_{\rm DM} \simeq 2 \times 10^{12} M_{\odot}$), which is close to the characteristic bimodality scale that separates blue, star-forming, disk-dominated systems and red, bulge-dominated systems with old populations (typically $M_{\rm star} \sim 3 \times 10^{10} M_{\odot}$, see e.g. Kauffmann et al., 2003; Baldry et al., 2004; Kannappan, 2004; Baldry et al., 2006; Cattaneo et al., 2006; Dekel & Birnboim, 2006).

Of course, for detailed treatments of galaxy morphology, this model is too simplistic. The inclusion of gas-richness in the efficacy of major mergers to disrupt morphology seems to greatly relieve the problem of disk stability, and the agreement between the observed early-type fraction from SDSS and the fraction of halos with at least one gas-poor major merger is quite remarkable. However, this is only a first step in understanding the distribution of galaxy morphologies. In detail, nothing we have investigated here can explain the prominence of "bulgeless" galaxies, as simulated gas-rich major mergers lead to galaxies with noticeable bulges and disks that are thicker and hotter than the Milky Way. Even cosmological simulations that produce thin disk galaxies (e.g. Governato et al., 2009) require significant smooth gas accretion from the hot halo after the most recent gas-rich merger in order to form a thin disk. Such intricate details are beyond the scope of this chapter, as we are primarily concerned with providing the most robust predictions possible, only using N-body dark matter halo merger trees and empirical relations between $M_{\rm DM}$, $M_{\rm star}$, and $M_{\rm gas}$ to determine gas-rich and gas-poor merger statistics.

Any model that predicts detailed bulge-to-disk mass ratios or estimates the thinness or thickness of the galactic disk resulting from a merger event must require further

assumptions about the detailed morphological effects of any given merger event, which are still relatively uncertain. We refer the reader to Hopkins et al. (2009b) for a more detailed galaxy formation model that generates bulge and disk mass estimates due to merger events as a function of merger mass ratio, gas fraction and orbital parameters. Using a semi-empirical assignment of gas and stars to dark matter halos similar (but distinct) from our own treatment, they find that cosmologically motivated merger trees lead to consistent distributions of B/T (bulge mass to total galaxy mass) values as a function of halo mass and redshift.

4.4.2 Alternative definitions for major merger

The middle and right panels of Figure 4.2 explore how the implied merger fraction trends change when one chooses to define major mergers using the stellar-mass ratio, $(m/M)_{\rm star} > 0.3$, and total baryonic galaxy mass ratio, $(m/M)_{\rm gal} > 0.3$, respectively, rather than the total mass ratio in dark matter. Clearly, the implied trends between merger fraction and galaxy halo mass depend sensitively on whether dark matter mass ratios, stellar mass ratios, or baryonic galaxy mass ratios are considered (also see Maller, 2008; Stewart, 2009). As seen by the solid black line in the middle panel, high stellar-mass ratio events are rare in small galaxy halos and common in high mass halos. This follows directly from the fact that low-mass halos tend to have a higher stellar-mass to dark matter mass ratios (see Figure 4.1). The trend changes dramatically when the full baryonic mass of the galaxy is considered in the ratio (right panel). In this case, even small galaxy halos are expected to have had common mergers with galaxies of a comparable total baryonic mass (note that the range of the vertical axis has changed in the right-hand panel). It is clear from this comparison alone that most of the major mergers experienced by small galaxies must be gas-rich.

We note that the fraction of systems that have experienced at least one gas-rich merger (and consequently, the total merger fractions as well) show qualitatively different behavior depending on these definitions. Gas-rich *halo* mergers ($(m/M)_{\rm DM} > 0.3$) are relatively frequent for $M_{\rm DM} = 10^{11.5} M_\odot$ systems (40% since $z = 2$), with a smoothly declining merger fraction for increasing halo mass (roughly linear in $\log M_{\rm DM}$), while the gas-rich *stellar* merger fractions decline in a qualitatively similar fashion but are universally less common, with merger fractions $< 20\%$ for $M_{\rm DM} = 10^{11.5} M_\odot$. In contrast, the fraction of halos with at least one major *galaxy* merger ($(m/M)_{\rm gal} > 0.3$) shows completely different behavior, with extremely high fractions ($40 - 90\%$) and non-monotonic evolution with $\log M_{\rm DM}$ (with a maximum value at $M_{\rm DM} \sim 10^{12.2} M_\odot$).

The behavior of *gas-poor* merger fractions, on the other hand, remains remarkably similar in each case. Regardless of these three merger ratio definitions, the fraction of halos which have experienced a gas-poor major merger is negligible at small halos masses ($M_{\rm DM} \sim 10^{11.5} M_\odot$) and increases roughly linearly with $\log M_{\rm DM}$ to a fraction of $65 - 75\%$ at $M_{\rm DM} = 10^{13.2} M_\odot$. Because these gas-poor merger fractions appear somewhat independent of the merger ratio definition used (and they remain consistent with observed morphological fractions as a function of halo mass) we again suggest that a dark matter halo's gas-poor merger history may be a particularly useful tracer of galaxy morphology—more so than the merger history of all mergers.

One might be tempted to conclude that the total major merger rate in the middle panel (major stellar mergers) is sufficiently steep to account for the change in morphological fraction with halo mass reported by W06 and W09, without bothering to account for the gas content of these mergers. Encouragingly, only $\sim 30\%$ of $10^{12} M_\odot$ halos have experienced a $(m/M)_{\rm star} > 0.3$ merger since $z = 2$. It is important to note that even relatively minor, $(m/M)_{\rm DM} = 0.1$ dark matter halo mergers with *negligible* stellar content $(m/M)_{\rm star} \sim 0.03$ are capable of heating and thickening a galactic

disk beyond the properties of the Milky Way (Purcell et al., 2009). (However, a galaxy need not contain a disk as thin as the Milky Way in order to be classified as late-type in either W06 or W09, so systems similar to those studied in Purcell et al. (2009) would still be labeled as "surviving" disks in our simple model.) Still, it is important to keep in mind that major dark matter mergers do not necessarily correspond to major stellar mergers, especially at halos less massive than the Milky Way (see e.g. Maller, 2008; Stewart, 2009). For example, consider a $M_{\rm star} = 10^{10} M_{\odot}$ galaxy experiencing a stellar merger at $z = 0, 1, 2$ that is just below our definition of "major," with $(m/M)_{\rm star} = 0.2$. The corresponding dark matter halo ratios of these merger events will be $\sim 0.4, 0.4$, and 0.5, respectively. Even if we consider a more minor stellar merger, with $(m/M)_{\rm star} = 0.1$ at these redshifts, such merger events still correspond to major dark matter mergers, with dark matter halo ratios of $\sim 0.3, 0.3, 0.4$, respectively. If gas content is ignored, a substantial fraction of these events will easily be capable of destroying disk morphologies altogether (not simply thickening and heating the existing disk). Still, these mergers would be classified as "minor" stellar mergers, with a stellar merger ratio < 0.3, even while the total dark matter mass ratios may approach $2:1$. In addition, the opposite effect occurs at large galaxy masses. For example, a major stellar mergers into a $M_{\rm star} = 10^{11} M_{\odot}$ galaxy with a $(m/M)_{\rm star} = 0.3$ at $z = 0$ only corresponds to a dark matter halo mass ratio of ~ 0.1, which is less likely to be morphologically destructive. This is why the total merger fraction in the middle panel (at high galaxy mass) exceeds that in the left panel: major stellar mergers only correspond to minor dark halo mergers at this mass regime. Thus, we conclude that the major stellar merger fractions in the middle panel likely present an uneven, and potentially incomplete picture of possible means of disk destruction via mergers.

4.4.3 Gas Delivery Via Mergers

In Chapter 3, we discuss the observational implications of two well-known consequences of galaxy halo mergers: merger-induced starbursts and morphological disturbance (also, Stewart et al., 2009a). A third potentially important consequence of mergers is the direct, cumulative deposition of cold baryons (gas and stars) onto galaxies. We are now concerned with the exact baryonic content of each merging galaxy, whereas we have previously only focused on whether or not a given halo lies above or below an arbitrary gas fraction threshold. As such, we impose an additional constraint to our method for assigning gas (as outlined in §4.3). Specifically, when estimating the gas content of halos at high redshift, blindly extrapolating equation 4.1 to arbitrarily small stellar masses sometimes results in more baryons in a given halo than the universal baryon fraction of matter in the Universe. This is an unphysical situation that arises from extrapolation far beyond the regime where $M_{\rm gas}(M_{\rm star})$ is well-constrained. In order to avoid unphysically high gas content of low mass halos at high redshift, we present two models for assigning upper limits to the gas content of low stellar mass galaxies. In the model A (left panel of figure 4.3), we set an upper limit on equation 4.1 such that $M_{\rm gas} + M_{\rm star} \leq f_b M_{\rm DM}$, where $f_b = 0.17$. In model B, we define the upper limit by the ratio of gas mass to halo mass: ($f_{lim} \equiv M_{\rm gas}/M_{\rm DM}$ at $M_{\rm star} = 3 \times 10^8 M_\odot$). For galaxies with stellar mass lower than this threshold, we then set $M_{\rm gas} = f_{lim} M_{\rm DM}$. This model, which always assigns less (or equal) gas per galaxy than the first model, is used to construct the right panel of figure 4.3.

In both panels of Figure 4.3, the solid black lines show the fraction of a central galaxy's current ($z = 0$) baryonic mass ($M_{\rm gal} = M_{\rm gas} + M_{\rm star}$) acquired directly via major mergers as a function of halo mass $f_{\rm merged} \equiv M_{\rm merged}/M_{\rm gal}(z = 0)$. Specifically, $M_{\rm merge}$ includes all of the baryonic mass in mergers obeying $(m/M)_{\rm DM} > 0.3$ since $z = 2$. Focusing on the left panel (model A: $M_{\rm gas} + M_{\rm star} \leq f_b M_{\rm DM}$) the first clear result is

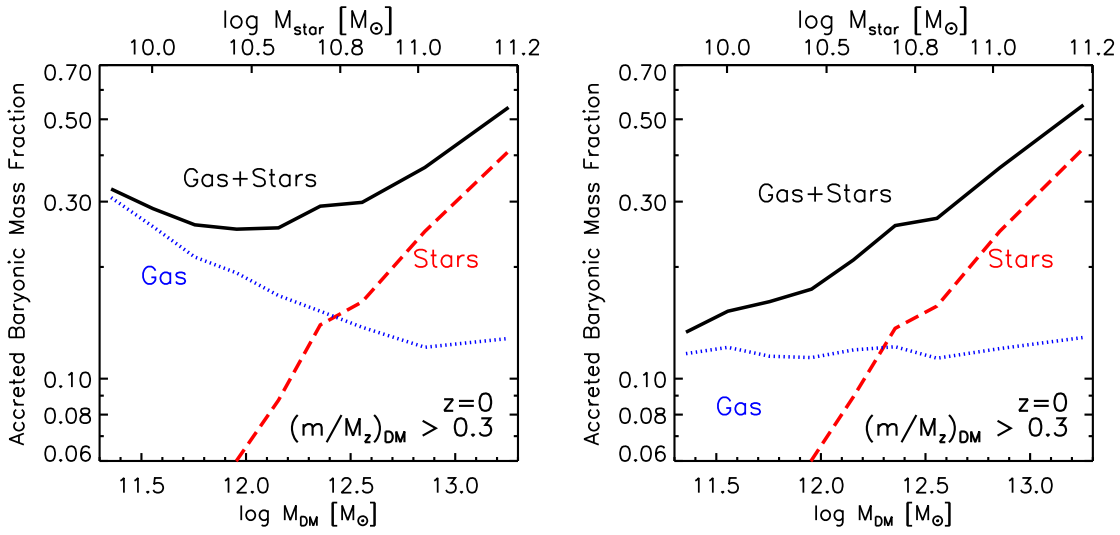

Figure 4.3: The fraction of a $z = 0$ galaxy's total baryonic mass that was accreted directly via major mergers or moderately sized mergers since $z = 2$, as a function of halo mass. *Left:* model A, in which we assign gas by Equation 4.1, but impose an upper limit due to the universal baryon fraction, such that $M_{\rm gas} + M_{\rm star} \leq f_b M_{\rm DM}$. *Right:* model B, in which we assign gas by Equation 4.1, but impose an upper limit such that $M_{\rm gas} \leq f_{lim} M_{\rm DM}$, where f_{lim} at each redshift is the value of $M_{\rm gas}/M_{\rm DM}$ when $M_{\rm star} = 3 \times 10^8 M_\odot$ at that redshift. In both panels, the dotted (blue) and dashed (red) lines show the accreted baryonic mass fraction from gas and stars, respectively, while the solid (black) line shows the total.

that the merged baryonic fraction is significant: $\sim 30-50\%$ of the final galaxy mass is accreted directly in the form of major mergers. Given the effectiveness of dynamical friction in major mergers, we expect the majority of the accreted baryonic material in these events to be deposited in the central galaxy itself. In principle, this limits the fraction of a galaxy's baryons that can be acquired by direct hot halo cooling, cold flows, or minor mergers to $50-70\%$, depending on the halo mass of interest. Of course, (gaseous) baryons deposited via major mergers could in principle be blown out by energetic feedback, but all in all, this result on major merger deposition (much like known results on cold flows) would seem to make the 'overcooling' problem in galaxy formation more difficult. While the fraction of baryons accreted directly as cold gas via major mergers is less substantial in the right panel (model B: $M_{\rm gas} \leq f_{lim} M_{\rm DM}$),

we still find significant accretion: $15-50\%$ of the final galaxy mass.

The dotted (blue) and dashed (red) lines in Figure 4.3 separate the total baryonic accretion fraction from major mergers into contributions from gas and stars, respectively (this is not a division between gas-rich and gas-poor mergers as before, but rather an integrated accounting of all material regardless of the makeup of the merged progenitors). We see that in both models, the baryonic accretion onto smaller halos ($M_{\rm DM} \lesssim 10^{12.3} M_{\odot}$) is typically dominated by the gas content of the infalling galaxies, while the baryonic makeup of merged material into more massive systems is dominated by the infalling galaxies' *stellar* content. For Milky Way-size systems ($M_{\rm DM} = 10^{12} M_{\odot}$), we find in model A (B) that typically $\sim 30\%(20\%)$ of a galaxy's baryonic content was accreted in the form of gas and stars directly via major mergers, with most of this accretion dominated by cold gas. In both models, more massive systems ($M_{\rm DM} = 10^{13} M_{\odot}$) typically accrete $\sim 30\%(10\%)$ of their baryons as stars (gas) via major mergers, with no noticeable discrepancies between the two models. Though not shown, we find that most baryonic accretion from major mergers ($70-80\%$ of stars, $50-70\%$ of gas) occurred at later times.

How do our results change if we include more minor mergers in our accounting? If we count up all of the baryonic acquisition in mergers larger than $(m/M)_{\rm DM} > 0.1$, we find that the mass fraction accreted as stars is boosted by a factor of of ~ 1.5 from the panels shown, while the accreted gas is amplified by a factor of ~ 1.7, both roughly independent of halo mass. We caution, however, that the importance of minor mergers in delivering baryons to central galaxies is significantly less clear than it is with major mergers. While the baryons associated with major mergers almost certainly become deposited directly onto the central galaxy (see e.g. the simulations of Purcell et al. 2008b) the ultimate fate of the baryons in minor mergers will depend sensitively on the orbital properties of the secondary and on the potential presence of

hot gas halo around the primary galaxy. Past work has demonstrated that the *stellar* material in minor mergers will likely contribute to extended diffuse light components like stellar halos or intracluster light (e.g., Bullock & Johnston, 2005; Purcell et al., 2007; Conroy et al., 2007; Purcell et al., 2008), but the destiny of accreted *gas* (which is the dominant component for galaxy halos) in these minor mergers is relatively unexplored. One possibility is that the gas in minor mergers is quickly liberated via ram pressure stripping (see, e.g. Grcevich et al., 2008) and that it either evaporates into the hot halo itself or eventually rains down onto the galaxy, possibly in the form of high-velocity clouds. These interesting possibilities are clearly beyond the scope of the present work but provide important avenues for future investigation.

The relation between gas mass and stellar mass below $M_{\rm star} = 3 \times 10^8 M_\odot$ remains relatively uncertain, making it impossible to know which panel of this figure is a more accurate representation of galaxy formation. In detail, we expect our two models to bracket reasonable expectations for the true relation between $M_{\rm star}$ and $M_{\rm gas}$ in this regime. Nevertheless, focusing on model A for the time being (left panel), we find it interesting that there appears to be a minimum in merged baryon fraction at the $M_{\rm DM} \sim 10^{12} M_\odot$ scale, which corresponds closely to the well-known mass scale of maximum galaxy formation efficiency ($\sim L_*$ in the galaxy luminosity function). Although it is unclear whether this minimum exists in reality, or is merely an artifice of the manner in which we have assigned gas, we speculate on a possible correspondence between galaxy formation efficiency and the merged baryon fraction. Specifically, a minimum in the merged baryon fraction naturally implies a maximum in the baryon fraction accreted via smooth gas accretion from the hot halo or from cold streams. We speculate that smooth gas accretion might allow for a higher efficiency in star formation than accreting large clumps of gas via major mergers, because gas-rich mergers are likely to trigger massive starbursts that may blow significant gas content out of the central galaxy. We also speculate that accretion of stars via mergers

may also be inefficient, since some fraction of a satellite galaxy's stars is likely to be distributed into the stellar halo before reaching the central galaxy within massive halos. If this is the case, that smooth gas accretion forms stars most efficiently, then it would be reasonable to expect a maximum in the baryon fraction of smoothly accreted gas to correlate with the maximum galaxy formation efficiency. However, we emphasize that this possible correlation between minimum merged baryonic fraction and maximum star formation efficiency is not a robust prediction of our model, but merely a speculation (for example, model B results in no such minimum in the merged baryonic fraction).

4.4.4 Redshift Evolution

While the cumulative fraction of halos that have *ever* experienced a gas-rich or gas-poor major merger (since $z = 2$) is the most pertinent question for morphological evolution and disk survivability (see §4.4.1), another point of interest is the redshift evolution of a more instantaneous measure of the merger rate of gas-poor and gas-rich mergers. Figure 4.4 shows the fraction of halos that have experienced at least one major merger with $(m/M)_{\rm DM} > 0.3$ in the past halo dynamical time, τ [3]. As in Figure 4.2, the solid (black) line shows the total merger fraction for dark matter halos, while the dotted (blue) and dashed (red) lines show the major merger fraction for gas-poor ($f_g < 50\%$) and gas-rich ($f_g > 50\%$) mergers, respectively. Because the quantitative values of these merger fractions depend sensitively on the merger timescale in question at each redshift, we choose to focus on two important *qualitative* results from this figure. We refer the reader to Chapter 3 for a more detailed discussion of the evolution of the halo merger rate (and merger fractions) with redshift, halo mass, and merger

[3] As in Chapter 3, in which we studied the evolution of the halo merger rate with redshift, we again adopt $\tau(z) = R/V \propto (\Delta_v(z)\,\rho_u(z))^{-1/2}$, such that the halo dynamical time evolves with redshift, but is independent of halo mass.

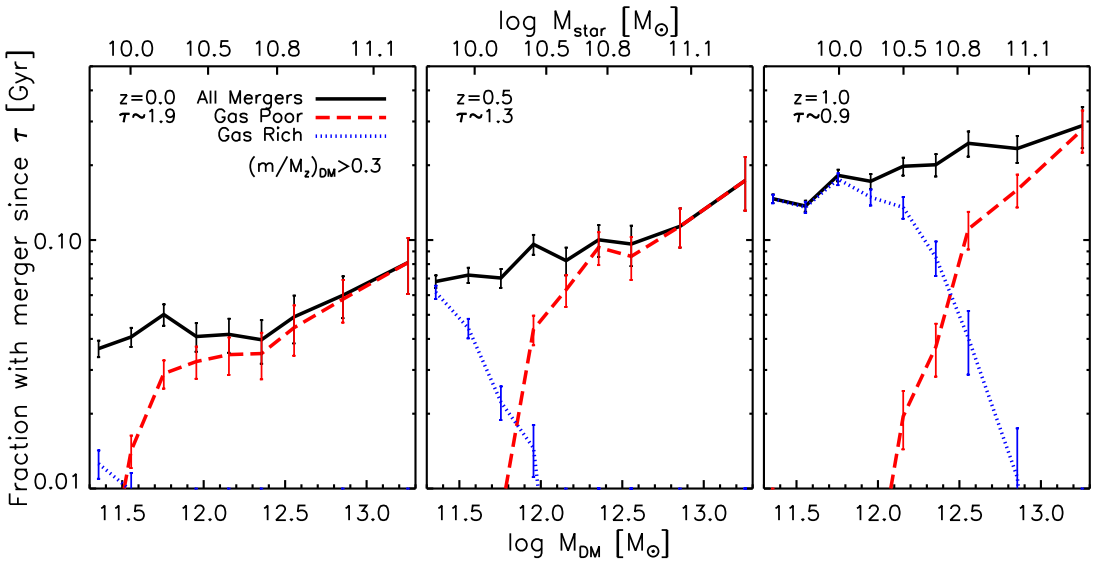

Figure 4.4: Major merger fraction within the past dynamical time of the halo, τ, as a function of halo mass. The solid (black) line shows the total merger fraction for dark matter halos (no baryons included). The dashed (red) line shows the merger fraction while only considering gas poor mergers ($f_g < 50\%$). The dotted (blue) line shows only gas-rich mergers ($f_g > 50\%$). The three panels show results for $z = 0$, $z = 0.5$, and $z = 1$, for which the halo dynamical time, $\tau \simeq 1.9, 1.3, 0.9$ Gyr, respectively. We primarily focus on the decomposition of these merger fractions into gas-rich and gas-poor mergers. We refer the reader to Chapter 3 for a detailed analysis of the dependence of dark matter of merger rates and merger fractions on redshift, halo mass, and mass ratio.

mass ratio (see also Fakhouri & Ma, 2009, for the effects of halo environment on the merger rate).

The first feature of note in this figure is the presence of a typical transition mass, $(M_t)_{\rm DM}$, such that most of the recent major mergers into halos less massive than $(M_t)_{\rm DM}$ are gas-rich, while most of the recent major mergers into halos more massive than $(M_t)_{\rm DM}$ are gas-poor. The existence of this transition mass is primarily due to the strong dependence of galaxy gas fractions on stellar mass (and thus, halo mass) at fixed redshift. In addition to creating this transition mass, the dependence of gas fraction on halo mass also results in a very limited mass range for which mixed mergers (where one galaxy is gas-poor and the other is gas-rich) constitute

a significant portion of all mergers (at most $\sim$ 50%). This effect is apparent in Figure 4.4 where the combined total of the gas-poor and gas-rich merger fractions fall significantly short of the total. Not unexpectedly, this range of importance for mixed mergers is centered on $(M_t)_{\rm DM}$.

The other important result from Figure 4.4 is that $(M_t)_{\rm DM}$ is more massive at higher redshifts, with $(M_t)_{\rm DM} \simeq 10^{11.4}, 10^{11.9}, 10^{12.8} M_\odot$ at $z = 0.0, 0.5, 1.0$, respectively. This arises naturally from the strong increase in galaxy gas fractions to higher redshift. The corresponding galaxy stellar mass transitions at $z = 0.0, 0.5$, and 1.0, are $(M_t)_{\rm star} \sim 10^{9.7}, 10^{10.3}, 10^{11.0} M_\odot$ (upper horizontal axis in Figure 4.4. Of course, the precise value of M_t at each redshift will depend to some degree on our definitions of "gas-rich" and "gas-poor," but the *existence* of this transition mass, and its qualitative evolution with redshift should be robust to changes in these definitions.

Consider recent major mergers into Milky-Way size $10^{12} M_\odot$ halos. At $z = 0$, mergers of this kind are very uncommon. Only $\sim$ 5% of Milky-Way size halos should have experienced a major dark matter accretion event with $(m/M)_{\rm DM} > 0.3$ in the last $\tau \sim 2$ Gyr. However, when these major mergers do occur at $z = 0$ they are very likely gas-poor ($\sim 0.04/0.05 = 80\%$ of the time). On the other hand major mergers are fairly common in $10^{12} M_\odot$ halos at $z \sim 1$, with $\sim$ 15% experiencing such a merger in the last $\tau \sim 1$ Gyr. Nevertheless, these higher redshift mergers are almost universally gas-rich. Under the presumption that gas-rich mergers do not destroy disk morphologies, the evolution of the merger rate with redshift and in the associated gas-rich transition mass makes it increasingly likely that major mergers *build* disk galaxies at high redshift rather than destroy them (c.f. Robertson et al. 2006a, Robertson & Bullock 2008). If we were to boldly extrapolate our trends to higher redshift, we would expect that nearly *all* major mergers into halos with $M_{\rm DM} < 10^{12} M_\odot$ should be gas-rich ($f_g > 50\%$) at $z > 1$.

Encouragingly, Lin et al. (2008) observe a similar redshift evolution between gas-rich and gas-poor mergers by studying the close-pair counts of galaxies from the DEEP2 Redshift Survey. While our definitions vary in detail from theirs (they divide galaxy pairs into wet and dry mergers based on galaxy colors, and bin their sample by total galaxy luminosity, while we use galaxy gas fractions to define gas-poor versus gas-rich mergers, and bin by galaxy stellar mass) they also find that at fixed luminosity (stellar mass) the percentage of major mergers that are dry (gas-poor) should decrease with increasing redshift, while the percentage of major mergers that are wet (gas-rich) should increase. We reserve a more detailed comparison to their results for a future study, but we find the qualitative agreement encouraging.

4.4.5 Comparison to Previous Work

Recent studies of galaxy formation at high redshift using hydrodynamic simulations have stressed the importance of smooth accretion of cold gas from filamentary streams. For example, Kereš et al. (2009) compared the accretion rate of gas onto galaxies via cold flows and via mergers, and found that at $z = 1 - 2$, only about half of all gas accretion (onto galaxies corresponding to $M_{\rm DM} \gtrsim 10^{11.3} M_{\odot}$) is in the form of mergers, (where gas from mergers was defined as any gas that was added to galaxies in dense baryonic clumps). Similarly, Dekel et al. (2009) found that half of cold gas infall onto massive $z = 2$ galaxies is acquired via mergers with $(m/M)_{\rm DM} > 0.1$, and the other acquired from cold flows. Indeed, even studies that focus primarily on the importance of galaxy mergers also note that smooth gas accretion is at least as dominant as galaxy mergers in the mass buildup of galaxies (e.g. Maller et al., 2006). Our results do not contradict these expectations. As demonstrated in Figure 4.3, we expect that $\sim 30 - 40\%$ of a typical galaxy's baryons should have been accreted directly via major mergers with $(m/M)_{\rm DM} > 0.3$. This leaves significant room for

cold-flow gas to contribute to the baryonic assembly of small galaxies and for cooling to contribute to the buildup of larger galaxies. Though, as mentioned above, we do expect that the percentage of merger-delivered baryons could rise to as much as $\sim 60\%$ if all of the baryonic material from $(m/M)_{\rm DM} > 0.1$ mergers is able to find its way into the central galaxy.

Brooks et al. (2009) used a high-resolution cosmological hydrodynamic simulation to study the gas accretion onto four disk galaxies within halos of masses $10^{10.7-12.7} M_{\odot}$, and also found that smooth accretion of gas (either shocked or un-shocked) dominates the mass buildup of their galaxies. When comparing smooth gas accretion to gas infall from mergers (using a generous definition of what qualifies as a merger) they found that $\sim$ 25% of the total gas infall into their Milky Way-size galaxy derives from mergers, with $\sim 10\%$ of the final stellar content at $z = 0$ being accreted directly as stars from mergers. While their detailed results (and definitions) differ slightly from our own, the rough consistency between their simulation and our own semi-empirical approach is quite encouraging.

One point of caution associated with the discussion of cold flows is that these predictions are based entirely on simulations that do not generally reproduce the observed baryonic mass function and stellar mass function of galaxies. It is possible that the cold flows are somehow restricted in the real universe in a way that solves the well-known over-cooling problem in galaxy formation. Due to the inherent difficulties in detecting cold filaments of gas locally and at high redshift, there has yet to be an observational confirmation of a star forming galaxy fueled by the smooth accretion of cold gas along filaments, as seen in hydrodynamic simulations. In contrast, our predictions for the accretion of stars and gas via major mergers is solidly normalized against observations, and is arguably inevitable in the context of LCDM merger histories. Of course, baryonic material (especially gas) that is delivered via major

mergers need not remain in the central galaxy indefinitely. Gas accreted either along cold flows or through major mergers may be subsequently expelled via supernovae or AGN feedback (e.g. Benson et al., 2003; Di Matteo et al., 2005; Springel et al., 2005a; Somerville et al., 2008). In this respect, Figure 4.4 represents an upper limit on the baryonic contribution from major mergers, with respect to the total amount of barons *currently* exist in the galaxy.

4.5 Conclusion

We have used dark matter halo merger trees from a large cosmology N-body simulation together with observationally-normalized relationships between dark matter halo mass, galaxy stellar mass, and galaxy gas mass to explore the baryonic content of galaxy mergers back to redshift $z = 2$. Though our adopted associations between halo mass and the baryonic content of galaxies cannot be precisely correct, it is almost certainly accurate in its scalings with halo mass and redshift, and has the added advantage that it is *independent of any uncertain galaxy formation physics*. Indeed, any self-consistent galaxy formation model that is set within the LCDM framework would certainly need to reproduce our gross baryonic assignments in order to reproduce the observed universe. Our main results based on this methodology may be summarized as follows:

1. The vast majority ($\sim 85\%$) of the major mergers experienced by Milky-Way size galaxies since $z = 2$ should have been gas-rich, and this fraction drops significantly towards higher mass systems (see Figure 4.2. Remarkably, the fraction of galaxies with gas-poor major mergers matches well to the observed fraction of bulge-dominated galaxies as a function of halo mass from $M_{\rm DM} = 10^{11}$ to $10^{13} M_{\odot}$.

2. Though *recent* major mergers are expected to be rare for small galaxies in the local universe, the recent mergers that do occur should typically be gas poor. At higher redshift, recent mergers become more common and the probability that such a merger is gas-rich also increases (see Figure 4.4). One can define a transition dark matter halo mass M_t, below which most of the recent major mergers are gas-rich and above which they are gas poor, and this transition mass increases with redshift: $(M_t)_{\rm DM} \sim 10^{11.4}, 10^{11.9}, 10^{12.8} M_\odot$ at $z = 0.0, 0.5, 1.0$. As a result, the vast majority of recent major mergers into galaxy-size $M_{\rm DM} < 10^{12} M_\odot$ dark matter halos are expected to be gas-rich at $z < 1$.

3. A significant fraction $(20 - 50\%)$ of the baryonic mass in field galaxies at $z = 0$ should have been deposited directly via major mergers since $z = 2$. For less massive galaxies, $M_{\rm DM} \sim 10^{11.5} M_\odot$, the vast majority of the merger-acquired baryons are gaseous, while in more massive galaxies $M_{\rm DM} \sim 10^{13} M_\odot$, major mergers bring in mostly stars (see Figure 4.3. For Milky Way-size systems, major mergers since $z = 2$ bring in $\sim 30\%$ of the galaxy's $z = 0$ baryonic mass, with most of this contribution in the form of gas.

Many of these conclusions lend support to the conjecture of Robertson et al. (2006a) and Brook et al. (2007a), who were the first to forcefully suggested a scenario where gas-rich mergers play an important role in building and stabilizing disk galaxies at high redshift. Though our conclusions are far from a sufficient test of this idea, we have demonstrated that gas-rich mergers should be common enough to make it viable for serious consideration.

Among our most interesting results is the similarity between our predicted gas-poor merger fraction with halo mass and the observed early-type galaxy fraction with halo mass (Figure 4.2, left panel). Of course, even if gas-rich mergers do preserve disks, there are many openings for concern. For example, the current presentation

leaves little room for the production of bulge-dominated systems by means *other* than major mergers. In an extreme yet illustrative example, Bournaud et al. (2007) used a suite of focused simulations to show that bulge-dominated galaxies may be formed by successive minor mergers. Disk galaxies can also grow massive bulges by secular processes (typically bulges formed in this way show kinematically distinct properties from classical bulges, and are referred to as "pseudobulges") (e.g. Courteau et al., 1996; Kormendy & Kennicutt, 2004; Kormendy & Fisher, 2005, 2008).

An interesting possibility in this context of disk survival and secular evolution is that we have been too conservative in our classification of 'gas-rich'. Our fiducial division between gas-rich and gas poor at $f_g = 50\%$ was motivated by the idealized simulations studied by Robertson et al. (2006a) and Hopkins et al. (2008). However Governato et al. (2009) used a cosmologically self-consistent hydrodynamic simulation to demonstrate the creation of spiral galaxy at $z = 0$ within a system that experienced a very major ($(m/M)_{\rm DM} > 0.8$) merger at $z = 0.8$. The two progenitor galaxies in this case were only moderately gas-rich ($f_g \sim 20\%$). Despite these relatively low gas fractions, the merger remnant was able to quickly reform a disk via the cooling of gas from the hot phase. If we use this result as motivation to focus on the more lenient ($f_g > 30\%$) definition of gas-rich in Figure 4.2, our gas-poor merger fractions drop to $10 - 20\%$ smaller than the observed bulge-dominated fractions, leaving room for processes other than gas-poor major mergers to cause a significant portion of morphological transformations.

The general semi-empirical findings we have presented here may be regarded as accurate (not precise) predictions based on merger histories of LCDM halos and observed relations. As such, it is reassuring that our almost unavoidable qualitative trends are consistent with a growing body of work that stresses the importance of gas-richness in preserving disk morphologies during mergers (Barnes, 2002; Brook et al., 2004;

Springel & Hernquist, 2005; Robertson et al., 2006a; Brook et al., 2007b,a; Governato et al., 2007, 2009; Hopkins et al., 2009a; Robertson & Bullock, 2008). Although we have focused primarily on issues of morphological transformation, disk survival, and baryonic accretion via mergers in this chapter, we believe that in future work, the semi-empirical approach we have used here may provide a useful tool in exploring a vast array of galaxy properties and evolutionary mechanisms.

4.6 Acknowledgements

The contents of this chapter were previously published by Stewart, Bullock, Wechsler and Maller (2009) in The Astrophysics Journal, September 2009 (v702, p307). The simulation used in this chapter was run on the Columbia machine at NASA Ames. We would like to thank Anatoly Klypin for running the simulation and making it available to us. We are also indebted to Brandon Allgood for providing the merger trees. We thank Charlie Conroy for sharing his abundance matching data so we could assign stellar masses to dark matter halos, and Lisa Wei (and collaborators) for sharing gas fraction data from an upcoming paper.

Chapter 5

Invisible Major Mergers: Defining Galaxy "Merger Ratios"

5.1 Chapter Abstract

The mapping between dark matter halo mass, galaxy stellar mass, and galaxy cold gas mass is not a simple linear relation, but is influenced by a wide array of galaxy formation processes. We implement observationally-normalized relations between dark matter halo mass, stellar mass, and cold gas mass to explore these mappings, with specific emphasis on the correlation between different definitions of a major galaxy merger. We always define a major merger by a mass ratio $m/M > 0.3$, but allow the masses used to *compute* this ratio to be defined in one of three ways: dark matter halo masses, galaxy stellar masses, or galaxy baryonic masses (stars and cold gas). We find that the merger ratio assigned to any particular merger event depends strongly on which of these masses is used, with the mapping between different mass ratio definitions showing strong evolution with halo mass and redshift. For example, major dark

matter mergers (> 0.3) in small galaxies ($M_{\rm DM} < 10^{11} M_{\odot}$) typically correspond to very minor *stellar* mergers ($< 1/20$). These mergers contain significant dark matter mass, and should cause noticeable morphological disruption to the primary galaxy, even though there is no observable bright companion. In massive galaxies, there is an opposite effect, with bright companion galaxies corresponding to only minor dark matter mergers. We emphasize that great care must be taken when comparing mergers based on different mass ratio definitions.

5.2 Introduction

In the cold dark matter (CDM) model of structure formation, galaxy mergers are believed to play an important role in galaxy evolution. Typically, these mergers are divided into two categories. "Minor" mergers (with mass ratios $< 1/3$) are often thought to trigger moderate bursts of increased star formation and/or morphological disturbances, as well as contributing to the deposition of diffuse light components of galaxies. "Major" mergers (with mass ratios $> 1/3$) are likely to influence stronger morphological disturbances responsible for the transformation from disk-dominated to bulge-dominated morphologies, in addition to triggering stronger starburst and AGN activity.

Despite this commonly adopted distinction between major and minor mergers at merger mass ratios of $\sim 1/3$, there is still ambiguity in what mass is used to *define* this ratio. Theoretical investigations of dark matter halo merger rates typically define merger ratios in terms of dark matter halo masses, the most theoretically robust prediction from cosmological N-body simulations (e.g. Chapter 2, and references within). But because estimates of dark matter halo masses are difficult to obtain observationally, it is also common to define merger ratios by comparing the stellar

masses or the total baryonic masses of galaxies.

In attempting to compare theoretically derived merger statistics (in terms of dark matter mass ratios) to observational investigations of galaxy mergers (in terms of stellar or galaxy mass ratios), it is important to understand the mapping between these definitions. Galaxy merger rates, for example, are quite sensitive to the merger mass ratio being considered (Chapter 3). In order to explore the fundamental differences between major mergers as defined by dark matter halo, stellar, and galaxy merger ratios, we adopt a semi-empirical methodology to estimate the stellar and cold gas content of dark matter halos as a function of halo mass and redshift. We give a very brief overview of this method before presenting our findings, but we refer reader to Chapter 4 for a more in-depth discussion of this method.

5.3 Assigning Baryons and Defining Masses

In order to assign stars to our halos, we assume a monotonic relationship between halo mass and stellar mass. Using this technique, provided we know $n_g(> M_{\rm star})$ (the cumulative number density of galaxies with stellar mass more massive than $M_{\rm star}$) we may determine the associated dark matter halo population by finding the halo mass above which the number density of halos (including subhalos) matches that of the galaxy population, $n_h(> M_{\rm DM}) = n_g(> M_{\rm star})$. Specifically, we adopt the relation found by Conroy & Wechsler, 2009a (interpolated from the data in their Figure 5.2). Of course, a simple relation of this kind cannot be correct in detail, but in an average sense, it provides a good characterization of the relationship between halo mass and galaxy stellar mass that must hold in order for LCDM to reproduce the observed universe.

In order to assign gas to the central galaxies within our halos, we quantify observationally-inferred relations between gas fraction and stellar mass. Specifically, we characterize the data from McGaugh, 2005 (disk-dominated galaxies at $z = 0$) and Erb et al., 2006 (UV-selected galaxies at $z \sim 2$) with a relatively simple function of stellar mass and redshift, as in Chapter 4, and find that this adopted characterization is also consistent with a number of other observationally motivated works (e.g., Kannappan, 2004; Baldry et al., 2008).

Having estimated the stellar and cold gas content of dark matter halos as a function of halo mass and redshift, we define three different means of identifying the mass of a galaxy (and thus, define merger mass ratios):

1. The mass (or mass ratio) of each dark matter halo, $(m/M)_{\rm DM}$. We will refer to these as the *DM mass (ratio)* of a galaxy (merger).
2. The mass (mass ratio) of the stellar mass of each dark matter halo's central galaxy, $(m/M)_{\rm star}$. We refer to this definition as the *stellar mass (ratio)*.
3. The mass (mass ratio) of the total baryonic mass of each dark matter halo's central galaxy, $(m/M)_{\rm gal}$. In this case, we define a galaxy's baryonic mass as a combination of its stellar mass and cold gas mass ($M_{\rm gal} \equiv M_{\rm star} + M_{\rm gas}$). We refer to this definition as the *galaxy mass (ratio)*.

Using these mass definitions, we show the stellar and galaxy mass of a dark matter halo's central galaxy as a function of halo mass (and normalized by halo mass) in Figure 5.1, where solid and dashed lines represent galaxies at $z = 0$ and $z = 1$, respectively. We emphasize that these mass fractions are a strong function of halo mass, and evolve with redshift. It is clear from this figure that a single merger event between galaxies may have a drastically different mass ratio in dark mater compared to its mass ratio in stars (or baryons). This could have important implications for

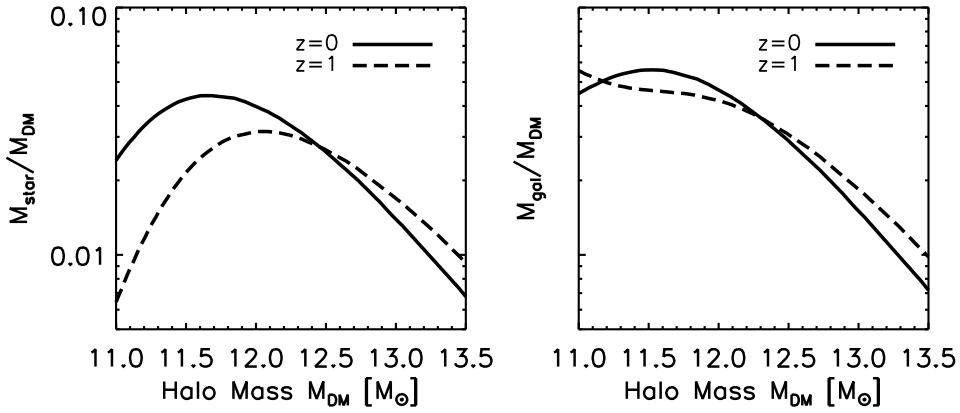

Figure 5.1: A comparison of the baryonic properties of central galaxies to their dark matter halo masses. *Left:* Ratio of stellar mass to dark matter halo mass, as a function of halo mass. *Right:* Ratio of total baryonic mass (stars and cold gas) to halo mass, as a function of halo mass. In both panels, the solid and dashed lines correspond to $z = 0$ and $z = 1$, respectively. Note that these relations vary significantly with halo mass and redshift.

observational efforts to measure the merger rate: morphological disturbances will be affected by high total mass ratio events, while pair count estimates will be more sensitive to the mass ratio in visible light.

5.4 Mapping Between Mass Ratios

We explore the various mappings between major mergers using different mass definitions in Figure 5.2. In the top panels we focus on mergers with $(m/M)_{\rm DM} = 0.3$ (henceforth *major DM mergers*), with the dashed and dotted lines showing the corresponding stellar and galaxy mass ratios of these mergers. In the bottom panels, we instead focus on *major stellar mergers*, defined by $(m/M)_{\rm star} = 0.3$. In these panels, the solid and dotted lines correspond to the DM and galaxy mass ratios of these mergers. The left and right panels show relations at $z = 0$ and $z = 1$, respectively.

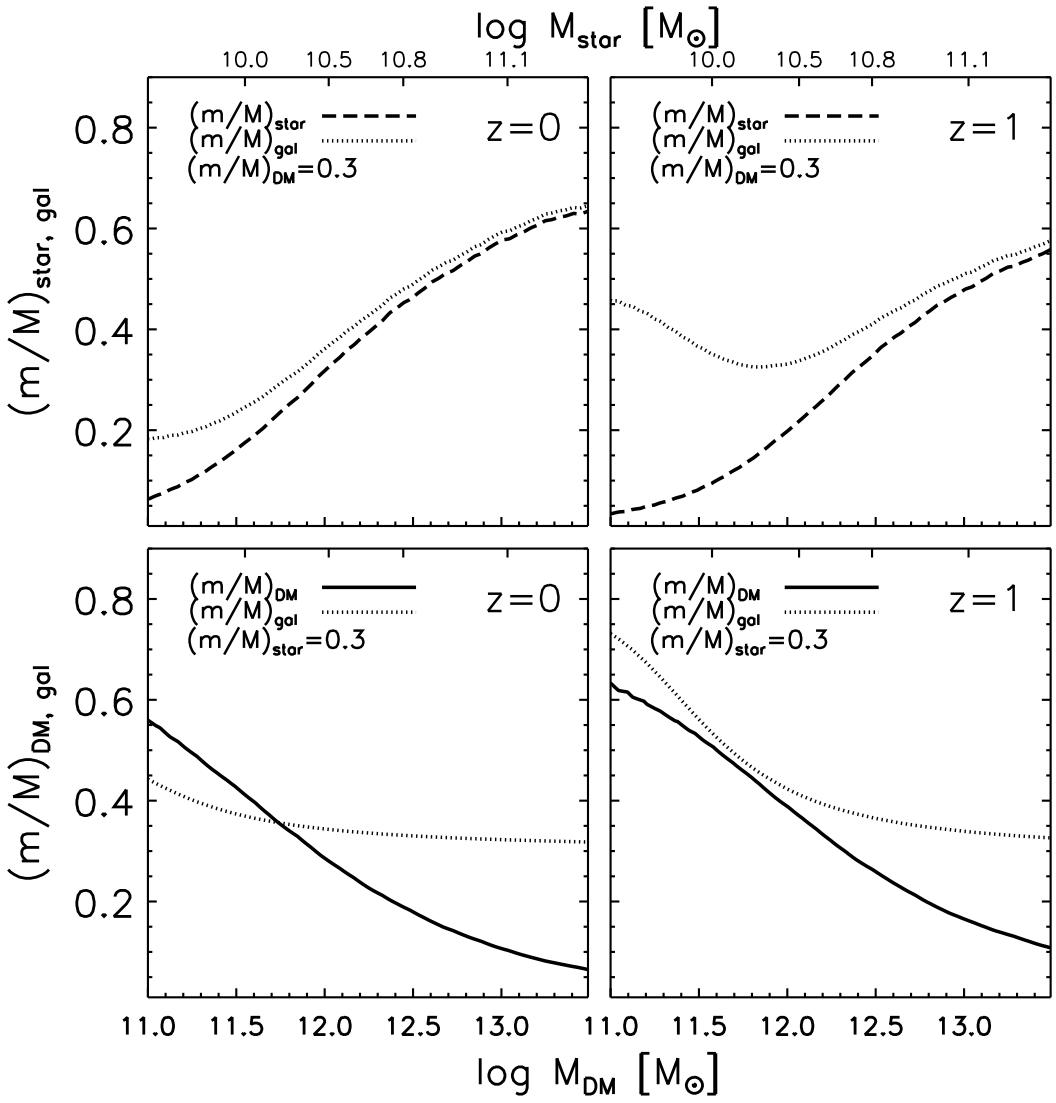

Figure 5.2: Conversion between major merger ratios defined by dark matter halo mass ($M_{\rm DM}$), stellar mass ($M_{\rm star}$), or galaxy (baryonic) mass ($M_{\rm gal}$). In the top panels, the dashed and dotted lines show the stellar and galaxy mass ratios of major DM mergers with $(m/M)_{\rm DM} = 0.3$, as a function of halo mass (lower axis) and stellar mass (top axis). Similarly, the solid and dotted lines in the bottom panels show the DM and galaxy mass ratios corresponding to major stellar mergers with $(m/M)_{\rm star} = 0.3$. The left and right panels give these relations at $z = 0$ and $z = 1$, respectively.

We emphasize that, in general, the DM mass ratio between two galaxies is *not* the same as the stellar (or galaxy) mass ratio. Specifically, major DM mergers (top panels) correspond to stellar mass ratios ranging from $\sim 5-60\%$ $(5-50\%)$ and galaxy mass ratios of $\sim 20-60\%$ $(35-50\%)$ for $10^{11-13} M_\odot$ halos at $z = 0$ (1). Similarly, major

stellar mergers (bottom panels) correspond to DM mass ratios from $\sim 10-55\%$ $(15-65\%)$ and galaxy mass ratios of $\sim 30-45\%$ $(35-75\%)$ for $10^{11-13}M_{\odot}$ halos at $z=0$ (1). Indeed, the *only* broad regime where different mass definitions result in similar merger ratios is for stellar and galaxy merger ratios of massive galaxies, where galaxy gas fractions are typically low enough that $M_{\rm star} \sim M_{\rm gal}$.

Note that in $M_{\rm DM} < 10^{11}M_{\odot}$ halos, major DM mergers should contain stellar mass ratios $< 1/20$. The smaller galaxy in these mergers contain significant mass in dark matter, and should be capable of triggering severe morphological disruption in the primary galaxy, but they are observationally "invisible," with negligible luminous content with respect to the primary. The existence of these "invisible" major mergers is a robust, testable prediction of LCDM.

5.5 Example Consequence: Measuring the Merger Rate

While theoretical investigations into dark matter halo merger rates define mergers by DM mass ratios, observed merger rates (specifically, those based on close-pair counts of galaxies) typically select pairs based on luminosity (stellar mass), and should thus constitute major *stellar* mergers. The mapping between stellar and DM mass ratios has two important qualitative effects in this case. First, for smaller halos, major DM mergers should correspond to substantially smaller stellar mass ratios, and may not be distinguishable as a luminous close-pair when observed (ie. faint/invisible major mergers). Second, for massive halos, some observed close-pairs with comparable luminosities (major stellar mergers) may correspond to substantially smaller *DM* mass ratios, and would be counted as *minor* (not major) mergers in theoretical predictions

from N-body simulations (ie. bright minor mergers).

For a more quantitative analysis, we adopt the fitting function for dN/dt from Chapter 3 (Table 3.1, infall, "simple fit"), which provides the rate of mergers more massive than $(m/M)_{\rm DM}$ into dark matter halos of mass $M_{\rm DM}$ (per halo, per Gyr) as a function of redshift, mass, and mass ratio. For $10^{11} M_{\odot}$ dark matter halos and DM merger ratios $> 30\%$ at $z = 0 - 1$, the merger rate increases from $\sim 0.015 - 0.075$. Now consider an identical halo mass, but for mergers selected on *stellar* mass ratios $> 30\%$, corresponding to a DM mass ratio of $\sim 7\%$ (4%) at $z = 0$ (1). Because of the minor DM mergers being considered, this selection would result in an artificial increase of the observed merger rate by a factor of $3-4$ compared to DM merger rates ($\sim 0.05-0.30$ from $z = 0-1$), with a redshift evolution that is too steep (and does not appear to fit well to $dN/dt \propto (1+z)^{\alpha}$; see Chapter 3). Thus, using different mass ratios to define mergers has a substantial effect on predictions of galaxy merger rates, and great care must be taken when comparing studies of galaxy or halo mergers, if the merger mass ratios have been defined by different criterion.

Chapter 6

Stealth Galaxies in the Halo of the Milky Way

6.1 Chapter Abstract

We predict that there is a population of low-luminosity dwarf galaxies orbiting within the halo of the Milky Way that have surface brightnesses so low that they have escaped detection in modern star-count surveys. The overall count of stealth galaxies is sensitive to the presence (or lack) of a low-mass threshold in galaxy formation. These systems have luminosities and stellar velocity dispersions that are similar to those of known ultrafaint dwarf galaxies but they have more extended stellar distributions ($R_{\rm e} \gtrsim 100$ pc) because they inhabit dark subhalos that are slightly less massive than their higher surface brightness counterparts. We show that a typical ultrafaint galaxy with $L = 10^3 L_\odot$ and $\sigma_\star = 5$ km s^{-1} will have a peak surface brightness fainter than 30 mag arcsec^{-2} if it inhabits a dark subhalo with maximum circular velocity smaller than about 15 km s^{-1}, or equivalently, with a mass within 300 pc less than

about $10^7 M_\odot$. One implication is that the inferred common mass scale for Milky Way dwarfs may be an artifact of selection bias. We use results from the Via Lactea II N-body simulation to show that if there is no sharp threshold in galaxy formation at low halo mass then ultrafaint galaxies like Segue I represent the high-mass, early forming tail of a much larger population of objects that have typical peak circular velocities of about ~ 8 km s^{-1} and masses within 300 pc of $\sim 5 \times 10^6 M_\odot$. In this case, there should be hundreds of stealth galaxies in the halo of the Milky Way, making up about half of potentially-observable systems. Alternatively, if we impose a low-mass threshold in galaxy formation in order to explain the unexpectedly high densities of the ultrafaint dwarfs, then we expect only a handful of stealth galaxies in the halo of the Milky Way. We expect a similar paucity of stealth galaxies if the power spectrum is truncated of if the dark matter is warm. A complete census of these objects will require deeper sky surveys, 30m-class follow-up telescopes, and more refined methods to identify extended, self-bound groupings of stars in the halo.

6.2 Introduction

Approximately twenty-five new dwarf galaxy companions of the Milky Way (MW) and M31 have been discovered since 2004, more than doubling the known satellite population in the Local Group in five years (Willman et al., 2005; Zucker et. al, 2006; Grillmair, 2006; Majewski et al., 2007; Belokurov et al., 2007; Grillmair, 2009; Belokurov et al., 2009; Martin et al., 2009). The majority of these newly-discovered dwarfs are less luminous than any galaxy previously known. The most extreme of these, the ultra-faint MW dwarfs, have luminosities smaller than an average globular cluster $\mathrm{L}_V \simeq 10^2 - 10^4$ $\mathrm{L}_\odot$, and were discovered by searches for stellar overdensities in the wide-field maps of the Sloan Digital Sky Survey (SDSS) and the Sloan Ex-

tension for Galactic Understanding and Exploration (SEGUE). Follow-up kinematic observations showed that these tiny galaxies have surprisingly high stellar velocity dispersions for their luminosities and sizes ($\sigma_\star \sim 5\,\mathrm{km\,s^{-1}}$, Martin et al., 2007; Simon & Geha, 2007; Geha et al., 2009) and subsequent mass modeling has shown that they are the most dark matter dominated galaxies known (Strigari et al., 2008; Wolf et al., 2009). Remarkably, these extreme systems are not only the faintest, most dark matter dominated galaxies in the universe but they are also the most metal poor stellar systems yet studied (Kirby et al., 2008; Geha et al., 2009).

Perhaps the most exciting aspect of these recent discoveries is that they point to a much larger population. Detection in the SDSS is complete only to ~ 50 kpc for the least luminous dwarfs (Koposov et al., 2008; Walsh et al., 2009) and straightforward cosmologically motivated luminosity bias and coverage corrections suggest that there are $\sim$ 500 ultra-faint dwarf galaxies within 400 kpc of the Milky Way (Tollerud et al., 2008), with an ever increasing number beyond. Moreover, the luminosity-distance detection limits only apply for systems with peak surface brightness obeying $\mu_V < 30$ mag arcsec^{-2} (Koposov et al., 2008). Any satellite galaxy with a luminosity of $L \sim 1000\,L_\odot$ and a projected half-light radius R_e larger than about 100 pc would have evaded detection with current star-count techniques.

Here we argue that there should be a population of dwarf galaxies surrounding the Milky Way (and by extension, throughout the universe) that are so diffuse in stellar density that they would have thus far avoided discovery. Our predictions rely on the fact that the effective radius R_e of a dark matter dominated, dispersion-supported galaxy with fixed stellar velocity dispersion will increase as its dark matter halo mass decreases. One implication of this idea is that the known ultrafaint dwarf spheroidals (dSphs) may represent the high (dark matter) mass tail of a larger distribution of stealth galaxies. These undiscovered systems should preferentially inhabit the lowest

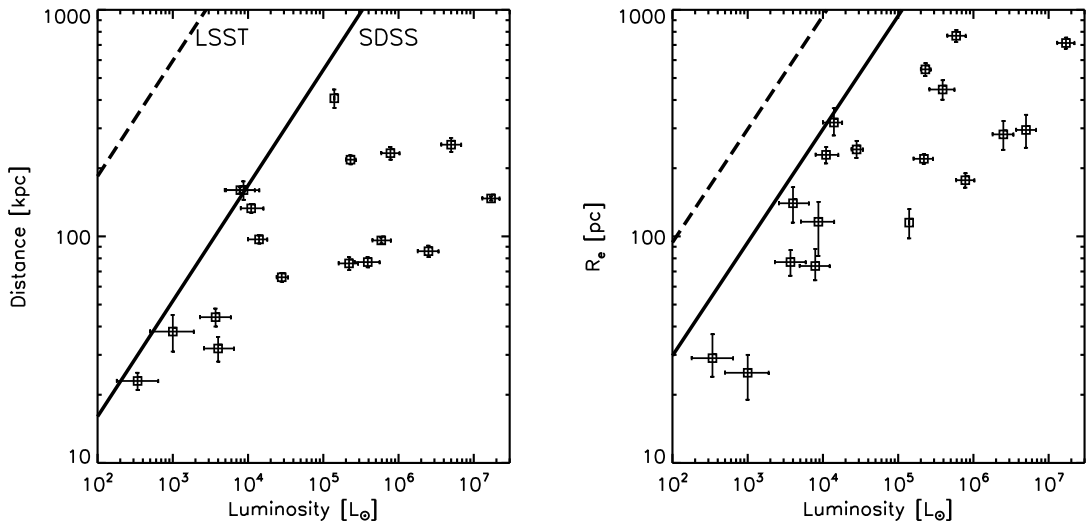

Figure 6.1: Projected helio-centric distance vs. V=band luminosity (left) and half-light radius R_e vs. V-band luminosity (right) and for Milky Way dSph galaxies. The lines in the left panel show SDSS luminosity completeness limits from Walsh et al. (2009) and an estimate for LSST completeness following Tollerud et al. (2008). In the right panel, galaxies above the solid line, with surface brightness fainter than $\mu = 30$ mag arcsec^{-2} are currently undetectable. For reference, the dashed line in the right panel corresponds to $\mu = 35$ mag arcsec^{-2}.

mass dark matter subhalos that host stars, and may provide an important missing link for the satellite-subhalo problem in Cold Dark Matter (CDM) models (Klypin et al., 1999b; Moore et al., 1999; Bullock et al., 2000; Stoehr et al., 2002; Zentner & Bullock, 2003; Kazantzidis et al., 2004; Strigari et al., 2007; Macciò et al., 2009; Busha et al., 2009; Muñoz et al., 2009; Kravtsov, 2009; Okamoto & Frenk, 2009).

Mass determinations for MW dSphs based on current stellar kinematic samples reveal a surprising lack of trend between inferred dark matter halo masses and galaxy luminosities (Strigari et al., 2008; Peñarrubia et al., 2008; Walker et al., 2009; Wolf et al., 2009). The tiniest satellite galaxies have dark matter densities indicative of dark matter halos that are at least as massive as those of systems 10,000 times more luminous. For example, Strigari et al. (2008) found that the integrated mass [1]

[1]The radius 300 pc provides a good benchmark radius for comparison for two reasons. First, it represents a typical three-dimensional half-light radius for the bulk population of MW dSphs

within 300 pc for each galaxy shows no evidence for a relationship with luminosity: $M_{300} \propto L^{0.03\pm0.03}$. The normalization of this relation at $M_{300} \simeq 10^7 M_\odot$ is indicative of the central densities of *massive* dark matter subhalos ($V_{\rm max} \gtrsim 15$ km s^{-1}) and is therefore fairly easy to explain in CDM-based models of galaxy formation for the most luminous satellites (Strigari et al., 2008; Macciò et al., 2009; Busha et al., 2009; Muñoz et al., 2009; Kravtsov, 2009; Li et al., 2009; Okamoto & Frenk, 2009). However, the lack of observed correlation between L and mass is quite unexpected. To put the lack of measured slope in the $M_{300} - L$ relation in perspective, consider the relationship between dark matter halo $V_{\rm max}$ and galaxy luminosity required to match the faint-end slope of the galaxy luminosity function: $L \propto V_{\rm max}^b$ with $b = 7.1$ (Busha et al., 2009). For dark matter halos of interest, with maximum circular velocities $V_{\rm max} \simeq 15 - 45$ km s^{-1}, we expect $M_{300} \propto V_{\rm max}$ (assuming NFW fits to halos in Springel et al., 2008) such that the observed trend $M_{300} \propto L^{0.03}$ would naively imply $L \propto V_{\rm max}^b$ with $b \simeq 33$. One possible explanation for this lack of mass trend is that it reflects a scale in galaxy formation, where the scatter in L at fixed $V_{\rm max}$ becomes very large (Strigari et al., 2008; Macciò et al., 2009; Okamoto & Frenk, 2009, and §6.4 below). Another possibility, outlined below, is that the lack of an observed trend between mass and luminosity is the product of selection bias: most ultrafaint galaxies do inhabit halos with $M_{300} \lesssim 10^7 M_\odot$, but they are too diffuse to have been discovered.

In the next section, we explain why we expect surface brightness selection bias to

(Strigari et al., 2008; Wolf et al., 2009), and second, it is the largest radius that can currently be well-resolved in CDM N-body simulations (Springel et al. 2008 and Diemand et al. 2008). There are four galaxies that lack stellar tracers that extend to 300 pc. In these cases, the inferred mass within 300 pc requires an extrapolation based on a physically-motivated prior (Strigari et al., 2008). Such an extrapolation is perfectly reasonable because CDM subhalos have strong (predicted) correlations between the density at some inner radius (e.g. 100 pc) and at a larger radius (e.g. 300 pc) and we aim to compare to CDM predictions. It is reassuring to note that If one performs the same comparison between galaxies using a smaller benchmark radius (100 pc, Strigari et al., 2008) or using the 3d half-light radius for each galaxy (Wolf et al., 2009) or using the 3d mass within the 2d half-light radius of each galaxy (Walker et al. 2009) then one reaches the same conclusion: there is no observed trend between inferred halo mass (or $V_{\rm max}$) and luminosity.

limit the discovery of satellite galaxies in small subhalos. In §6.4 we use a simple model to estimate the number of low surface brightness stealth galaxies within the vicinity of the Milky Way. Our estimates rely on the public subhalo catalogs provided by the Via Lactea 2 N-body simulation group (Diemand et al., 2008). We explore two models. Our Fiducial Scenario connects each subhalo's mass and accretion time to a galaxy luminosity L by extrapolating the halo mass-light relationship required to match the asymptotic slope of the galaxy stellar mass function (Moster et al., 2009). Our secondary model (Threshold Scenario) explores a scenario where galaxy formation is truncated sharply below a characteristic dark halo mass scale. We present our findings in §6.5 and conclude in §6.6.

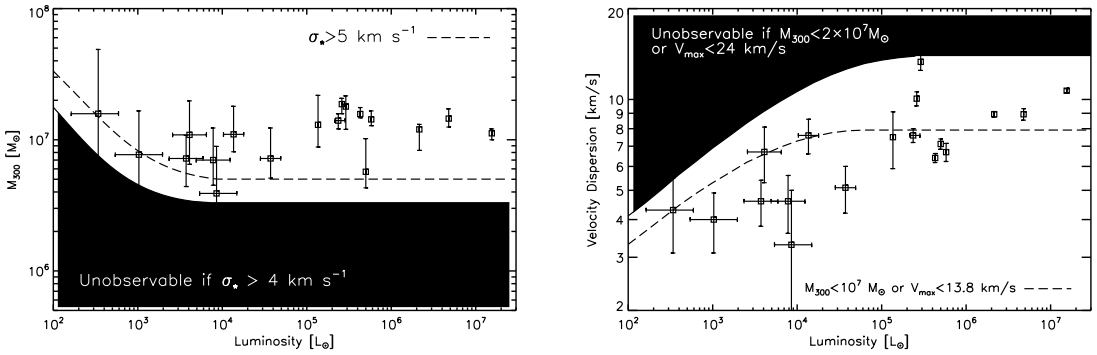

Figure 6.2: Mass within 300 pc vs. luminosity (left) and measured stellar velocity velocity dispersion, $\sigma_\star$, vs. luminosity (right) for Milky Way dwarf spheroidal galaxies (data points with error bars). In the left panel, galaxies within in the shaded region (below dashed line) will remain hidden ($\mu > 30$ mag arcsec^{-2}) if they have $\sigma_\star > 4\mathrm{km\,s^{-1}}$ ($\sigma_\star > 5\,\mathrm{km\,s^{-1}}$). In the right panel, galaxies in the shaded region will be stealth ($\mu > 30$) if they have $M_{300} < 2 \times 10^7 M_\odot$ and galaxies below the dashed line will be stealth if they have $M_{300} < 10^7 M_\odot$.

6.3 Motivations

The left panel of Figure 6.1 shows the known MW dSphs plotted in the plane of heliocentric distance vs. V-band luminosisty. The solid line (labeled SDSS) illustrates the

distance to which dwarfs of a given luminosity can be detected in SDSS with 90% efficiency from Walsh et al. (2009). Similar results were presented by Koposov et al. (2008). The upper line shows the same limit adjusted up by scaling to the limiting magnitude of the full co-added LSST survey (Tollerud et al., 2008; Ivezic et. al, 2008). Clearly, the known dwarf galaxies cluster at the current completeness edge of the diagram, indicating a high likelihood for future discoveries (Koposov et al., 2008; Tollerud et al., 2008; Walsh et al., 2009).

The distance-luminosity completeness limits presented by Walsh et al. (2009) and Koposov et al. (2008) are only applicable for systems with surface brightness brighter than $\mu_V = 30$ mag arcsec^{-2} (Koposov et al., 2008, and G. Gilmore, M. Geha, and B. Willman, private communications). Systems more diffuse than this limit cannot be detected in SDSS with current methods, no matter their helio-centric distance. This phenomenon is illustrated qualitatively in the right panel of Figure 6.1, which presents the same set of MW dSphs in the plane of $R_{\rm e}$ vs. L. The solid line shows a constant peak (central) surface brightness for a Plummer profile

$$\Sigma_{\rm peak} = \frac{L}{\pi R_{\rm e}^2} = 0.036\, L_\odot\, {\rm pc}^{-2}, \tag{6.1}$$

and corresponds to $\mu_V = 30$ mag arcsec^{-2} for solar absolute magnitude $M_{\odot V} = 4.83$. As in the distance-luminosity figure, the tendency for many of the fainter dwarfs to "pile up" near the surface brightness detection limit is suggestive. There is nothing ruling out the presence of a larger population of more extended systems that remain undetected because of their low surface brightness.

If a large number of diffuse, undetected galaxies do exist, they are likely associated with low-mass dark matter subhalos. One can understand this expectation by considering a spherically-symmetric galaxy with stellar density distribution $\rho_*(r)$ and

radial velocity profile $\sigma_r(r)$ that is embedded within a gravitationally-dominant dark matter halo mass profile $M(r)$. The Jeans equation implies

$$M(r) = \frac{r\,\sigma_r^2}{G}\,(\gamma_\star + \gamma_\sigma - 2\beta)\,, \tag{6.2}$$

where $\beta(r) \equiv 1 - \sigma_t^2/\sigma_r^2$ characterizes the tangential velocity dispersion and $\gamma_\star \equiv -\mathrm{d}\ln\rho_\star/\mathrm{d}\ln r$ and $\gamma_\sigma \equiv -\mathrm{d}\ln\sigma_r^2/\mathrm{d}\ln r$. If we make the simplifying assumption that $\beta = 0$ and $\sigma(r) \simeq \sigma_\star = \text{constant}$, with $\gamma_\sigma \ll 1$ then $M(r) = r\,G^{-1}\,\sigma_\star^2\,\gamma_\star$. For a fixed velocity dispersion, a more spatially extended profile (smaller $\gamma_\star$) requires a lower mass at fixed radius.

The same basic expectation follows in a more general context from the recent work of Wolf et al. (2009), who showed [2] that the total mass of a quasi-spherical dSph galaxy within its 3d half-light radius $r_{1/2} \simeq 1.3\,R_\mathrm{e}$ may be determined accurately from the luminosity weighted line-of-sight velocity dispersion $\sigma_\star$ for general β: $M(r_{1/2}) = 3\,G^{-1}\,r_{1/2}\,\sigma_\star^2$. Mass determinations at larger and smaller radii require an extrapolation of the mass profile from that point, but given a theoretical prediction for the shape of the dark matter mass profile one can perform this extrapolation.

It is useful to rewrite the Wolf et al. (2009) mass estimator in terms of the implied circular velocity at $r_{1/2}$:

$$V_c(r_{1/2}) = \sqrt{3}\,\sigma_\star. \tag{6.3}$$

Consider then a galaxy with velocity dispersion $\sigma_\star$ and luminosity L embedded within a gravitationally-dominant dark matter halo described by a circular velocity curve that increases with radius as an approximate power law: $V_c(r) = V_{300}\,(r/300\mathrm{pc})^\alpha$.

[2] Under the assumption that the observed stellar velocity dispersion remains fairly flat with projected radius, as is the case with all of the well-studied systems.

Equation 6.3 implies $r_{1/2} = 300\mathrm{pc}\,(\sqrt{3}\sigma_\star/V_{300})^{1/\alpha}$. For an NFW halo (Navarro et al., 1997) with $r_s \gg 300$ pc we have $\alpha = 1/2$ and $r_{1/2} \propto V_{300}^{-2} \propto M_{300}^{-1}$. Clearly, the galaxy becomes puffier as we decrease M_{300} or V_{300}. One implication is that if a galaxy has a stellar density that is just large enough to be detected, another galaxy with identical L and $\sigma_\star$ will be undetectable if it happens to reside within a slightly less massive halo.

Figure 6.2 provides a more detailed exploration of the relationship between halo mass parameters (M_{300} or $V_{\rm max}$) and associated dSph observables $\sigma_\star$, L, and $R_{\rm e}$. Points in the left panel of Figure 6.2 present M_{300} vs. L for MW dSph galaxies, with masses from Strigari et al. (2008) and luminosities updated as in Wolf et al. (2009). The right panel shows $\sigma_\star$ vs. L for the same galaxies culled from Table 1 of Wolf et al. (2009).

The shaded bands and dashed lines in each panel of Figure 6.2 illustrate the way in which surface brightness incompleteness may affect these diagrams. In determining these regions we have assumed each dSph is dark-matter dominated, such that its gravitating mass profile produces an NFW circular velocity curve $V_c(r) = V_{\rm NFW}(r)$. Given the NFW shape, the rotation curve is fully specified by its peak value $V_{\rm max}$ and the radius where the peak occurs $r_{\rm max}$ (e.g., Bullock et al., 2001a). We assume for simplicity that subhalos of a given $V_{\rm max}$ map in a one-to-one way to a rotation curve shape using $r_{\rm max} = 650\,\mathrm{pc}\,(V_{\rm max}/10\mathrm{km\,s^{-1}})^{1.35}$, which is indicative of median subhalos in high-resolution N-body simulations (intermediate between the normalizations of Springel et al. 2008 and Diemand et al. 2008). With this assumption in place, given a halo mass variable (e.g., M_{300} or $V_{\rm max}$), we may determine the implied half-light radius $R_{\rm e} \simeq 0.75\,r_{1/2}$ associated with any $\sigma_\star$ using $V_{\rm NFW}(r_{1/2}) = \sqrt{3}\,\sigma_\star$ (Equation 6.3).

In the right panel of Figure 6.2, galaxies residing in the shaded region are unobservable

if they sit within dark matter halos less massive than $M_{300} = 2 \times 10^7$ or (equivalently for our assumptions) with peak circular velocity smaller than $V_{\rm max} = 24\,{\rm km\,s^{-1}}$. Similarly, galaxies residing above the dashed line are too diffuse to be detected if they have $M_{300} < 10^7 M_\odot$ or $V_{\rm max} \lesssim 14\,{\rm km\,s^{-1}}$. Galaxies need to have deep potential wells if they are to remain observable at low luminosity for $\sigma_\star \sim 5\,{\rm km\,s^{-1}}$. If there are low-luminosity galaxies with M_{300} values smaller than $\sim 10^7 M_\odot$ they would remain hidden as long as they have stellar velocity dispersions comparable to those of the known dwarfs. [3]

A related set of limits is depicted in the left panel of Figure 6.2. Galaxies sitting in the shaded band will have $R_{\rm e}$ too large to be observable if they have $\sigma_\star > 4\,{\rm km\,s^{-1}}$. Slightly hotter galaxies, with $\sigma_\star > 5\,{\rm km\,s^{-1}}$ will be unobservable if they sit below the dashed line. As expected, the hotter the galaxy, the deeper the potential well needs to be in order keep the stars confined to an observable surface brightness. We see that galaxies with $L \sim 10^3\,L_\odot$ residing in a halos less massive than $M_{300} \simeq 8 \times 10^6\,M_\odot$ will be too diffuse to be seen if they have $\sigma_\star = 5\,{\rm km\,s^{-1}}$. Note that for $L \gtrsim 10^4 L_\odot$ the constraint on allowed M_{300} values is flat with L because halos smaller than this value are kinematically forbidden via Equation 6.3. Specifically, kinematic mass determinations demand $V_{\rm max} \geq \sqrt{3}\,\sigma_\star$.

Implicit in the above discussion is the idea that a galaxy's $\sigma_\star$ can be considered independently of its halo mass. Dynamically, the only constraint is that $\sigma_\star \leq V_{\rm max}/\sqrt{3}$ (Equation 6.3). One is more inclined to suspect that $\sigma_\star$ in an ultrafaint dSph is governed by star formation and galaxy formation processes, with an absolute minimum set by the effective temperature of the star forming ISM. Even for a very cold primor-

[3] In deriving these regions, we have explicitly assumed that the stellar systems are dark-matter dominated within their half-light radii. The same arguments cannot be applied to globular cluster systems, some of which do inhabit the shaded regions in the right panel of Figure 6.2 without any discernible dark matter halo. These systems have large velocity dispersions simply because they have very high stellar densities.

dial effective ISM temperature, $T_{ISM} \sim 300$K, we expect $\sigma_{ISM} \sim 2\,\mathrm{km\,s^{-1}}$, and this ignores turbulent and magnetic pressure terms. The vast majority of globular clusters have stellar velocity dispersions larger than this (Pryor & Meylan, 1993). Moreover, dark matter halos of all masses are expected to have experienced significant mergers in their early histories (e.g., Stewart et al., 2008). These mergers would have heated (the oldest) stars beyond any primoridal pressurized motions. This realization is important because larger $\sigma_\star$ values will produce more extended stellar distributions within dark halos of fixed mass. In the next section we consider the implications of a model where $\sigma_\star$ is correlated with luminosity L in a way that tracks the observed relationship (right panel of Figure 6.2). In principle, there could be a floor in the $\sigma_\star$ values allowed for dwarf galaxies. We do not impose such a floor in our calculations, but if one does exist, then our estimates will under-predict the fraction of stealth galaxies.

6.4 Model

We rely on the publicly released subhalo catalogs of the Via Lactea II N-body simulation (VL2 hereafter) as described in Diemand et al. (2008). The simulation adopts cosmological parameters from WMAP3 (Spergel et al., 2007) and tracks the formation of a Milky Way size dark matter halo with a highest particle-mass resolution of $4,100 M_\odot$ and force resolution of 40 pc. The main halo has a radius of 402 kpc, defined to enclose a mean density that is 200 times the mean matter density of the universe, and an associated mass of $M_{\rm DM} = 1.9 \times 10^{12} M_\odot$. The public subhalo catalogs include M_{300}, $V_{\rm max}$, and $r_{\rm max}$ parameters for each bound system, as well as merger history information that allows us to track the redshift of infall $z_{\rm inf}$ for each subhalo and to determine its maximum attained mass $M_{\rm max}$ prior to infall. Tests by the VL2 team

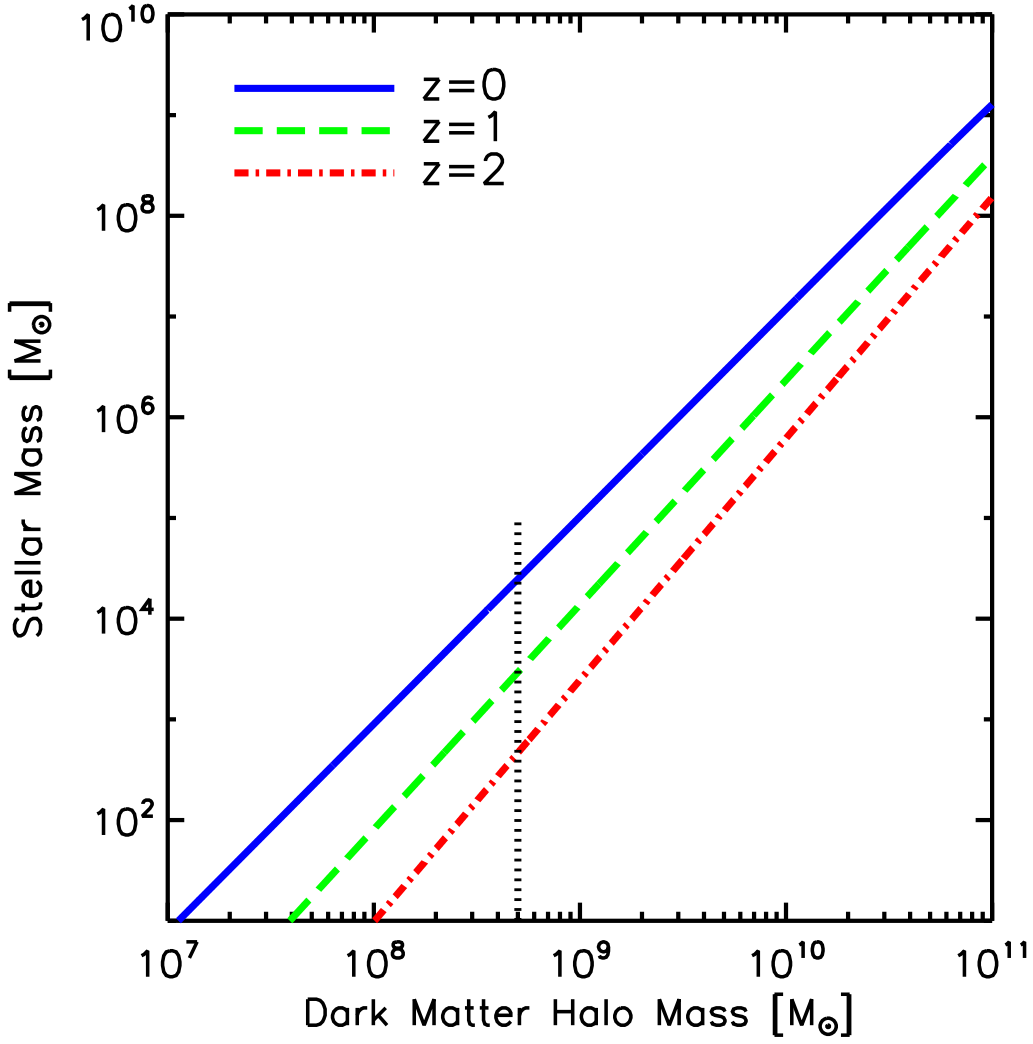

Figure 6.3: Model stellar mass - halo mass relation (Moster et al., 2009) shown at three example redshifts. Our Fiducial Scenario assumes that the $M_{\rm halo} - M_\star$ relation extrapolates smoothly to very small masses. Our Threshold Scenario imposes a sharp truncation mass at $M_{\rm halo} = 5 \times 10^8 M_\odot$ (vertical dotted line) below which all halos are assumed to form no stars.

suggest that the measured M_{300} masses are good to about 20% (random) owing to resolution effects (J. Diemand, private communication).

We assign light to each of our accreted dark matter subhalos by assuming that at each redshift z there is a monotonic relationship between halo mass $M_{\rm DM}$ and galaxy

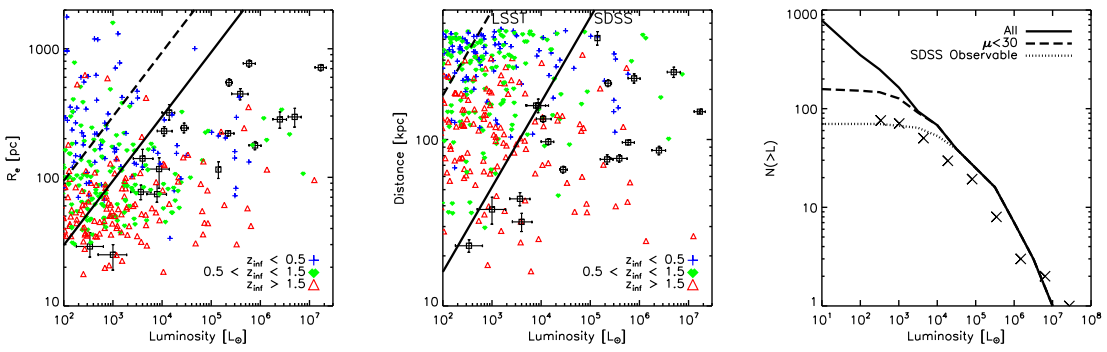

Figure 6.4: Fiducial Scenario galaxy size vs. luminosity relation (colored points, left); distance vs. luminosity relation (middle); and luminosity functions for different completeness cuts (right). *Left Panel:* The solid line corresponds to the current detection limit at a peak surface brightness of $\mu = 30$ mag arcsec^{-2} and the dashed line corresponds to $\mu = 35$ mag arcsec^{-2}, for reference. The small colored points represent model galaxies and the point-type scheme maps to the redshift of infall into the host dark halo: open triangles have $z_{\rm inf} > 1.5$, green circles have $0.5 \leq z_{\rm inf} \leq 1.5$, and blue plusses were accreted since $z = 0.5$. The black squares with error bars are known MW dSph galaxies. *Middle Panel:* The solid and dashed lines indicate luminosity-distance completeness in the SDSS and LSST, respectively, for systems with $\mu < 30$ mag arcsec^{-2}. The point types are the same as in the left panel. *Right Panel:* The symbols shown as X's reflect the current census of MW dSphs, corrected for the sky coverage completeness of SDSS as in Tollerud et al. (2008). The uncertainty in this correction corresponds roughly to the size of the symbols we use. The dotted line shows the predicted cumulative luminosity function of satellite galaxies that are bright enough to have been detected by SDSS according to the Walsh et al. (2009) limits. The dashed line shows the predicted luminosity function of all satellites with surface brightness meeting the $\mu < 30$ mag arcsec^{-2} threshold, most of which should be detectable by LSST. The solid line shows all satellite galaxies, including the stealth population. We see that the majority of ultrafaint dwarfs are expected to have surface brightnesses so low that they will avoid detection without revised techniques for discovery.

stellar mass $M_\star$. This general approach is motivated by its demonstrated success in producing the clustering properties of galaxies larger than $M_\star \simeq 10^9 M_\odot$ (Kravtsov et al., 2004; Tasitsiomi et al., 2004; Vale & Ostriker, 2004; Conroy et al., 2006; Berrier et al., 2006; Purcell et al., 2007; Marín et al., 2008; Stewart et al., 2009a; Conroy & Wechsler, 2009b). Of course, cosmological abundance matching cannot be applied directly at the smallest stellar masses because of completeness issues. In our Fiducial Scenario we simply adopt the asymptotic $M_{\rm DM}$ – $M_\star$ relationship suggested by the

most complete stellar mass functions, which effectively assumes that there is no new (or abrupt) mass scale that truncates galaxy formation in small halos. We also explore a Threshold Scenario that imposes such a truncation scale (see below).

For our Fiducial Scenario, we assign $M_\star$ to each subhalo by extrapolating the fitting formula presented by Moster et al. (2009) to small stellar masses. Moster et al. (2009) derived the relationship using N-body halo catalogs together with observationally inferred stellar mass functions for $M_\star \gtrsim 10^{8-9} M_\odot$ galaxies out to redshift $z \sim 3$. The implied (extrapolated) relationship between stellar mass and dark halo mass is presented in Figure 6.3 for three example redshifts. We see that $M_\star$ must decrease at high redshift for a fixed $M_{\rm DM}$ in order to explain the evolving stellar mass function. Low-mass halos at high redshift have not had time to form as many stars as their $z \sim 0$ counterparts. For our Threshold Scenario we adopt the same mapping for massive halos but we impose a sharp truncation in the $M_\star$ - $M_{\rm DM}$ relation at $M_{\rm DM} = 5 \times 10^8 M_\odot$ (dotted line in Figure 6.3).

We assume that star formation is quenched in each subhalo at a time $\tau_{\rm q}$ after the redshift of accretion into the VL2 host. Specifically, subhalo light content is determined at redshift z_q (set at a time τ_q after the accretion redshift) using the appropriate Moster et al. (2009) mapping with $M = M_{\rm max}$, the maximum mass each subhalo progenitor obtained prior to infall. If the subhalo is accreted at a time less than $\tau_{\rm q}$ before $z = 0$ we adopt the Moster et al. (2009) relation at $z_{\rm q} = 0$. For the figures we present below we use a quenching timescale that is roughly a dynamical time for the host halo $\tau_{\rm q} = 2$ Gyr. We find that the value of $\tau_{\rm q}$ only affects our predictions for the largest satellites $M_\star \gtrsim 10^6\, M_\odot$. For example, if we set $\tau_{\rm q} = 0$, we under-predict the number of luminous satellites by a few, but the low-luminosity satellite count is largely unaffected. The main conclusions of this paper regarding the least luminous, stealth satellites are not sensitive to the choice of $\tau_{\rm q}$. For all satellites, we convert

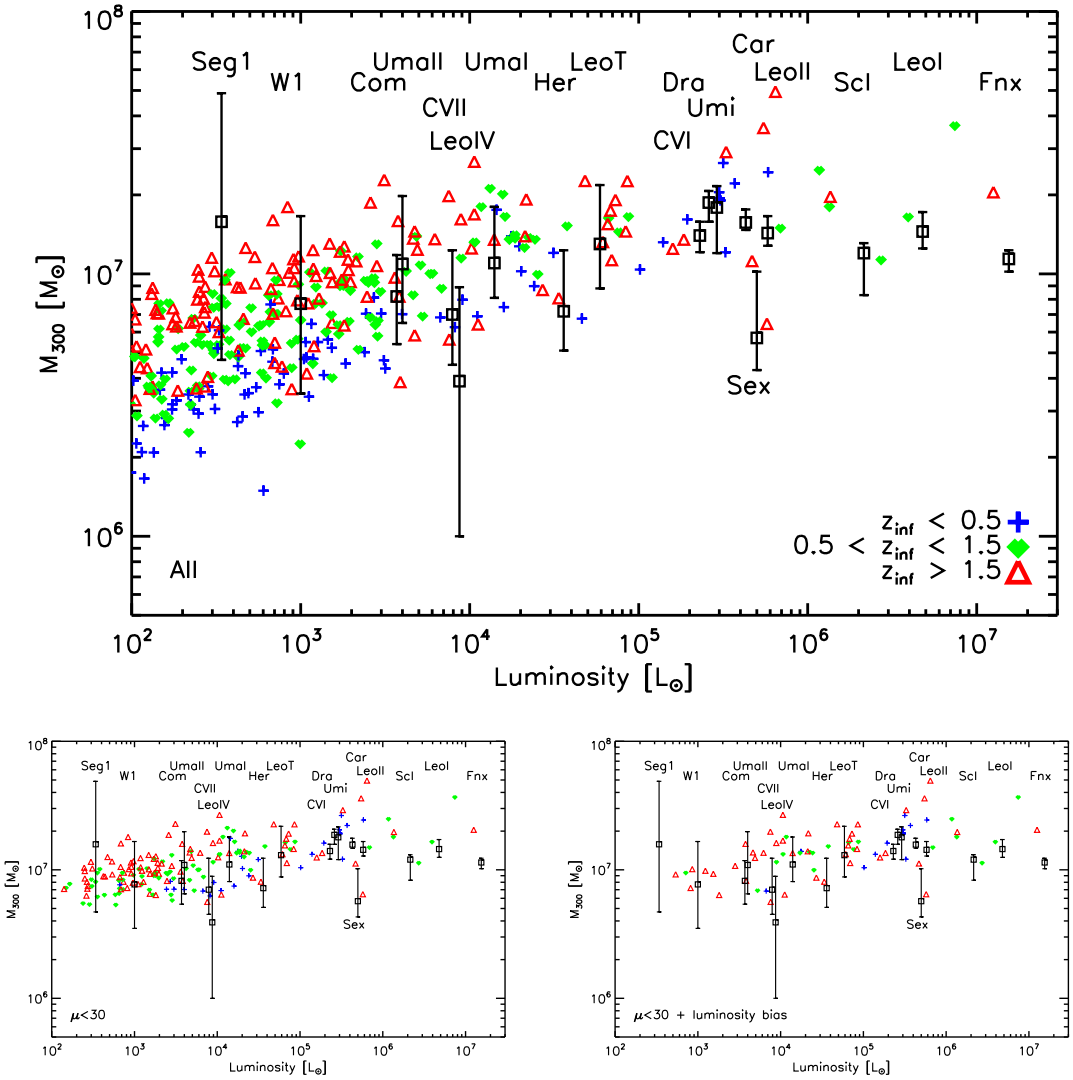

Figure 6.5: Mass within 300 pc as a function of luminosity. Milky Way dSph galaxies are shown as black squares. Fiducial model galaxies are show as smaller colored points, with the point type and color mapped to the time they fell in to the virial radius of the VL2 main halo. Earlier accretions are red and recent accretions are blue as in Figure 6.4 and as indicated in the upper panel legend. The *upper panel* presents all predicted satellites and the *bottom left panel* shows only model satellites that are concentrated enough to be detected with current methods, with $\mu < 30$ mag arcsec^{-2}. The *bottom right panel* includes only the subset of $\mu < 30$ mag arcsec^{-2} galaxies that are close enough to have been detected by SDSS, according to the 90% completeness limits in Walsh et al. (2009).

from stellar mass to V-band luminosity using $M_\star/L = 2\,[M_\odot/L_\odot]$, which is typical for Milky Way dSphs according to Martin et al. (2008) for a Kroupa IMF.

Once L is determined for each subhalo, we assign a stellar velocity dispersion by adopting the empirical relation shown in the right panel of Figure 6.2:

$$\sigma_\star = 6.9\,\mathrm{km\,s^{-1}}\left(\frac{L}{10^5\,L_\odot}\right)^{0.09}, \tag{6.4}$$

with a log normal scatter of $\Delta \log_{10}\sigma = 0.1$ at fixed L. [4] We then determine $R_\mathrm{e} \simeq 0.75\,r_{1/2}$ using $V_{NFW}(r_{1/2}) = \sqrt{3}\,\sigma_\star$ (Equation 2). The V_max and r_max values that define $V_{NFW}(r)$ are those measured for each subhalo in the simulation. We note that in $\sim 90\%$ of cases we find $r_{1/2} < r_\mathrm{max}$, such that the NFW assumption for $V(r)$ provides a reasonable description for the dark matter profiles of subhalos. In reality, subhalo rotation curves decline more rapidly than NFW at $r \gtrsim r_\mathrm{max}$ because of tidal effects (e.g. Kazantzidis et al., 2004). The few systems that we do have with $r_{1/2} > r_\mathrm{max}$ represent systems with stellar content that is currently being tidally stripped. We will not explore the observational implications of this evaporating population here, but this definition may prove useful for future theoretical explorations aimed at predicting the fraction of dwarf satellites that should be showing signs of ongoing stellar stripping.

With $R_\mathrm{e} \simeq 0.75\,r_{1/2}$ in hand, we may now assign a surface brightness to each system. For simplicity, we assume that each dwarf galaxy follows a Plummer profile, with a peak surface density given by Equation 6.1. As discussed above, galaxies with $\Sigma_\mathrm{peak} < 0.036\,L_\odot\,\mathrm{pc^{-2}}$ are assumed to be undetectable with standard techniques.

Before moving on to our results, we mention that the halo finder and the associated

[4] We do not account for any systematic surface brightness bias that would lead to high $\sigma_\star$ systems being missed (as these are the systems that will have large R_e). By ignoring this effect we are systematically *under-estimating* the possible number of stealth galaxies.

definition of halo mass used by Moster et al. (2009) in our stellar mass assignment differ slightly from those used in the VL2 catalogs. We estimate that this amounts to a $\sim 20\%$ difference in dark matter halo mass association for any individual object, a difference that is not significant given the exploratory nature of this work.

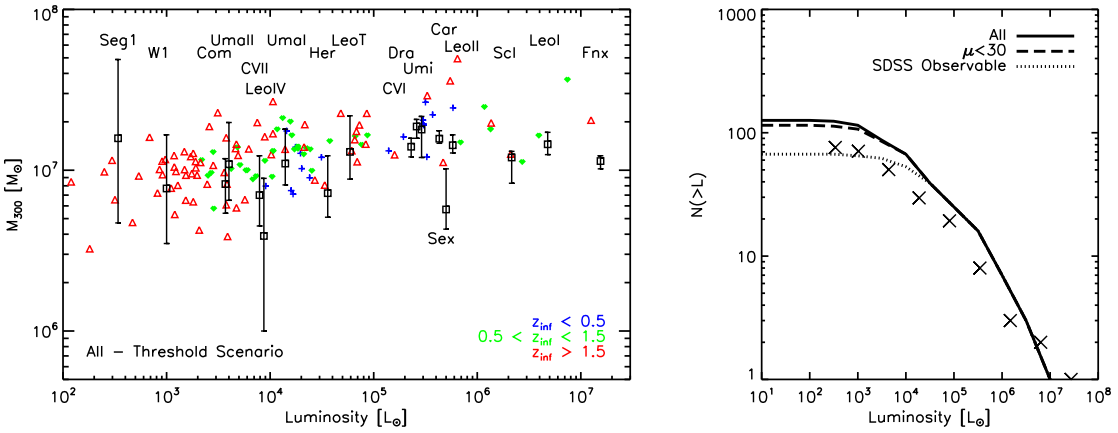

Figure 6.6: Threshold Scenario predictions for the Strigari plot (left) and luminosity function (right). The symbols and line types are identical to those in Figure 6.5 and the right panel of Figure 6.4, respectively. This model imposes a sharp truncation in galaxy formation efficiency at $M_{\rm DM} = 5 \times 10^8 M_\odot$, which drastically reduces the expected number of stealth galaxies.

6.5 Results

Figure 6.4 provides a summary of our fiducial model predictions compared to current observations: galaxy $R_{\rm e}$ vs. luminosity (left), helio-centric distance vs. luminosity (middle), and cumulative number vs. luminosity (right). The small colored symbols in the left and middle panels are model galaxies, with color and symbol type indicating three infall redshift bins with $z_{\rm inf} > 1.5$ (red triangles), $0.5 \leq z_{\rm inf} \leq 1.5$ (green circles), and $z < 0.5$ (blue plusses). The larger, black squares reproduce the MW dSph data from Figure 6.1. In the middle panel, the helio-centric distance for model galaxies is measured from an arbitrary point 8 kpc from the host dark matter halo center. Our

gross results are independent of this choice for solar location.

Model galaxies above the solid line in the left panel of Figure 6.4 are too diffuse to have been detected. Clearly, this population is significant. At fixed luminosity, systems above the solid line ($\mu = 30$ mag arcsec^{-2}) tend to have been accreted more recently (blue) than their higher-surface brightness counterparts (red). This trend follows directly from our redshift-dependent mapping between L and halo mass – at fixed stellar mass, the required halo mass increases with redshift (Figure 6.3) and, as discussed above, more massive halos tend to host more concentrated stellar distributions for a given $\sigma_\star$ and L. We also see that there is a slight tendency for early-accreted galaxies to be closer to the Sun than more recently-accreted galaxies (middle panel).

The dotted line in the right panel of Figure 6.4 shows the predicted luminosity function of satellites that are observable for an SDSS-like survey covering the full sky according to the luminosity-distance completeness limits of Walsh et al. (2009). This should be compared to the data points, which reflect the current MW satellite population corrected for sky-coverage as in Tollerud et al. (2008). The uncertainty in the in the sky-coverage correction (associated with the possibility of an anisotropic satellite distribution on the sky) is similar to the size of the points (Tollerud et al. 2008). We see that the predicted and observed populations are roughly consistent. The solid line shows the predicted luminosity function for all satellites within 400 kpc, without any allowance for observational incompleteness. The dashed line, on the other hand, shows the subset of those galaxies that have peak stellar surface densities that are bright enough to be discovered with standard techniques. We see that roughly half of the systems that are in principle luminous enough to be detected with deep surveys like LSST (with $L \lesssim 1000 L_\odot$) have peak surface densities that are too diffuse to be seen. Specifically, even a survey like LSST, with a very deep limiting magnitude, will

have difficulties detecting these systems without new observing strategies.

Figure 6.5 explores how detection bias affects the Strigari plot. In the upper panel, we show M_{300} vs. L for all model satellites within 400 kpc of the Sun (color/type scheme is the same as in Figure 6.4) compared to the MW dSphs (black squares). We see that unlike the data, there is a significant population of predicted galaxies with low central densities $M_{300} \lesssim 5 \times 10^6 M_\odot$ for $L \lesssim 5000 L_\odot$. Moreover, while the data follow a nearly common-mass relation $M_{300} \propto L^c$ with $c \simeq 0.05$ (using updated luminosities) the model points prefer a steeper trend $c \simeq 0.15$ (as expected from abundance matching). The model predictions are very similar to those presented in many past CDM-based explorations of satellite M_{300} values (e.g. Macciò et al., 2009; Busha et al., 2009; Muñoz et al., 2009). The similarity between our model results and those of Muñoz et al. (2009), in particular, are encouraging. These authors use the same VL2 catalog that we use, but they explored a more sophisticated model for assigning light to subhalos. Generally, a population of $L \lesssim 5000 L_\odot$ satellite galaxies with $M_{300} \lesssim 5 \times 10^6 M_\odot$ seems to be a fairly robust expectation for hierarchical models.

The bottom left panel of Figure 6.5 includes only those model galaxies that have peak surface brightness $\mu < 30$ mag arcsec^{-2}. We see that this requirement immediately removes the population of $M_{300} \lesssim 5 \times 10^6 M_\odot$ objects. The bottom right panel includes only those galaxies that meet both the surface brightness requirement and the luminosity-distance requirement for SDSS discovery. We see that the resultant population of observable model galaxies has M_{300} values that are very much in line with those of the known MW dSphs. The model we have adopted therefore reproduces both the luminosity function and the mass function of Milky Way dwarfs, once all of the relevant selection bias effects are taken into account. It is therefore reasonable to take the implied model prediction seriously: there is a large, undiscovered population of very low surface brightness MW satellite galaxies that preferentially inhabit the

lowest mass dark matter halos to host stars.

Of course, if the smallest dark matter halos do not contain galaxies at all, then the likelihood for a significant stealth galaxy population is much reduced. We explore this expectation with our Threshold Scenario, which imposes a sharp scale in galaxy formation at $M_{\rm DM} = 5 \times 10^8 M_\odot$. Below this scale dark matter halos are completely devoid of stars (vertical line in Figure 6.3). The resultant Strigari plot and luminosity functions for this model are shown in Figure 6.6. Like the Fiducial Scenario, the Threshold Scenario also reproduces the observed satellite luminosity function (right panel). However, unlike in the Fiducial Scenario, we now expect only a handful of stealth galaxies that remain undiscovered (solid vs. dashed lines). The Threshold case also yields a Strigari relation that is in reasonable agreement with the data (left panel), without appealing to any selection bias. Another distinct difference in the Threshold scenario is that all of the low-luminosity galaxies are expected to be quite old (or at least to have been accreted early $z_{inf} > 1.5$).

Before concluding we note that the MW dSph M_{300} masses in Figures 6.5 and 6.6 are taken directly from Strigari et al. (2008). A more recent analysis of membership in the Hercules dwarf (labeled Her in Figures 6.5 and 6.6) by Adén et al. (2009) suggests that the actual M_{300} mass for this system is about a factor of ~ 3 lower than the value used in our Figure 6.5. Though this result does not change the fact that there is no strong observed trend between M_{300} and L in the data, it does make the mass of Hercules more difficult to explain in our model (and in almost all CDM-based models to date). The newly-derived velocity dispersion from Adén et al. (2009) is $\sigma_\star \simeq 3.7 {\rm km\,s^{-1}}$, which is low enough that this system would not be expected to be stealth according to our definition. Of course, as the most elongated of the dSphs known, the systematic error associated with any spherically-symmetric mass determination in Hercules is likely to be significant. More work on the issue of

membership and mass modeling in this interesting object is certainly warranted.

6.6 Conclusions and Discussion

We have argued that there is likely a population of low-luminosity satellite galaxies orbiting within the halo of the Milky Way that are too diffuse to have been detected with current star-count surveys, despite the fact that they have luminosities similar to those of known ultrafaint MW dSphs. These stealth galaxies should preferentially inhabit the smallest dark matter subhalos that host stars ($V_{\rm max} \lesssim 15$ km s^{-1}). One implication is that selection bias (Figures 6.2 and 6.5) may play a role explaining the apparent common mass scale for MW dSph galaxies (Strigari et al., 2008; Peñarrubia et al., 2008; Walker et al., 2009; Wolf et al., 2009).

We developed a plausible estimate for the number and character of MW stealth satellites using the subhalo catalogs of the VL2 simulation (Diemand et al., 2008). We assigned light to subhalos by extrapolating the dark matter mass-light relationship required to reproduce bright galaxy number counts (Moster et al., 2009) and we assigned stellar velocity dispersions to each system by adopting the empirical relationship between $\sigma_\star$ and L for known Milky Way dwarfs. Finally, galaxy sizes were computed using the dynamical relationship between $R_{\rm e}$ and $\sigma_\star$ for the measured dark matter halo densities in each subhalo (Equation 6.3). The resultant model galaxy population includes a substantial fraction of ultrafaint galaxies that are stealth, with peak surface brightness $\mu > 30$ mag arcsec^{-2}. According to our fiducial estimate, about half of the several hundred satellite galaxies that should be potentially observable by surveys like LSST fall into this category (Figure 6.4).

We also explored the possibility that there is a sharp threshold in galaxy formation

at a halo mass of $M_{\rm DM} = 5 \times 10^8 M_\odot$. This idea follows from the common mass conjecture in Strigari et al. (2008) and remains viable since it reproduces the observed Milky Way satellite luminosity function as well as a fairly weak M_{300} vs. L trend without appealing to selection bias (Figure 6.6). In this scenario, there are no low-mass halos that host satellite galaxies, and therefore the number of predicted stealth galaxies (which preferentially inhabit the smallest dark matter halos) is significantly reduced (Figure 6.6). Moreover, we expect that all of the low-luminosity satellites will have been accreted since $z \simeq 1.5$ (Figure 6.6) and that they will all host old stellar populations. This is not necessarily the case in our Fiducial Scenario, where the most distant and low-mass subhalos may host ultrafaint galaxies that contain intermediate-age stars.

It is well known that galaxy formation has a primary scale – the scale that gives rise to the L_* cutoff in galaxy counts at the bright end of the luminosity function. We do not know if there is a second scale at the low-luminosity end. One implication of our findings is that a complete search for very low surface brightness satellite galaxies of the Milky Way can help determine whether or not there is a second scale in galaxy formation. Of course, the lack of stealth galaxies is fundamentally an indication that there are no very low mass halos that host stars. A similar effect would be seen if there were simply a truncation in the power spectrum, as might be expected in ~ 1 KeV WDM models (Strigari et al., 2008; Maccio' & Fontanot, 2009). In this sense, the discovery of many stealth galaxies in the halo would provide a means to constrain dark matter particle properties in addition to galaxy formation physics.

It is possible that the structure known as the Pices Overdensity (or Structure J) at a distance of ~ 85 kpc represents the first detection of a stealth dwarf galaxy with $\mu > 30$ (Kollmeier et al., 2009), though deeper imaging and spectroscopic follow-up will be required to test this suggestion. Unlike the well-known ultrafaint dSphs of

the Milky Way, which were discovered as overdensities in RGB or MS turnoff stars, this system was discovered as an excess in RR Lyrae variables in the multi-epoch SDSS Stripe-82 (Watkins et al., 2009; Sesar et. al, 2007). Repeated sky surveys like Pan-STARRS and LSST may provide the best hope for discoveries of this kind in the future.

More generally, upcoming deep, time-resolved sky surveys and associated follow-up campaigns with 30m-class telescopes offer significant hope for the discovery of hundreds of new dwarf galaxy companions of the Milky Way (Tollerud et al. 2008). These data will definitively constrain the overall count of stealth galaxies that lurk at very low surface brightness and provide unparalleled constraints on the efficiency of galaxy formation in the smallest dark matter halos.

6.7 Acknowledgements

The contents of this chapter have been submitted for publication in The Astrophysics Journal as Bullock, Stewart, Kaplinghat, and Tollerud (2010) . We thank M. Geha, G. Gilmore, J. Simon, and B. Willman for useful discussions.

Chapter 7

Future Work

7.1 A Systematic Approach to Cosmological Hydrodynamic Simulations

So far, the work presented here has specialized in analyzing cosmological dark matter simulations to understand the merger statistics of dark matter halos. While dark matter halo merger rates and merger statistics are well understood in the current ΛCDM framework, the underlying baryonic physics is much more complicated. In the work presented so far, we have used semi-empirical techniques such as the observed stellar mass function and relations between galaxy stellar mass and cold gas mass to estimate baryonic properties of DM halos in a statistical sense. This method is statistically reliable for large samples of halos, however, the scatter in these relations make such an approach impossible for studying the detailed evolution of galaxies on a case-by-case basis. An alternate approach is to use the initial conditions for a smaller subregion of a large dark matter simulation as a starting point for a smooth particle hydrodynamic (SPH) simulation, that includes treatment of gas, star forma-

tion, supernova feedback, metal enrichment and cooling, etc. While some of these processes are not yet fully understood (for example, the precise details in how energy from supernovas effects gas in the surrounding regions) such simulations have become increasingly successful in producing realistic galaxies in recent years (e.g., Governato et al., 2007, 2009).

One drawback of hydrodynamic simulations is that they are computationally expensive, making a statistical analysis difficult. Indeed, it is often unclear how statistically commonplace a given hydrodynamic simulation is, once placed in a cosmological context. As a future avenue of study, I plan to run a suite of hydrodynamic simulations of Milky Way-sized dark matter halos ($M \sim 10^{12} M_{\odot}$), sampling a systematic distribution of merger accretion histories and halo environments for halos of this mass. For example, it is well known that statistically averaged mass accretion histories of dark matter halos are well-described by an exponential, $M(z) = M_0 e^{-\alpha z}$ (Wechsler et al., 2002). However, while this relation holds true in an average sense, on an individual basis, $\sim 1/3$ of Milky Way-size halos exhibit steep late growth compared to this exponential form, with $\sim 1/3$ showing shallow late growth and $\sim 1/3$ fitting quite well the the average exponential form (McBride et al., 2009). Would steep, shallow, and exponential late growth halos produce galaxies with noticeable differences, if run in a self-consistent cosmological hydrodynamic simulation? What about the resulting differences between the $\sim 30\%$ of Milky Way-size halos without a single large ($m > 10^{11} h^{-1} M_{\odot}$) merger since $z = 2$, the $\sim 40\%$ of halos with exactly one such merger, and the $\sim 30\%$ of halos with two or more such mergers (as in Chapter 2, Figure 2.5, right panel)? A suite of hydrodynamic simulations covering a statistical range of common merger histories is necessary to answer these questions. An example simulations, similar to the suite of simulations I intend to run, is shown in Figure 7.1, and briefly discussed below.

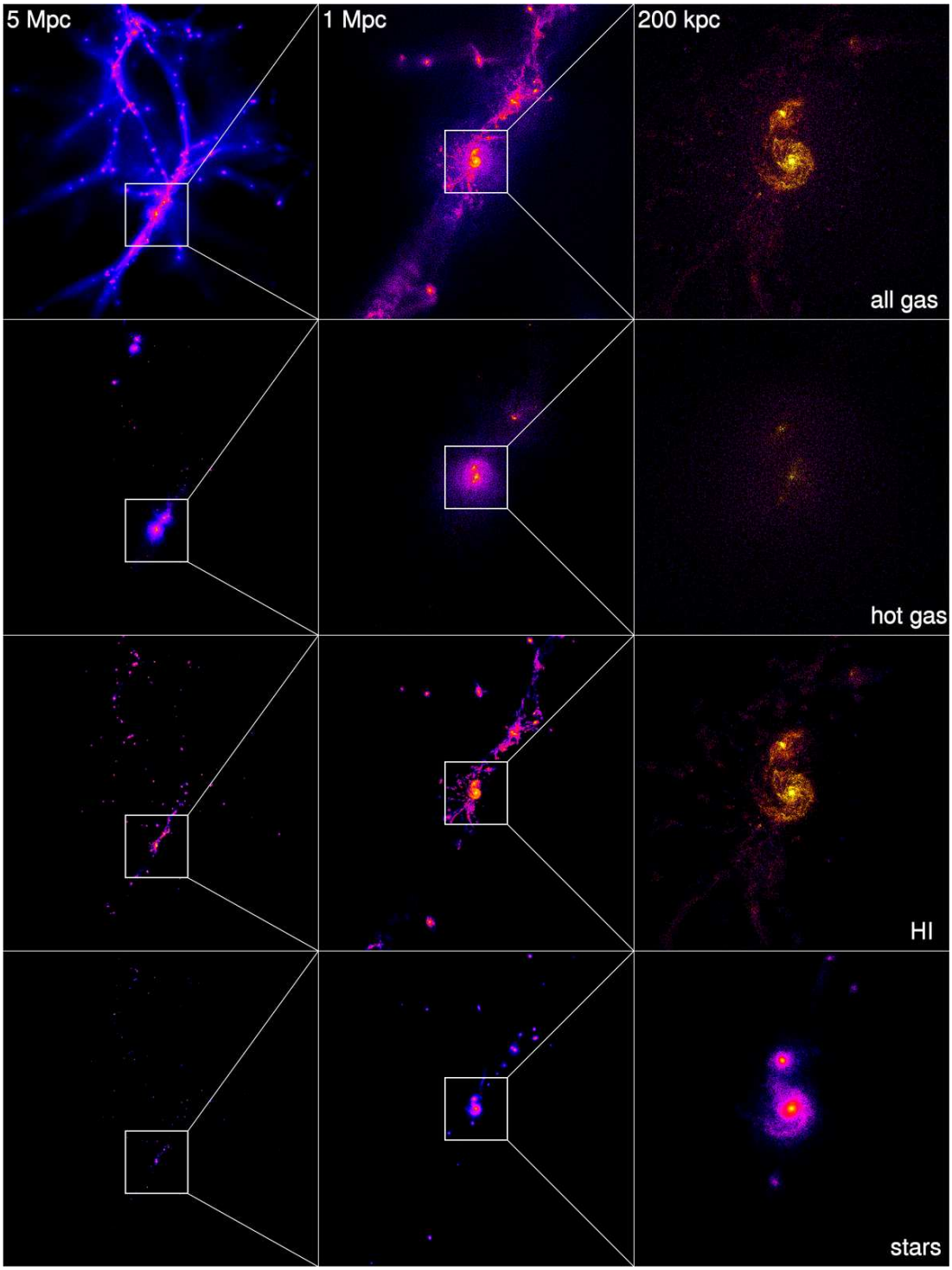

Figure 7.1: A sample visualization from our simulation. Panel widths correspond to 5 Mpc, 1 Mpc, and 200 kpc (comoving). The white squares in the middle and left columns show the "zoom in" area of panels to the right. From top to bottom, rows show 3-d density maps (blue less dense; white most dense) of: all gas, hot ($T > 500,000K$) gas, cold gas (neutral hydrogen), and stellar mass. This figure shows the main progenitor galaxy about to experience a major merger at $z \sim 1.5$.

7.2 Example Simulation: "Via Lactea II" with SPH code "GASOLINE"

Our "VL2gas" simulation, shown in Figure 7.1, implements the same initial conditions as the Via Lactea II simulation from Diemand et al. (2008). The main galaxy has a dark halo mass of $M_{\rm vir}(z=0) \sim 2 \times 10^{12} M_{\odot}$. We implement the "zoom in" technique to properly account for large-scale tidal torques as described in Katz & White (1993). The simulation is contained within a 40 comoving kpc cube, with the highest resolution region (which includes all the gas and star particles) limited to a ~ 4 comoving kpc cube volume. The simulation uses the smooth particle hydrodynamics (SPH) code GASOLINE (Wadsley et. al, 2004) to treat the behavior of gas. In the highest resolution region, the masses per particle of our simulation are: $(m_{\rm dark}, m_{\rm gas}, m_{\rm star}) = (3.7, 3.4, 1.0) \times 10^5 M_{\odot}$, with a force softening of 332 pc, and a minimum SPH smoothing length of 0.05 times the force softening. There are no strong momentum-driven winds in our simulation, nor is there AGN feedback. The code implements Compton and radiative cooling, as well as star formation and the "blastwave feedback" prescriptions detailed in Katz et al. (1996) and Stinson et. al (2006), while the the cosmic UV field implemented is described in Haardt & Madau (1996). These prescriptions are identical to those implemented in recent simulations (Governato et al., 2007, 2009) that have shown great success in producing realistic disk-type galaxies. We refer the reader to these works for a more detailed description of the workings of the code, though we will give a brief overview here.

Criteria for gas particles to form star particles (star formation) are: 1) the gas particle temperature is $< 30,000K$; 2) local gas density is > 0.1 cm^{-3}; 3) other local gas particles (in our case, the 32 nearest neighbors) define a converging flow. Stars form according to the Schmidt Law (Kennicutt, 1998), with a Kroupa IMF Kroupa et al.

(1993). We assume that energy from supernova feedback creates turbulent motions in nearby gas particles (again, the 32 nearest neighbors) that keeps these gas particles from cooling and forming stars. Once a star particle is formed, it is treated as a single population with uniform metallicity. We also keep track of mass loss from stellar winds, with star particles losing $\sim 30 - 40\%$ of their mass over time, depositing this mass into nearby gas particles, and enriching the ISM with metals from both supernovae types Ia and II (adopting yields from Thielemann et al. (1986) and Weaver & Woosley (1993) respectively). As with feedback, these metals are distributed to the 32 nearest neighbors. We note that the only two free parameters in this star formation and feedback model (star formation efficiency and the fraction of SN energy that is coupled to the ISM) have both been fixed based on the results of Governato et al. (2007), in order to produce galaxies with realistic star formation rates, disk thickness, gas turbulence, and Schmidt law over a range in dynamic masses. In addition, this pre-set scheme has also been shown to match observed trends between metallicity and stellar mass (Brooks et al., 2007) and the abundance of Damped Lyman α systems at $z = 3$ (Pontzen et al., 2008).

Chapter 8

Summary and Concluding Remarks

The aim of this thesis has been to bridge theoretical expectations of ΛCDM cosmology and observations. In order to do this, we have used dark matter halo merger histories from dissipationless cosmological N-body simulations to characterize globally averaged merger statistics as a function of redshift, merger mass ratio and halo mass. We have demonstrated a good agreement between theory and observations in regards to more direct measurements of the galaxy merger rate, such as the morphologically disturbed fraction of galaxies and close-pair counts of galaxies as a function of redshift, to within the margins of error of both theory and observations (as discussed in Chapter 3). It is important to note in such comparisons that often observation will define merger mass ratios in terms of galaxy baryonic mass (stars and cold gas) or stellar mass, whereas observations typically use dark matter halo mass. Because there is not a simple linear relation between these quantities, and the merger rate of galaxies is strongly dependent on merger mass ratio, it is important to keep this distinction in mind when comparing theory to observation (as discussed in detail in Chapter 5).

We have also focused on the issue of disk survivability. With mergers being as common as they are in ΛCDM, how are disk-dominated galaxies formed at high redshift expected to survive subsequent major mergers until $z = 0$, such that the majority of Milky Way-sized galaxies are disks? We quantified the extent of this problem in Chapter 2, showing that 70% of Milky Way-sized galaxies have experienced at least one dark matter halo merger with more mass than the Milky Way's own baryonic disk ($m > 10^{11} h^{-1} M_{\odot}$) in the last 10 Gyr ($z \sim 2$). And only a small fraction of the final halo mass was built via subsequent minor mergers. As such, in order for theory and observations to agree, mergers this massive must *not always* destroy disk morphologies. One possible explanation for this seeming contradiction is the role of gas in mergers. Recent simulations have stressed that gas-rich major mergers may in fact result in disk galaxies, and are consistent with the kinematics of disk galaxies at $z \sim 2$ (Brook et al., 2004; Robertson et al., 2006a; Robertson & Bullock, 2008). In order to explore the extent to which this may resolve the issue of disk survival, we implemented empirically motivated prescriptions for stellar mass and cold gas mass as a function of halo mass and redshift. Given these prescriptions, we find astonishing agreement between the observed bulge-dominated fraction as a function of halo mass, and the theoretical fraction of halos with a gas-poor major merger since $z = 2$. Although this by no means "solves" the problem of disk survival, it is strongly suggestive that if gas-rich mergers do indeed preserve disk morphologies, then cosmologically expected merger histories are consistent with observed morphological fractions.

Finally, we used the very high resolution dark matter simulation "Via Lactea II" in combination with the empirically motivated stellar mass–halo mass relation to explore cosmological expectations for the substructure of the Milky Way. Our model shows good agreement with the observed luminosity function of galaxies, as well as the "Strigari" plot (M_{300} vs. Luminosity for Milky Way dwarf galaxies), once we account for luminosity and peak surface brightness selection biases. Our model

also suggests that the flat slope shown in the Strigari plot (Strigari et al., 2008) may be the result of this selection bias, and we predict a population of very low surface brightness "stealth" galaxies within the halo of the Milky Way, which have luminosities comparable to observed ultrafaint dwarfs, but reside is less massive halos, resulting in low surface brightnesses that cannot be detected with current methods.

Recent SPH simulations have become increasingly successful in producing realistic disk-dominated galaxies that match a number of empirical relations (e.g., Governato et al., 2007, 2009). However, since such simulations are typically computationally expensive, they lack the statistical power of cosmological N-body simulations of dark matter substructure, and it is often unclear what methods were used in choosing the initial conditions for such simulations. As computational resources increase, it will be important to begin choosing halos for hydrodynamic resimulation in a systematic manner, probing statistically representative merger histories across a wide range of parameters. Only then can we hope to address how the results of these simulations may be generalized to more global populations of galaxies in ΛCDM.

Bibliography

Abadi, M. G., Navarro, J. F., Steinmetz, M., & Eke, V. R. 2003, ApJ, 591, 499

Adelberger, K. L., Erb, D. K., Steidel, C. C., Reddy, N. A., Pettini, M., & Shapley, A. E. 2005, ApJ, 620, L75

Adén, D., Wilkinson, M. I., Read, J. I., Feltzing, S., Koch, A., Gilmore, G. F., Grebel, E. K., & Lundström, I. 2009, ApJL, Accepted, ArXiv:0910.1348

Agertz, O., Teyssier, R., & Moore, B. 2009, MNRAS, 397, L64

Allgood, B., Flores, R. A., Primack, J. R., Kravtsov, A. V., Wechsler, R. H., Faltenbacher, A., & Bullock, J. S. 2006, MNRAS, 367, 1781

Baldry, I. K., Balogh, M. L., Bower, R. G., Glazebrook, K., Nichol, R. C., Bamford, S. P., & Budavari, T. 2006, MNRAS, 373, 469

Baldry, I. K., Glazebrook, K., Brinkmann, J., Ivezić, Ž., Lupton, R. H., Nichol, R. C., & Szalay, A. S. 2004, ApJ, 600, 681

Baldry, I. K., Glazebrook, K., & Driver, S. P. 2008, MNRAS, 388, 945

Barnes, J. E. 1988, ApJ, 331, 699

—. 2002, MNRAS, 333, 481

Barnes, J. E. & Hernquist, L. 1996, ApJ, 471, 115

Barton, E. J., Arnold, J. A., Zentner, A. R., Bullock, J. S., & Wechsler, R. H. 2007, ApJ, 671, 1538

Bell, E. F., McIntosh, D. H., Katz, N., & Weinberg, M. D. 2003, ApJ, 149, 289

Bell, E. F., Phleps, S., Somerville, R. S., Wolf, C., Borch, A., & Meisenheimer, K. 2006, ApJ, 652, 270

Bell, E. F., Zucker, D. B., Belokurov, V., Sharma, S., Johnston, K. V., Bullock, J. S., Hogg, D. W., Jahnke, K., de Jong, J. T. A., Beers, T. C., Evans, N. W., Grebel, E. K., Ivezić, Ž., Koposov, S. E., Rix, H., Schneider, D. P., Steinmetz, M., & Zolotov, A. 2008, ApJ, 680, 295

Bell et al. 2005, ApJ, 625, 23

Belokurov, V., Walker, M. G., Evans, N. W., Gilmore, G., Irwin, M. J., Mateo, M., Mayer, L., Olszewski, E., Bechtold, J., & Pickering, T. 2009, MNRAS, 397, 1748

Belokurov, V., Zucker, D. B., Evans, N. W., Kleyna, J. T., Koposov, S., Hodgkin, S. T., Irwin, M. J., Gilmore, G., Wilkinson, M. I., Fellhauer, M., Bramich, D. M., Hewett, P. C., Vidrih, S., De Jong, J. T. A., Smith, J. A., Rix, H.-W., Bell, E. F., Wyse, R. F. G., Newberg, H. J., Mayeur, P. A., Yanny, B., Rockosi, C. M., Gnedin, O. Y., Schneider, D. P., Beers, T. C., Barentine, J. C., Brewington, H., Brinkmann, J., Harvanek, M., Kleinman, S. J., Krzesinski, J., Long, D., Nitta, A., & Snedden, S. A. 2007, ApJ, 654, 897

Benson, A. J., Bower, R. G., Frenk, C. S., Lacey, C. G., Baugh, C. M., & Cole, S. 2003, ApJ, 599, 38

Berrier, J. C., Bullock, J. S., Barton, E. J., Guenther, H. D., Zentner, A. R., & Wechsler, R. H. 2006, ApJ, 652, 56

Besla, G., Kallivayalil, N., Hernquist, L., Robertson, B., Cox, T. J., van der Marel, R. P., & Alcock, C. 2007, ApJ, 668, 949

Birnboim, Y. & Dekel, A. 2003, MNRAS, 345, 349

Blanton et al. 2003, ApJ, 594, 186

Blumenthal, G. R., Faber, S. M., Primack, J. R., & Rees, M. J. 1984, Nature, 311, 517

Bournaud, F., Jog, C. J., & Combes, F. 2007, A&A, 476, 1179

Bouwens, R. J., Illingworth, G. D., Franx, M., & Ford, H. 2007, ApJ, 670, 928

Boylan-Kolchin, M., Ma, C.-P., & Quataert, E. 2005, MNRAS, 362, 184

—. 2008, MNRAS, 383, 93

Brook, C., Richard, S., Kawata, D., Martel, H., & Gibson, B. K. 2007a, ApJ, 658, 60

Brook, C. B., Kawata, D., Gibson, B. K., & Freeman, K. C. 2004, ApJ, 612, 894

Brook, C. B., Veilleux, V., Kawata, D., Martel, H., & Gibson, B. K. Gas Rich Mergers in Disk Formation (Island Universes - Structure and Evolution of Disk Galaxies), 551–+

Brooks, A. M., Governato, F., Booth, C. M., Willman, B., Gardner, J. P., Wadsley, J., Stinson, G., & Quinn, T. 2007, ApJ, 655, L17

Brooks, A. M., Governato, F., Quinn, T., Brook, C. B., & Wadsley, J. 2009, ApJ, 694, 396

Bryan, G. L. & Norman, M. L. 1998, ApJ, 495, 80

Bullock, J. S. & Johnston, K. V. 2005, ApJ, 635, 931

Bullock, J. S., Kolatt, T. S., Sigad, Y., Somerville, R. S., Kravtsov, A. V., Klypin, A. A., Primack, J. R., & Dekel, A. 2001a, MNRAS, 321, 559

Bullock, J. S., Kravtsov, A. V., & Weinberg, D. H. 2000, ApJ, 539, 517

—. 2001b, ApJ, 548, 33

Bullock, J. S., Stewart, K. R., Kaplinghat, M., & Tollerud, E. J. 2009a

Bullock, J. S., Stewart, K. R., & Purcell, C. W. 2009b, in IAU Symposium, Vol. 254, IAU Symposium, ed. J. Andersen, J. Bland-Hawthorn, & B. Nordström, 85–94

Bundy, K., Fukugita, M., Ellis, R. S., Targett, T. A., Belli, S., & Kodama, T. 2009, ApJ, 697, 1369

Burkert, A., Naab, T., Johansson, P. H., & Jesseit, R. 2008, ApJ, 685, 897

Busha, M. T., Alvarez, M. A., Wechsler, R. H., Abel, T., & Strigari, L. E. 2009, ApJ, Submitted, ArXiv:0901.3553

Carlberg et al. 2000, ApJ, 532, L1

Carollo, C. M., Scarlata, C., Stiavelli, M., Wyse, R. F. G., & Mayer, L. 2007, ApJ, 658, 960

Cattaneo, A., Dekel, A., Devriendt, J., Guiderdoni, B., & Blaizot, J. 2006, MNRAS, 370, 1651

Choi, Y.-Y., Park, C., & Vogeley, M. S. 2007, ApJ, 658, 884

Cohn, J. D. & White, M. 2008, MNRAS, 385, 2025

Cole, S., Helly, J., Frenk, C. S., & Parkinson, H. 2008a, MNRAS, 383, 546

—. 2008b, MNRAS, 383, 546

Conroy, C., Shapley, A. E., Tinker, J. L., Santos, M. R., & Lemson, G. 2008, ApJ, 679, 1192

Conroy, C. & Wechsler, R. H. 2009a, ApJ, 696, 620

—. 2009b, ApJ, 696, 620

Conroy, C., Wechsler, R. H., & Kravtsov, A. V. 2006, ApJ, 647, 201

—. 2007, ApJ, 668, 826

Conselice, C. J., Bershady, M. A., Dickinson, M., & Papovich, C. 2003, AJ, 126, 1183

Courteau, S., de Jong, R. S., & Broeils, A. H. 1996, ApJ, 457, L73+

Cowie, L. L. & Barger, A. J. 2008, ApJ, 686, 72

Cox, T. J., Dutta, S. N., Di Matteo, T., Hernquist, L., Hopkins, P. F., Robertson, B., & Springel, V. 2006a, ApJ, 650, 791

Cox, T. J., Jonsson, P., Primack, J. R., & Somerville, R. S. 2006b, MNRAS, 373, 1013

Cox, T. J., Jonsson, P., Somerville, R. S., Primack, J. R., & Dekel, A. 2008, MNRAS, 384, 386

Cuesta, A. J., Prada, F., Klypin, A., & Moles, M. 2008, MNRAS, 389, 385

Dalcanton, J. J. & Bernstein, R. A. 2002, AJ, 124, 1328

Dalcanton, J. J., Seth, A., & Yoachim, P. 2005, arXiv:astro-ph/0509700

Davis, M., Efstathiou, G., Frenk, C. S., & White, S. D. M. 1985, ApJ, 292, 371

de Ravel et al. 2009, A&A, 498, 379

Dekel, A. & Birnboim, Y. 2006, MNRAS, 368, 2

Dekel, A., Birnboim, Y., Engel, G., Freundlich, J., Goerdt, T., Mumcuoglu, M., Neistein, E., Pichon, C., Teyssier, R., & Zinger, E. 2009, Nature, 457, 451

Di Matteo, T., Springel, V., & Hernquist, L. 2005, Nature, 433, 604

Diaferio, A., Kauffmann, G., Balogh, M. L., White, S. D. M., Schade, D., & Ellingson, E. 2001, MNRAS, 323, 999

Diemand, J., Kuhlen, M., & Madau, P. 2007, ApJ, 667, 859

Diemand, J., Kuhlen, M., Madau, P., Zemp, M., Moore, B., Potter, D., & Stadel, J. 2008, Nature, 454, 735

Erb, D. K., Steidel, C. C., Shapley, A. E., Pettini, M., Reddy, N. A., & Adelberger, K. L. 2006, ApJ, 646, 107

Faber et al. 2007, ApJ, 665, 265

Fakhouri, O. & Ma, C. 2009, MNRAS, 394, 1825

Fakhouri, O. & Ma, C.-P. 2008, MNRAS, 386, 577

Feldmann, R., Mayer, L., & Carollo, C. M. 2008, ApJ, 684, 1062

Förster Schreiber et al. 2006, The Messenger, 125, 11

Geha, M., Blanton, M. R., Masjedi, M., & West, A. A. 2006, ApJ, 653, 240

Geha, M., Willman, B., Simon, J. D., Strigari, L. E., Kirby, E. N., Law, D. R., & Strader, J. 2009, ApJ, 692, 1464

Genel, S., Genzel, R., Bouché, N., Naab, T., & Sternberg, A. 2009, ApJ, 701, 2002

Genzel et al. 2006, Nature, 442, 786

Gnedin, N. Y., Tassis, K., & Kravtsov, A. V. 2009, ApJ, 697, 55

Gottlöber, S., Klypin, A., & Kravtsov, A. V. 2001, ApJ, 546, 223

Governato, F., Brook, C. B., Brooks, A. M., Mayer, L., Willman, B., Jonsson, P., Stilp, A. M., Pope, L., Christensen, C., Wadsley, J., & Quinn, T. 2009, MNRAS, 398, 312

Governato, F., Gardner, J. P., Stadel, J., Quinn, T., & Lake, G. 1999, AJ, 117, 1651

Governato, F., Willman, B., Mayer, L., Brooks, A., Stinson, G., Valenzuela, O., Wadsley, J., & Quinn, T. 2007, MNRAS, 374, 1479

Grcevich, J., Putman, M., & Peek, J. E. G. 2008, in American Institute of Physics Conference Series, Vol. 1035, The Evolution of Galaxies Through the Neutral Hydrogen Window, ed. R. Minchin & E. Momjian, 159–162

Grillmair, C. J. 2006, ApJ, 645, L37

—. 2009, ApJ, 693, 1118

Haardt, F. & Madau, P. 1996, ApJ, 461, 20

Hammer, F., Flores, H., Puech, M., Athanassoula, E., Rodrigues, M., Yang, Y., & Delgado-Serrano, R. 2009a, submitted to A&A, ArXiv:0903.3962 [astro-ph],

Hammer, F., Flores, H., Yang, Y. B., Athanassoula, E., Puech, M., Rodrigues, M., & Peirani, S. 2009b, A&A, 496, 381

Hayashi, H. & Chiba, M. 2006, PASJ, 58, 835

Heckman, T. M., Smith, E. P., Baum, S. A., van Breugel, W. J. M., Miley, G. K., Illingworth, G. D., Bothun, G. D., & Balick, B. 1986, ApJ, 311, 526

Helmi, A. & White, S. D. M. 1999, MNRAS, 307, 495

Hernquist, L. 1993, ApJ, 409, 548

Hopkins, P. F., Cox, T. J., Younger, J. D., & Hernquist, L. 2009a, ApJ, 691, 1168

Hopkins, P. F., Hernquist, L., Cox, T. J., Younger, J. D., & Besla, G. 2008, ApJ, 688, 757

Hopkins, P. F., Somerville, R. S., Cox, T. J., Hernquist, L., Jogee, S., Kereš, D., Ma, C., Robertson, B., & Stewart, K. 2009b, MNRAS, 397, 802

Ilbert et al. 2006, A&A, 453, 809

Ivezic et. al. 2008, ArXiv:0805.2366

Jesseit, R., Naab, T., Peletier, R. F., & Burkert, A. 2007, MNRAS, 376, 997

Jogee et. al. 2008, in Astronomical Society of the Pacific Conference Series, Vol. 396, Astronomical Society of the Pacific Conference Series, ed. J. G. Funes & E. M. Corsini, 337–+

Johnston, K. V., Hernquist, L., & Bolte, M. 1996, ApJ, 465, 278

Jonsson, P., Cox, T. J., Primack, J. R., & Somerville, R. S. 2006, ApJ, 637, 255

Jurić et. al. 2008, ApJ, 673, 864

Kampczyk, P., Lilly, S. J., Carollo, C. M., Scarlata, C., Feldmann, R., Koekemoer, A., Leauthaud, A., Sargent, M. T., Taniguchi, Y., & Capak, P. 2007, ApJ, 172, 329

Kannappan, S. J. 2004, ApJ, 611, L89

Kartaltepe, J. S., Sanders, D. B., Scoville, N. Z., Calzetti, D., Capak, P., Koekemoer, A., Mobasher, B., Murayama, T., Salvato, M., Sasaki, S. S., & Taniguchi, Y. 2007, ApJ, 172, 320

Katz, N., Weinberg, D. H., & Hernquist, L. 1996, ApJ, 105, 19

Katz, N. & White, S. D. M. 1993, ApJ, 412, 455

Kauffmann, G., Heckman, T. M., White, S. D. M., Charlot, S., Tremonti, C., Peng, E. W., Seibert, M., Brinkmann, J., Nichol, R. C., SubbaRao, M., & York, D. 2003, MNRAS, 341, 54

Kaufmann, T., Mayer, L., Wadsley, J., Stadel, J., & Moore, B. 2007a, MNRAS, 53

Kaufmann, T., Wheeler, C., & Bullock, J. S. 2007b, MNRAS, 382, 1187

Kautsch, S. J., Grebel, E. K., Barazza, F. D., & Gallagher, III, J. S. 2006, A&A, 445, 765

Kazantzidis, S., Bullock, J. S., Zentner, A. R., Kravtsov, A. V., & Moustakas, L. A. 2008, ApJ, 688, 254

Kazantzidis, S., Mayer, L., Mastropietro, C., Diemand, J., Stadel, J., & Moore, B. 2004, ApJ, 608, 663

Kazantzidis, S., Zentner, A. R., & Bullock, J. S. 2009, in IAU Symposium, Vol. 254, IAU Symposium, ed. J. Andersen, J. Bland-Hawthorn, & B. Nordström, 417–422

Kennicutt, Jr., R. C. 1998, ApJ, 498, 541

Kereš, D., Katz, N., Fardal, M., Davé, R., & Weinberg, D. H. 2009, MNRAS, 395, 160

Kereš, D., Katz, N., Weinberg, D. H., & Davé, R. 2005, MNRAS, 363, 2

Khochfar, S. & Burkert, A. 2005, MNRAS, 359, 1379

Kirby, E. N., Simon, J. D., Geha, M., Guhathakurta, P., & Frebel, A. 2008, ApJ, 685, L43

Kitzbichler, M. G. & White, S. D. M. 2008, MNRAS, 391, 1489

Klypin, A. & Holtzman, J. 1997, ArXiv:astro-ph/9712217

Klypin, A., Kravtsov, A. V., Valenzuela, O., & Prada, F. 1999a, ApJ, 522, 82

—. 1999b, ApJ, 522, 82

Klypin, A., Zhao, H., & Somerville, R. S. 2002, ApJ, 573, 597

Koda, J., Milosavljević, M., & Shapiro, P. R. 2009, ApJ, 696, 254

Kolatt, T. S., Bullock, J. S., Somerville, R. S., Sigad, Y., Jonsson, P., Kravtsov, A. V., Klypin, A. A., Primack, J. R., Faber, S. M., & Dekel, A. 1999, ApJ, 523, L109

Kollmeier, J. A., Gould, A., Shectman, S., Thompson, I. B., Preston, G. W., Simon, J. D., Crane, J. D., Ivezić, Ž., & Sesar, B. 2009, ApJ, 705, L158

Komiya, Y., Suda, T., Habe, A., & Fujimoto, M. Y. 2008, in American Institute of Physics Conference Series, Vol. 990, First Stars III, ed. B. W. O'Shea & A. Heger, 462–466

Koposov, S., Belokurov, V., Evans, N. W., Hewett, P. C., Irwin, M. J., Gilmore, G., Zucker, D. B., Rix, H.-W., Fellhauer, M., Bell, E. F., & Glushkova, E. V. 2008, ApJ, 686, 279

Kormendy, J. & Fisher, D. B. 2005, in Revista Mexicana de Astronomia y Astrofisica Conference Series, Vol. 23, Revista Mexicana de Astronomia y Astrofisica Conference Series, ed. S. Torres-Peimbert & G. MacAlpine, 101–108

Kormendy, J. & Fisher, D. B. 2008, in Astronomical Society of the Pacific Conference Series, Vol. 396, Astronomical Society of the Pacific Conference Series, ed. J. G. Funes & E. M. Corsini, 297–+

Kormendy, J. & Kennicutt, Jr., R. C. 2004, ARAA&A, 42, 603

Kravtsov, A. V. 2009, ArXiv:0906.3295

Kravtsov, A. V., Berlind, A. A., Wechsler, R. H., Klypin, A. A., Gottlöber, S., Allgood, B., & Primack, J. R. 2004, ApJ, 609, 35

Kravtsov, A. V., Klypin, A. A., & Khokhlov, A. M. 1997, ApJ, 111, 73

Kriek et al. 2008, ApJ, 677, 219

Kroupa, P., Tout, C. A., & Gilmore, G. 1993, MNRAS, 262, 545

Lacey, C. & Cole, S. 1993, MNRAS, 262, 627

Law, D. R., Steidel, C. C., Erb, D. K., Larkin, J. E., Pettini, M., Shapley, A. E., & Wright, S. A. 2007a, ApJ, 669, 929

Law, D. R., Steidel, C. C., Erb, D. K., Pettini, M., Reddy, N. A., Shapley, A. E., Adelberger, K. L., & Simenc, D. J. 2007b, ApJ, 656, 1

Li, Y., Helmi, A., De Lucia, G., & Stoehr, F. 2009, MNRAS, 397, L87

Li, Y., Mo, H. J., van den Bosch, F. C., & Lin, W. P. 2007, MNRAS, 379, 689

Lin, L., Koo, D. C., Willmer, C. N. A., Patton, D. R., Conselice, C. J., Yan, R., Coil, A. L., Cooper, M. C., Davis, M., Faber, S. M., Gerke, B. F., Guhathakurta, P., & Newman, J. A. 2004, ApJ, 617, L9

Lin, L., Patton, D. R., Koo, D. C., Casteels, K., Conselice, C. J., Faber, S. M., Lotz, J., Willmer, C. N. A., Hsieh, B. C., Chiueh, T., Newman, J. A., Novak, G. S., Weiner, B. J., & Cooper, M. C. 2008, ApJ, 681, 232

Lotz, J. M., Davis, M., Faber, S. M., Guhathakurta, P., Gwyn, S., Huang, J., Koo, D. C., Le Floc'h, E., Lin, L., Newman, J., Noeske, K., Papovich, C., Willmer, C. N. A., Coil, A., Conselice, C. J., Cooper, M., Hopkins, A. M., Metevier, A., Primack, J., Rieke, G., & Weiner, B. J. 2008a, ApJ, 672, 177

Lotz, J. M., Jonsson, P., Cox, T. J., & Primack, J. R. 2008b, MNRAS, 391, 1137

Lucatello, S., Gratton, R. G., Beers, T. C., & Carretta, E. 2005, ApJ, 625, 833

Maccio', A. V. & Fontanot, F. 2009, ArXiv:0910.2460

Macciò, A. V., Kang, X., & Moore, B. 2009, ApJ, 692, L109

Majewski, S. R., Beaton, R. L., Patterson, R. J., Kalirai, J. S., Geha, M. C., Muñoz, R. R., Seigar, M. S., Guhathakurta, P., Gilbert, K. M., Rich, R. M., Bullock, J. S., & Reitzel, D. B. 2007, ApJ, 670, L9

Maller, A. H. 2008, in Astronomical Society of the Pacific Conference Series, Vol. 396, Astronomical Society of the Pacific Conference Series, ed. J. G. Funes & E. M. Corsini, 251–+

Maller, A. H., Katz, N., Kereš, D., Davé, R., & Weinberg, D. H. 2006, ApJ, 647, 763

Marchesini, D., van Dokkum, P., Quadri, R., Rudnick, G., Franx, M., Lira, P., Wuyts, S., Gawiser, E., Christlein, D., & Toft, S. 2007, ApJ, 656, 42

Marchesini, D., van Dokkum, P. G., Förster Schreiber, N. M., Franx, M., Labbé, I., & Wuyts, S. 2009, ApJ, 701, 1765

Marín, F. A., Wechsler, R. H., Frieman, J. A., & Nichol, R. C. 2008, ApJ, 672, 849

Martin, N. F., de Jong, J. T. A., & Rix, H.-W. 2008, ApJ, 684, 1075

Martin, N. F., Ibata, R. A., Chapman, S. C., Irwin, M., & Lewis, G. F. 2007, MNRAS, 380, 281

Martin, N. F., Mc Connachie, A. W., Irwin, M., Widrow, L. M., Ferguson, A. M. N., Ibata, R. A., Dubinski, J., Babul, A., Chapman, S., Fardal, M., Lewis, G. F., Navarro, J., & Rich, R. M. 2009, ApJ, 705, 758

McBride, J., Fakhouri, O., & Ma, C. 2009, MNRAS, 398, 1858

McGaugh, S. S. 2005, ApJ, 632, 859

McIntosh, D. H., Guo, Y., Hertzberg, J., Katz, N., Mo, H. J., van den Bosch, F. C., & Yang, X. 2008, MNRAS, 388, 1537

Melbourne, J., Ammons, M., Wright, S. A., Metevier, A., Steinbring, E., Max, C., Koo, D. C., Larkin, J. E., & Barczys, M. 2008, AJ, 135, 1207

Melbourne et al. 2005, ApJ, 625, L27

Mihos, J. C. & Hernquist, L. 1996, ApJ, 464, 641

Monaco, P., Theuns, T., & Taffoni, G. 2002, MNRAS, 331, 587

Moore, B., Ghigna, S., Governato, F., Lake, G., Quinn, T., Stadel, J., & Tozzi, P. 1999, ApJ, 524, L19

Moster, B. P., Somerville, R. S., Maulbetsch, C., van den Bosch, F. C., Maccio', A. V., Naab, T., & Oser, L. 2009, ApJ, Submitted, ArXiv:0903.4682

Muñoz, J. A., Madau, P., Loeb, A., & Diemand, J. 2009, MNRAS, Accepted, ArXiv:0905.4744

Naab, T. & Burkert, A. 2003, ApJ, 597, 893

Naab, T., Khochfar, S., & Burkert, A. 2006, ApJ, 636, L81

Navarro, J. F., Frenk, C. S., & White, S. D. M. 1997, ApJ, 490, 493

Navarro, J. F. & Steinmetz, M. 2000, ApJ, 538, 477

Neistein, E. & Dekel, A. 2008, MNRAS, 388, 1792

Newberg, H. J., Mayeur, P. A., Yanny, B., & the SEGUE collaboration. 2006, Memorie della Societa Astronomica Italiana, 77, 1049

Noeske et al. 2007, ApJ, 660, L47

Nordström, B., Mayor, M., Andersen, J., Holmberg, J., Pont, F., Jørgensen, B. R., Olsen, E. H., Udry, S., & Mowlavi, N. 2004, A&A, 418, 989

Okamoto, T. & Frenk, C. S. 2009, MNRAS, L315+

Okamoto, T. & Nagashima, M. 2001, ApJ, 547, 109

Park, C., Choi, Y.-Y., Vogeley, M. S., Gott, J. R. I., & Blanton, M. R. 2007, ApJ, 658, 898

Patton, D. R. & Atfield, J. E. 2008, ApJ, 685, 235

Patton et al. 2002, ApJ, 565, 208

Peñarrubia, J., McConnachie, A. W., & Navarro, J. F. 2008, ApJ, 672, 904

Peebles, P. J. E. 1982, ApJ, 263, L1

Pontzen, A., Governato, F., Pettini, M., Booth, C. M., Stinson, G., Wadsley, J., Brooks, A., Quinn, T., & Haehnelt, M. 2008, MNRAS, 390, 1349

Pryor, C. & Meylan, G. 1993, in Astronomical Society of the Pacific Conference Series, Vol. 50, Structure and Dynamics of Globular Clusters, ed. S. G. Djorgovski & G. Meylan, 357–+

Purcell, C. W., Bullock, J. S., & Zentner, A. R. 2007, ApJ, 666, 20

—. 2008, MNRAS, 391, 550

Purcell, C. W., Kazantzidis, S., & Bullock, J. S. 2009, ApJ, 694, L98

Quadri et al. 2007, AJ, 134, 1103

Quinn, P. J., Hernquist, L., & Fullagar, D. P. 1993, ApJ, 403, 74

Robertson, B., Bullock, J. S., Cox, T. J., Di Matteo, T., Hernquist, L., Springel, V., & Yoshida, N. 2006a, ApJ, 645, 986

Robertson, B., Bullock, J. S., Font, A. S., Johnston, K. V., & Hernquist, L. 2005, ApJ, 632, 872

Robertson, B., Cox, T. J., Hernquist, L., Franx, M., Hopkins, P. F., Martini, P., & Springel, V. 2006b, ApJ, 641, 21

Robertson, B., Hernquist, L., Cox, T. J., Di Matteo, T., Hopkins, P. F., Martini, P., & Springel, V. 2006c, ApJ, 641, 90

Robertson, B., Yoshida, N., Springel, V., & Hernquist, L. 2004, ApJ, 606, 32

Robertson, B. E. & Bullock, J. S. 2008, ApJ, 685, L27

Robertson, B. E. & Kravtsov, A. V. 2008, ApJ, 680, 1083

Rocha, M., Jonsson, P., Primack, J. R., & Cox, T. J. 2008, MNRAS, 383, 1281

Ryan, Jr., R. E., Cohen, S. H., Windhorst, R. A., & Silk, J. 2008, ApJ, 678, 751

Sawicki, M. & Thompson, D. 2006, ApJ, 642, 653

Sesar et. al. 2007, AJ, 134, 2236

Shapiro et al. 2008, ApJ, 682, 231

Shapley, A. E., Steidel, C. C., Adelberger, K. L., Dickinson, M., Giavalisco, M., & Pettini, M. 2001, ApJ, 562, 95

Siegel, M. H., Majewski, S. R., Reid, I. N., & Thompson, I. B. 2002, ApJ, 578, 151

Simon, J. D. & Geha, M. 2007, ApJ, 670, 313

Somerville, R. S., Hopkins, P. F., Cox, T. J., Robertson, B. E., & Hernquist, L. 2008, MNRAS, 391, 481

Somerville, R. S. & Kolatt, T. S. 1999, MNRAS, 305, 1

Sommer-Larsen, J., Götz, M., & Portinari, L. 2003, ApJ, 596, 47

Spergel, D. N., Bean, R., Doré, O., Nolta, M. R., Bennett, C. L., Dunkley, J., Hinshaw, G., Jarosik, N., Komatsu, E., Page, L., Peiris, H. V., Verde, L., Halpern, M., Hill, R. S., Kogut, A., Limon, M., Meyer, S. S., Odegard, N., Tucker, G. S., Weiland, J. L., Wollack, E., & Wright, E. L. 2007, ApJ, 170, 377

Springel, V., Di Matteo, T., & Hernquist, L. 2005a, MNRAS, 361, 776

Springel, V. & Hernquist, L. 2003, MNRAS, 339, 289

—. 2005, ApJ, 622, L9

Springel, V., Wang, J., Vogelsberger, M., Ludlow, A., Jenkins, A., Helmi, A., Navarro, J. F., Frenk, C. S., & White, S. D. M. 2008, MNRAS, 391, 1685

Springel, V., White, S. D. M., Jenkins, A., Frenk, C. S., Yoshida, N., Gao, L., Navarro, J., Thacker, R., Croton, D., Helly, J., Peacock, J. A., Cole, S., Thomas, P., Couchman, H., Evrard, A., Colberg, J., & Pearce, F. 2005b, Nature, 435, 629

Stewart, K. R. 2009, to appear in proceedings of to appear in proceedings of "Galaxy Evolution: Emerging Insights and Future Challenges", ArXiv:0902.2214 [astro-ph]

Stewart, K. R., Bullock, J. S., Barton, E. J., & Wechsler, R. H. 2009a, ApJ, 702, 1005

Stewart, K. R., Bullock, J. S., Wechsler, R. H., & Maller, A. H. 2009b, ApJ, 702, 307

Stewart, K. R., Bullock, J. S., Wechsler, R. H., Maller, A. H., & Zentner, A. R. 2008, ApJ, 683, 597

Stinson et. al. 2006, MNRAS, 373, 1074

Stoehr, F., White, S. D. M., Tormen, G., & Springel, V. 2002, MNRAS, 335, L84

Strigari, L. E., Bullock, J. S., Kaplinghat, M., Diemand, J., Kuhlen, M., & Madau, P. 2007, ApJ, 669, 676

Strigari, L. E., Bullock, J. S., Kaplinghat, M., Simon, J. D., Geha, M., Willman, B., & Walker, M. G. 2008, Nature, 454, 1096

Tasitsiomi, A., Kravtsov, A. V., Wechsler, R. H., & Primack, J. R. 2004, ApJ, 614, 533

Thielemann, F., Nomoto, K., & Yokoi, K. 1986, A&A, 158, 17

Tollerud, E. J., Bullock, J. S., Strigari, L. E., & Willman, B. 2008, ApJ, 688, 277

Toomre, A. & Toomre, J. 1972, ApJ, 178, 623

Toth, G. & Ostriker, J. P. 1992, ApJ, 389, 5

Tumlinson, J. 2007, ApJ, 665, 1361

Vale, A. & Ostriker, J. P. 2004, MNRAS, 353, 189

van den Bosch, F. C., Yang, X., Mo, H. J., Weinmann, S. M., Macciò, A. V., More, S., Cacciato, M., Skibba, R., & Kang, X. 2007, MNRAS, 376, 841

van der Marel, R. P., Alves, D. R., Hardy, E., & Suntzeff, N. B. 2002, AJ, 124, 2639

van Dokkum, P. G. 2008, ApJ, 674, 29

Villalobos, Á. & Helmi, A. 2008, MNRAS, 391, 1806

Wadsley et. al. 2004, New Astronomy, 9, 137

Walker, I. R., Mihos, J. C., & Hernquist, L. 1996, ApJ, 460, 121

Walker, M. G., Mateo, M., Olszewski, E. W., Peñarrubia, J., Wyn Evans, N., & Gilmore, G. 2009, ApJ, 704, 1274

Walsh, S. M., Willman, B., & Jerjen, H. 2009, AJ, 137, 450

Watkins, L. L., Evans, N. W., Belokurov, V., Smith, M. C., Hewett, P. C., Bramich, D. M., Gilmore, G. F., Irwin, M. J., Vidrih, S., Wyrzykowski, Ł., & Zucker, D. B. 2009, MNRAS, 398, 1757

Weaver, T. A. & Woosley, S. E. 1993, PhR, 227, 65

Wechsler, R. H., Bullock, J. S., Primack, J. R., Kravtsov, A. V., & Dekel, A. 2002, ApJ, 568, 52

Wechsler, R. H., Zentner, A. R., Bullock, J. S., Kravtsov, A. V., & Allgood, B. 2006, ApJ, 652, 71

Wei, L. H., Kannappan, S. J., Vogel, S. N., & Baker, A. J. 2009, ArXiv:0908.2868 [astro-ph]

Weinmann, S. M., Kauffmann, G., van den Bosch, F. C., Pasquali, A., McIntosh, D. H., Mo, H., Yang, X., & Guo, Y. 2009, MNRAS, 394, 1213

Weinmann, S. M., van den Bosch, F. C., Yang, X., & Mo, H. J. 2006, MNRAS, 366, 2

Wetzel, A. R., Cohn, J. D., & White, M. 2009, MNRAS, 395, 1376

Widrow, L. M. & Dubinski, J. 2005, ApJ, 631, 838

Willman, B., Dalcanton, J. J., Martinez-Delgado, D., West, A. A., Blanton, M. R., Hogg, D. W., Barentine, J. C., Brewington, H. J., Harvanek, M., Kleinman, S. J., Krzesinski, J., Long, D., Neilsen, Jr., E. H., Nitta, A., & Snedden, S. A. 2005, ApJ, 626, L85

Wolf, J., Martinez, G. D., Bullock, J. S., Kaplinghat, M., Geha, M., Munoz, R. R., Simon, J. D., & Avedo, F. F. 2009, MRNAS, submitted, ArXiv:0908.2995

Wolf et al. 2005, ApJ, 630, 771

Wong, T. & Blitz, L. 2002, ApJ, 569, 157

Woods, D. F., Geller, M. J., & Barton, E. J. 2006, AJ, 132, 197

Wright, S. A., Larkin, J. E., Law, D. R., Steidel, C. C., Shapley, A. E., & Erb, D. K. 2009, ApJ, 699, 421

Wyse, R. F. G. 2001, in Astronomical Society of the Pacific Conference Series, Vol. 230, Galaxy Disks and Disk Galaxies, ed. J. G. Funes & E. M. Corsini, 71–80

Wyse, R. F. G. 2006, in The Local Group as an Astrophysical Laboratory, ed. M. Livio & T. M. Brown, 33–46

Yepes, G., Kates, R., Khokhlov, A., & Klypin, A. 1997, MNRAS, 284, 235

Younger, J. D., Cox, T. J., Seth, A. C., & Hernquist, L. 2007, ApJ, 670, 269

Zentner, A. R. 2007, International Journal of Modern Physics D, 16, 763

Zentner, A. R., Berlind, A. A., Bullock, J. S., Kravtsov, A. V., & Wechsler, R. H. 2005, ApJ, 624, 505

Zentner, A. R. & Bullock, J. S. 2003, ApJ, 598, 49

Zhao, D. H., Mo, H. J., Jing, Y. P., & Börner, G. 2003, MNRAS, 339, 12

Zucker et. al. 2006, ApJ, 643, L103

Zurek, W. H., Quinn, P. J., & Salmon, J. K. 1988, ApJ, 330, 519